LA-UR-16-29624

Proton and Ion Linear Accelerators

8. Low-Medium-High Energy Beam Transports (LEBT-MEBT-HEBT)

Yuri Batygin
Los Alamos National Laboratory

U.S. Particle Accelerator School

July 15 - July 26, 2024

LEBT Functions and Requirements

LEBT Purposes:

- Extraction and low – energy acceleration of the beam
- Match beam out of the ion source to the transport channel
- Dispose of electrons emitted along with the ions
- Match beam into the RF Accelerator (RFQ)
- Provide beam diagnostics and test facilities
- Provide fast switching (chopping) before the RF Accelerator to introduce time structure of the beam

Beam Physics Issues:

- Electrostatic vs magnetostatic LEBT
- Minimization of emittance growth
- Beam space charge compensation
- Short neutralization time

Space Charge Effects in the Extraction Region of Particle Sources: Child-Langmuir Law

2.5.2

Planar Diode with Space Charge (Child–Langmuir Law)

Let us now include the effect of the space charge of the electron current in the diode on the potential distribution and electron motion. To simplify our analysis, we assume that all electrons are launched with initial velocity $\mathbf{v}_0 = 0$ from the cathode (i.e., they are moving on straight lines in the x-direction). This is an example of *laminar flow* where electron trajectories do not cross and the current density is uniform. We try to find the steady-state solution ($\partial/\partial t = 0$) in a self-consistent form. The electrostatic potential is determined from the space-charge density ρ via Poisson's equation, with $\phi = 0$, at $x = 0$ and $\phi = V_0$ at $x = d$, as in the previous case. The relationship between ρ, the current density $\mathbf{J}$, and the electron velocity $\mathbf{v}$ follows from the continuity equation ($\nabla \cdot \mathbf{J} = 0$ or $\mathbf{J} = \rho\mathbf{v} = \text{const}$). The velocity in turn depends on the potential ϕ and is found by integrating the equation of motion. Thus we have the following three equations:

$$\nabla^2\phi = \frac{d^2\phi}{dx^2} = -\frac{\rho}{\epsilon_0} \quad \text{(Poisson's equation)}, \tag{2.129}$$

$$J_x = \rho\dot{x} = \text{const} \quad \text{(continuity equation)}, \tag{2.130}$$

$$\frac{m}{2}\dot{x}^2 = e\phi(x) \quad \text{(equation of motion)}. \tag{2.131}$$

*From M.Reiser, Theory and Design of Charged Particle Beams, Wiley, 1994

Space Charge Effects in the Extraction Region of Particle Sources: Child-Langmuir Law (Con.)

Substituting $\dot{x} = [2e\phi(x)/m]^{1/2}$ from (2.131) into (2.130) and $\rho = J_x/\dot{x}$ from (2.130) into (2.129) yields

$$\frac{d^2\phi}{dx^2} = \frac{J}{\epsilon_0(2e/m)^{1/2}} \frac{1}{(\phi)^{1/2}}, \tag{2.132}$$

where the current density $J = -J_x$ is defined as a positive quantity. After multiplication of both sides of Equation (2.132) with $d\phi/dx$, we can integrate and obtain

$$\left(\frac{d\phi}{dx}\right)^2 = \frac{4J}{\epsilon_0(2e/m)^{1/2}}\phi^{1/2} + C. \tag{2.133}$$

Now $\phi = 0$ at $x = 0$, and if we consider the special case where $d\phi/dx = 0$ at $x = 0$, we obtain $C = 0$. A second integration then yields (with $\phi = V_0$ at $x = d$)

$$\frac{4}{3}\phi^{3/4} = 2\left(\frac{J}{\epsilon_0}\right)^{1/2}\left(\frac{2e}{m}\right)^{-1/4} x,$$

or

$$\phi(x) = V_0\left(\frac{x}{d}\right)^{4/3}, \tag{2.134}$$

with the relation

$$J = \frac{4}{9}\epsilon_0\left(\frac{2e}{m}\right)^{1/2}\frac{V_0^{3/2}}{d^2}. \tag{2.135}$$

Current-Voltage Curve

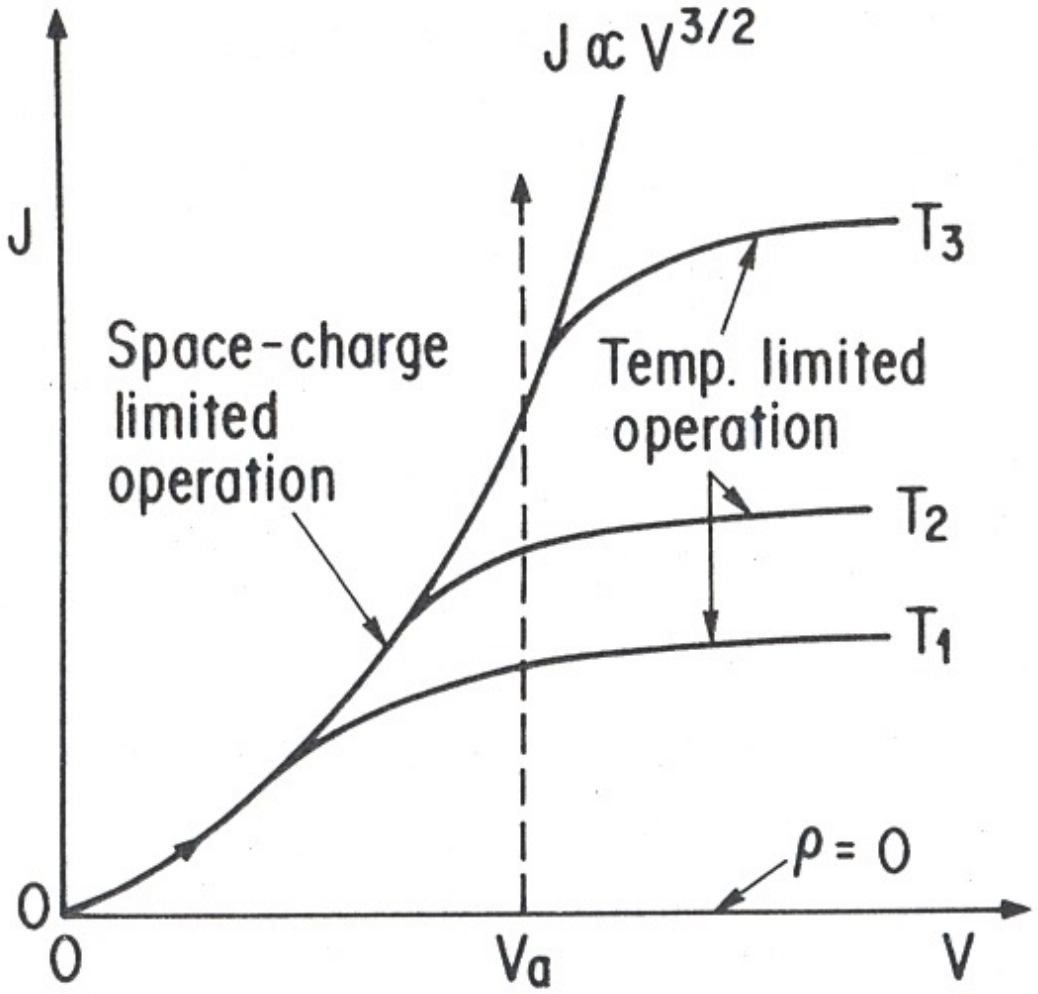

Current-voltage relation at constant cathode temperature (from S.Isagawa, Joint Accelerator School, 1996).

Child-Langmuir Law for Spherical Surfaces

In ion sources, the shape of plasma meniscus is determined by the balance between plasma pressure and applied electrostatic voltage for ion extraction.

To determine shape of plasma memiscus, let us consider self-consistent problem for the beam extracted from spherical emitter of radius R_1 (plasma) and spherical collector of radius R_2 ($R_2<R_1$). Saturated current density extracted from the plasma

$$j = n_i e \sqrt{\frac{kT_e}{m_i}}$$

Ion Source Beam Current

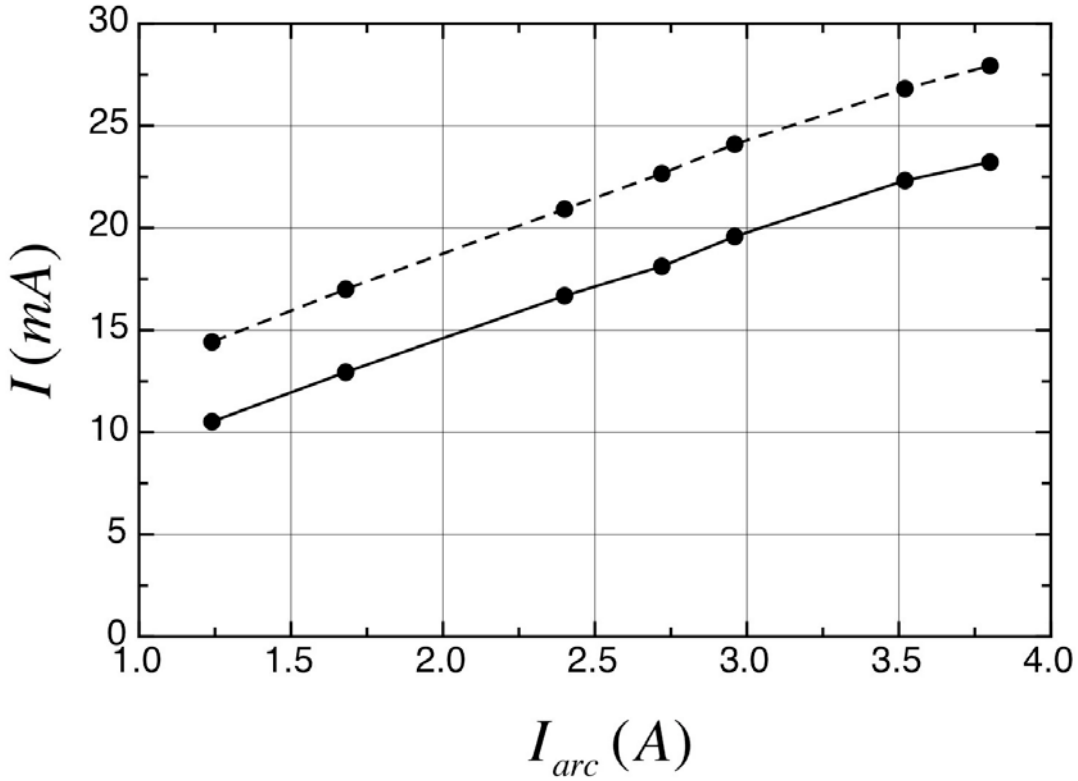

Beam current of Los Alamos duoplasmatron proton ion source at extraction voltage U_{ext} = 27 kV as a function of source arc current: (solid) H^+ beam current, (dashed) total $H^+/H_2^+/H_3^+$ current.

Child-Langmuir Law for Spherical Surfaces (cont.)

We will assume that all particle have the same extracted velocities, so the current density is $j = \rho\, v_r$ and particle velocity is

$$v_r = \sqrt{\frac{2qU}{m}}$$

where *U* is the potential between two spheres. Therefore, beam space charge density is

$$\rho = \frac{j}{\sqrt{\frac{2qU}{m}}}$$

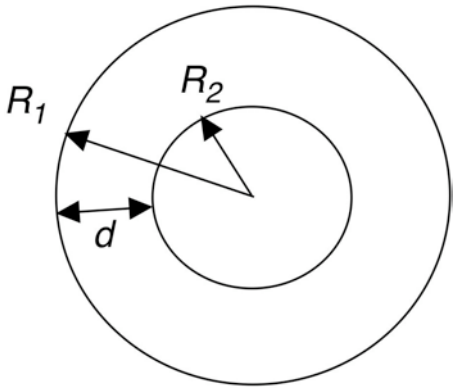

On derivation of Child-Langmuir law between spherical surfaces.

Child-Langmuir Law for Spherical Surfaces (cont.)

Let us substitute space charge density into Poisson's equation in spherical coordinates:

$$\frac{1}{r^2}\frac{d}{dr}\left(r^2\frac{dU}{dr}\right) = -\frac{1}{\varepsilon_o}\frac{j}{\sqrt{\frac{2qU}{m}}}$$

Solution of Poisson's equation for concentric spheres is

$$\frac{j}{U^{3/2}} = \frac{4\sqrt{2}}{9}\varepsilon_o\sqrt{\frac{q}{m}}\frac{1}{R_1^2\alpha^2}$$

where $\alpha = Y - 0.3Y^2 + 0.075Y^3$, $\quad Y = \ln\frac{R_2}{R_1}$

Child-Langmuir Law for Spherical Surfaces (cont.)

This is the Child-Langmuir law for spherical surfaces. When the distance between emitter and collector is much smaller than the raduses $d = R_1 - R_2 << R_1$, the following approximations can be used:

$$Y = \ln\left(\frac{R_1 - d}{R_1}\right) \approx -\frac{d}{R_1} - \frac{1}{2}\left(\frac{d}{R_1^2}\right)^2 - \frac{1}{2}\left(\frac{d}{R_1^2}\right)^3$$

$$\frac{1}{R_1^2 \alpha^2} \approx \frac{1}{d^2}\left(1 - 1.6\frac{d}{R_1}\right)$$

With this approximation, Child-Langmuir law is expressed as

$$\frac{j}{U^{3/2}} = \frac{4\sqrt{2}}{9}\varepsilon_o \sqrt{\frac{q}{m}}\frac{1}{d^2}\left(1 - 1.6\frac{d}{R_1}\right)$$

Child-Langmuir Law for Spherical Surfaces (cont.)

Let us apply now obtained result to the problem of plasma beam extraction from small extraction hole of the radius r_1. From Fig the relationship between extraction radius r_1 and radius R_1 is

$$R_1 = -\frac{r_1}{\sin\theta} \approx -\frac{r_1}{\theta}$$

where θ is the angle of ion emitting surface (plasma meniscus). Negative values of θ correspond to convergence of the beam (concave meniscus).

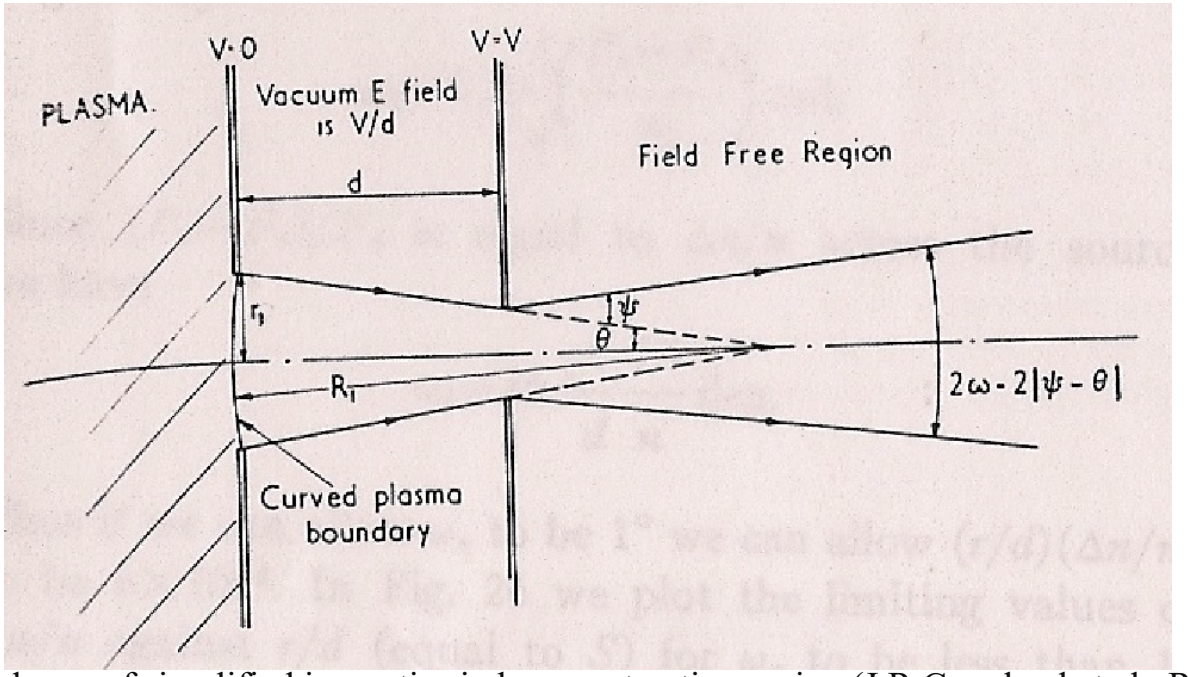

Scheme of simplified ion optics in beam extraction region (J.R.Coupland et al., Rev. Sci. Instruments, Vol. 44, No 9, (1973), p.1258.

Child-Langmuir Law for Spherical Surfaces (cont.)

Beam current density $$j = \frac{I}{\pi r_1^2}$$

Substitution of expression for beam current density into Child-Langmuir law reads:

$$\frac{I}{U^{3/2}} = \frac{4\sqrt{2}\pi}{9}\varepsilon_o\sqrt{\frac{q}{m}}\left(\frac{r_1}{d}\right)^2\left(1+1.6\frac{d}{r_1}\theta\right)$$

Beam perveance: $$P_b = \frac{I}{U^{3/2}}$$

Child-Langmuir perveance of one dimensional diode $$P_o = \frac{4\sqrt{2}\pi}{9}\varepsilon_o\sqrt{\frac{q}{m}}\left(\frac{r_1}{d}\right)^2$$

Extracted beam slope (plasma meniscus): $$\theta = 0.625\frac{r_1}{d}\left(\frac{P_b}{P_0}-1\right)$$

If $P_b << P_o$, it corresponds to the extracted beam with negligible intensity, and initial convergence of the beam is defined by extraction geometry only

$$\theta = -0.625\frac{r_1}{d}$$

Child-Langmuir Law for Spherical Surfaces (cont.)

According to Child-Langmuir law, the potential inside extraction gap has the following z-dependence:

$$U(z) = U_{ext} \left(\frac{z}{d_{ext}} \right)^{4/3}$$

Inside extraction gap particles move in the field, which, in the first approximation, has only longitudinal component

$$E_z = \frac{4}{3} U_{ext} \frac{z^{1/3}}{d_{ext}^{4/3}}$$

Outside extraction gap the field drops to zero.

Beam Defocusing in Extraction Gap

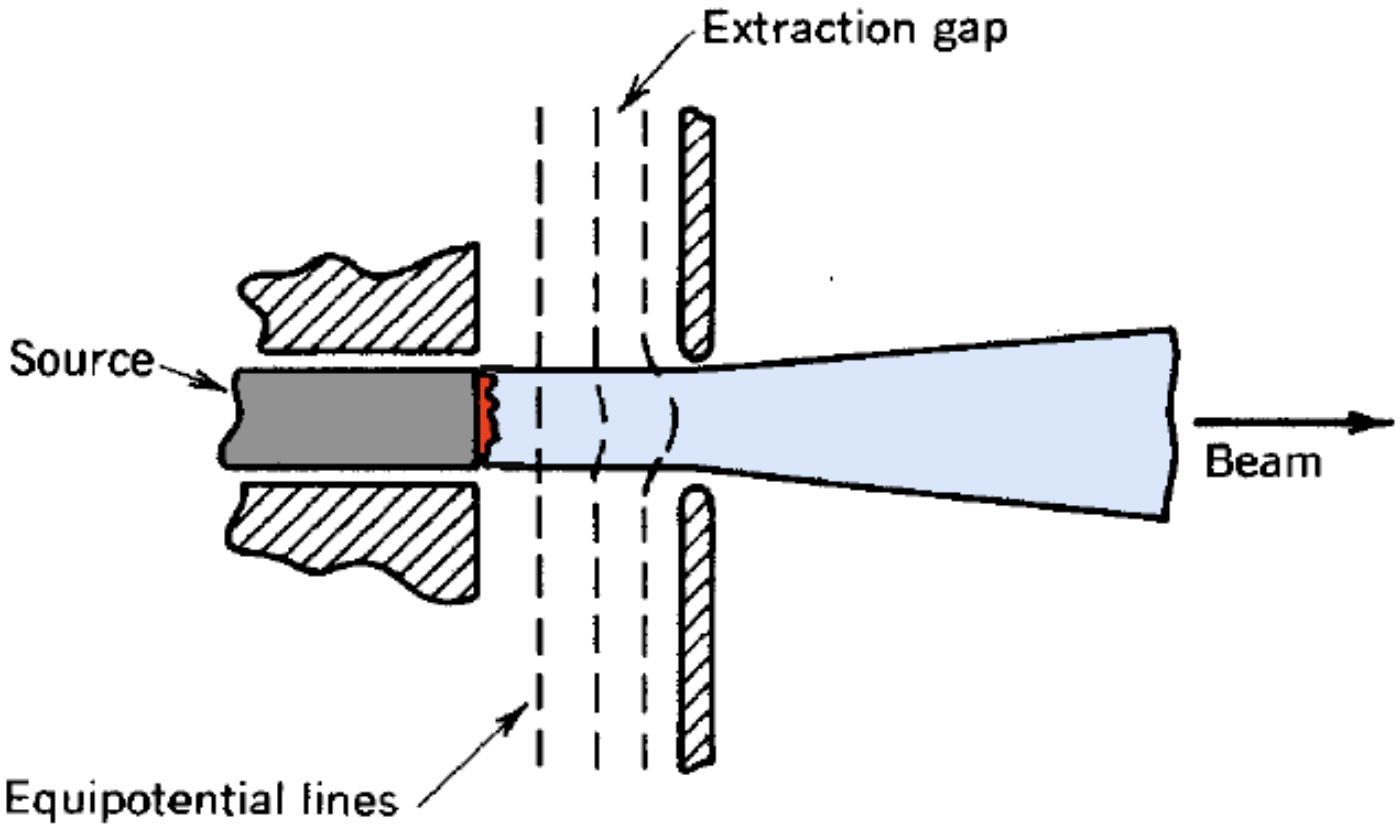

Extraction gap showing defocusing effect (S.Humphries, 1999).

Beam Defocusing in Extraction Gap (cont.)

Due to equation $$\text{div}\,\vec{E} = \frac{1}{r}\frac{\partial}{\partial r}(r\,E_r) + \frac{\partial E_z}{\partial z} = 0$$

any change in longitudinal field results in appearance of transverse field component, which (in this case) defocuses beam:

$$E_r = -\frac{1}{r}\int_0^r \frac{\partial E_z}{\partial z}\, r'\, dr' \approx -\frac{r}{2}\frac{\partial E_z}{\partial z}$$

Equation of particle motion: $$\frac{d^2 r}{dz^2} = -\frac{q}{mv_z^2} r \frac{1}{2}\frac{\partial E_z}{\partial z}$$

Slope of particle trajectory at the exit of the gap:

$$\psi = \Delta\left(\frac{dr}{dz}\right) = -\frac{q}{2mv_z^2} r \int \frac{\partial E_z}{\partial z} dz = \frac{q}{2mv_z^2} r E_z = \frac{r E_z}{4U_{ext}} = \frac{r}{3d}$$

Beam Defocusing in Extraction Gap (cont.)

Finally, divergence of the extracted beam is as follows:

$$\omega = |\theta + \psi| = \left| 0.625 \frac{r_1}{d} \left(\frac{P_b}{P_0} - 1 \right) + \frac{r_1}{3d} \right| = \left| 0.29 \frac{r_1}{d} \left(1 - 2.14 \frac{P_b}{P_0} \right) \right|$$

Condition for extracted beam with zero divergence

$$P_b = 0.47 P_o$$

Ratio of beam perveance to Chald-Langmuir perveance (matching parameter) is used to characterize conditions for the best extracted beam quality

$$\eta = \frac{P_b}{P_o} = \frac{9}{\sqrt{2} S^2} \frac{I}{I_c} \left(\frac{mc^2}{qU_{ext}} \right)^{3/2}$$

Aspect ratio:

$$S = \frac{r_1}{d}$$

Nonlinear Effects in Beam Optics (Lejeune, 1983)

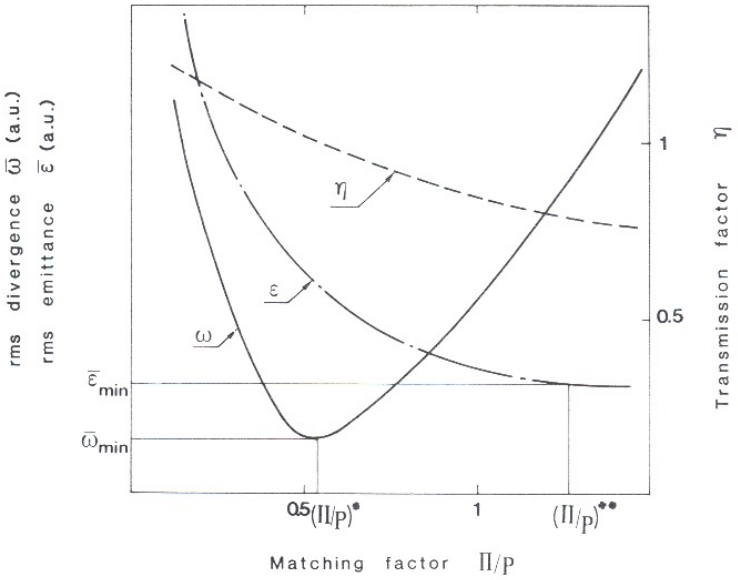

FIG. 32. Schematic representation of the three main graphs which characterize the performance of a triode extraction optics: rms divergence ($\bar{\omega}$), rms emittance ($\bar{\varepsilon}$), and transmission factor ($\bar{\eta}$) as functions of the matching factor (Π/P). These graphs may be summarized by the minimum values of $\bar{\omega}$ and $\bar{\varepsilon}$ and the respective optimal values of Π/P, as well as by the sensitivity factor Q, the definition of which is illustrated in Fig. 21.

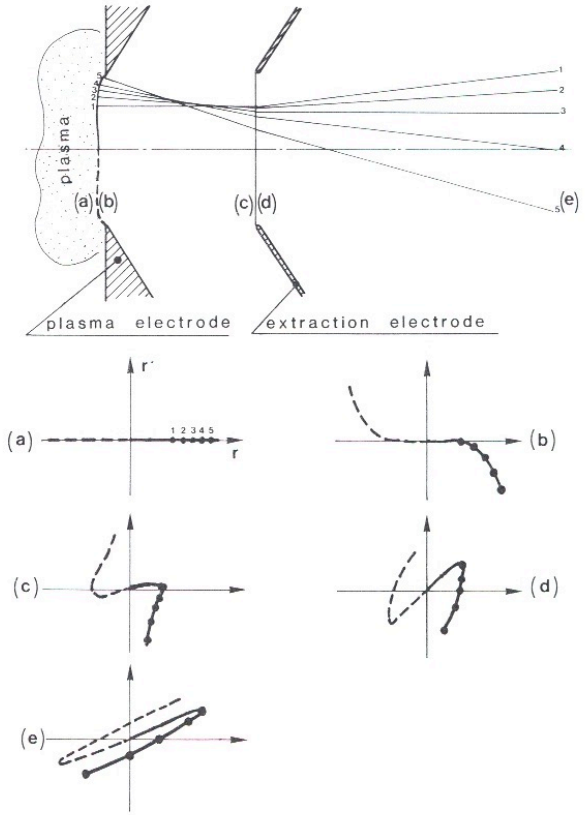

FIG. 24. Schematic illustration of the mechanism that produces an S-shaped emittance pattern for the beam emergent from an extraction optics if the radius of curvature of the plasma meniscus is not uniform. In the upper part of the figure are shown particular trajectories normally emitted from the rim of the plasma meniscus, where the radius of curvature varies strongly. In the lower diagrams the evolution of the beam emittance pattern is shown for several meaningful cross sections: (a) in the emitter section if the plasma meniscus is planar and without transverse thermal spread, (b) after the action of the concave plasma meniscus, (c) in the entrance plane of the extraction lens, (d) in the exit plane of this lens, and (e) in the probing section after a drift.

Nonlinear Optics: Simulations (Whealton et. al, 1980)

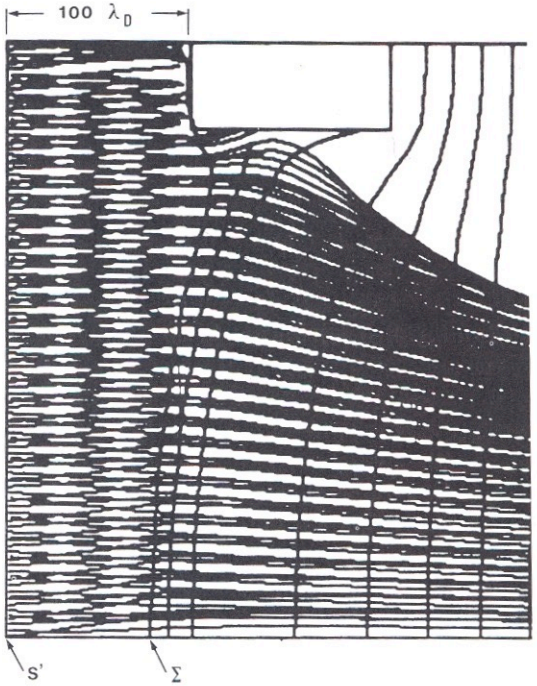

FIG. 11. Equipotential contours and ion trajectories in the region of the classical sheath edge Σ of a triode extraction optics. They are obtained from the ORNL nonlinear theory and code C (see text) (courtesy of Whealton and Whitson, 1980, and Gordon and Breach). The emissive surface (S') equivalent to the plasma is represented by the linear line on the left of the figure. The leftmost potential contour is halfway between the plasma and the screen potential and is illustrative of the position of the classical sheath edge Σ. The second contour just to the right of this is at the screen potential, and the third is at four times the difference between the plasma and the screen.

FIG. 4. Ion trajectories and potential distributions for a converged solution to Eqs. (9)—(12) showing the source-plasma sheath and nonlinear aberrrations near the plasma electrode: $S = 0.75$, $\Gamma = 4$, and $j = 0.45 j_0$.

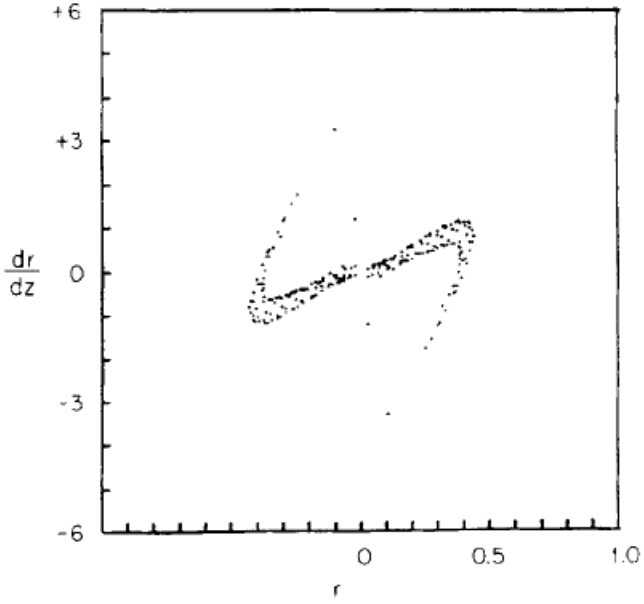

FIG. 5. Emittance diagram showing the slope and the position of exiting orbits for the case shown in Fig. 4.

Experimental Analysis of Extracted Beam Emittance (J.Aubert et al, 1983)

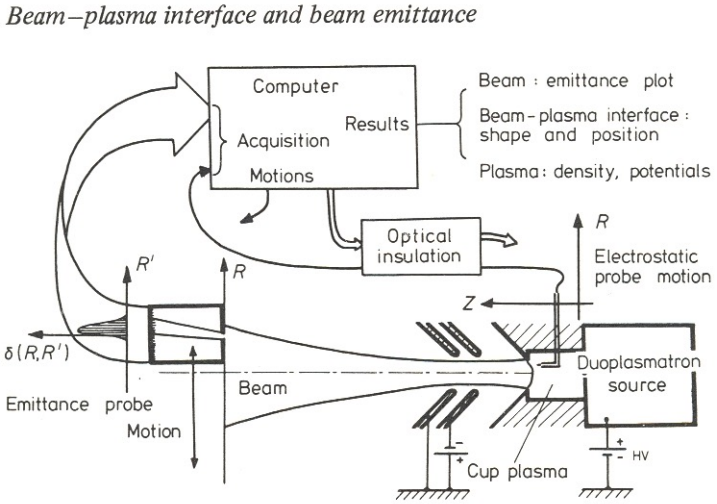

Figure 2. Principle of the computer-controlled experimental set-up.

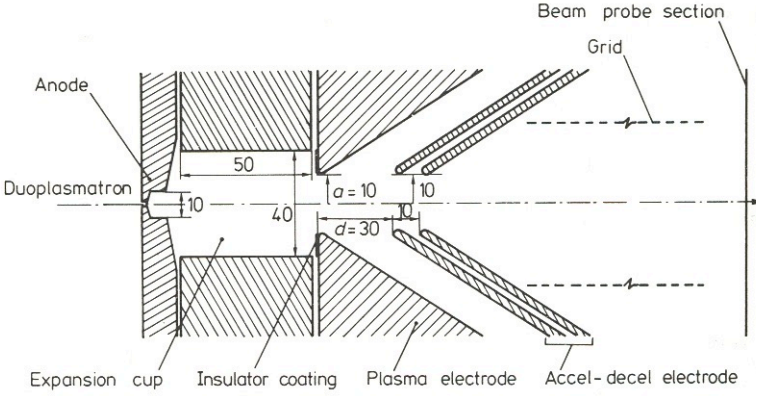

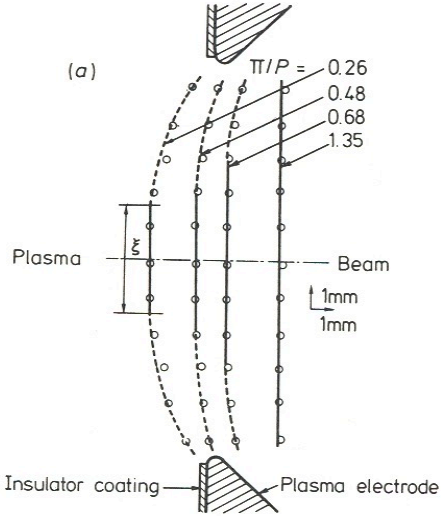

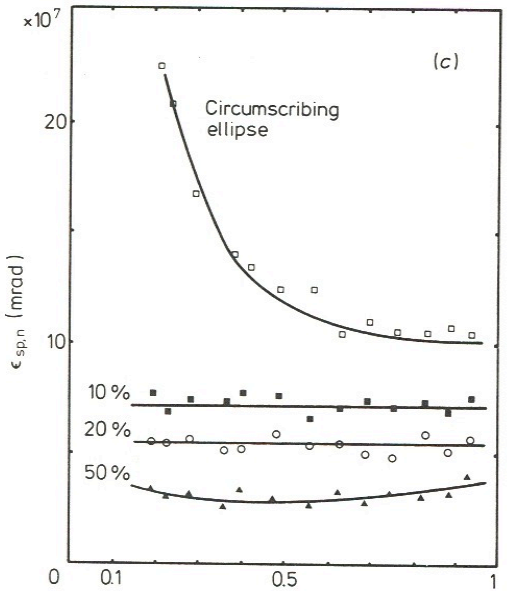

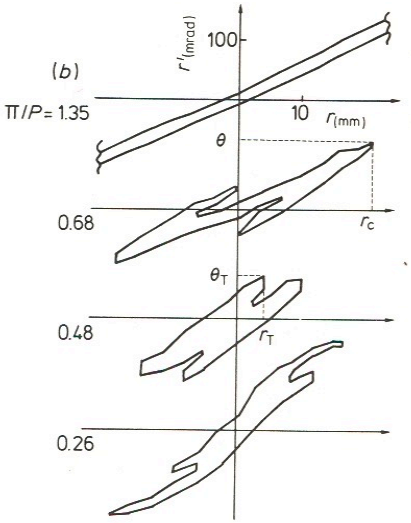

Figure 3. Beam–plasma interface for different values of the dimensionless parameter Π/P (*a*) and corresponding emittance contours (*b*). The intensity of the argon beam is constant (2 mA); the variation of Π/P is obtained from the variation of the accel voltage. (*c*) Fractional normalised emittance enclosed within equi-density contours and emittance of the circumscribing ellipse as functions of Π/P. The equi-density contours are defined by the quoted percentage of the maximum density.

LANL Proton Beam Brightness as a Function of Matching Parameter

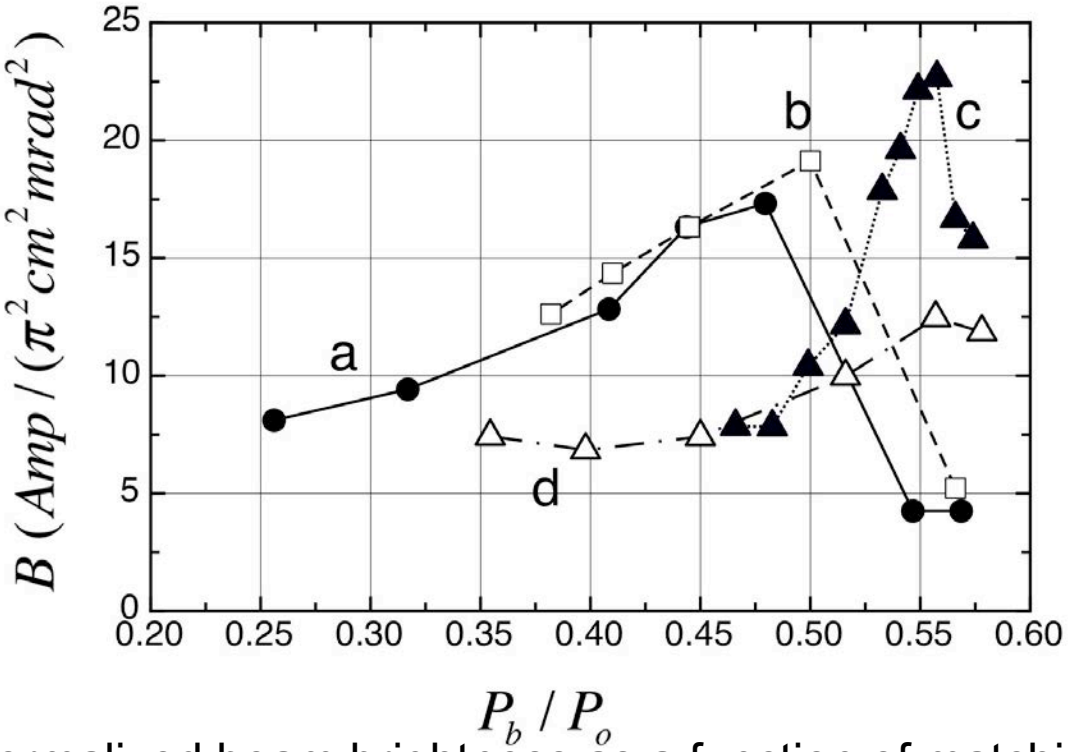

Normalized beam brightness as a function of matching parameter: (a) I = 10… 24 mA, U_{ext} = 27 kV, (b) U_{ext} = 24 ….30 kV, I = 18.5 mA, (c) I = 14… 17.5 mA, U_{ext} = 22 kV, (d) U_{ext} = 19.5 ….27 kV at I = 14.5 mA.

Y.B. et al, Rev. Sci. Instr., 85, 103301 (2014)

LANL Proton Beam Emittance versus Beam Intensity

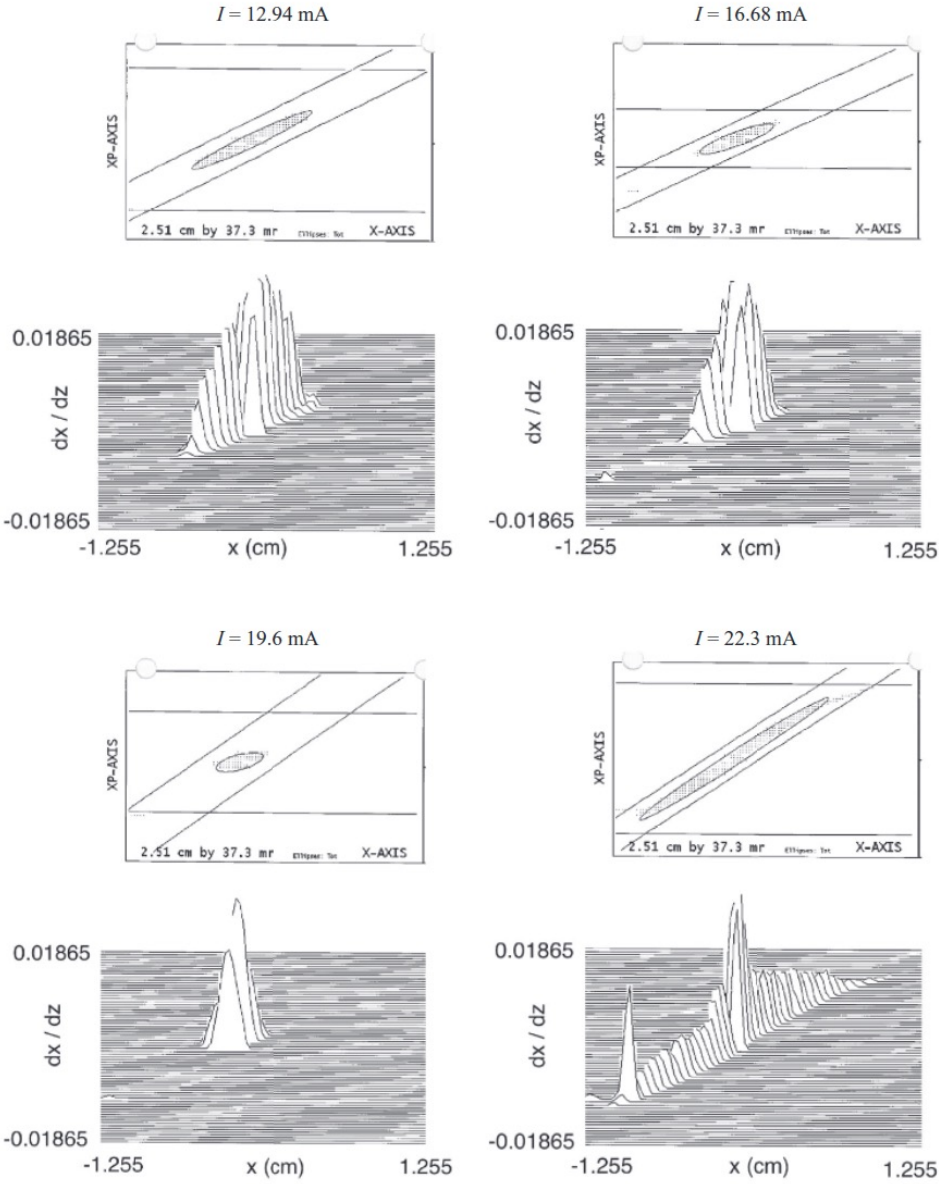

Horizontal beam emittance scans at extraction voltage of U_{ext} = 27 kV for different H^+ beam intensities.

Optimal Conditions for Proton Beam Extraction

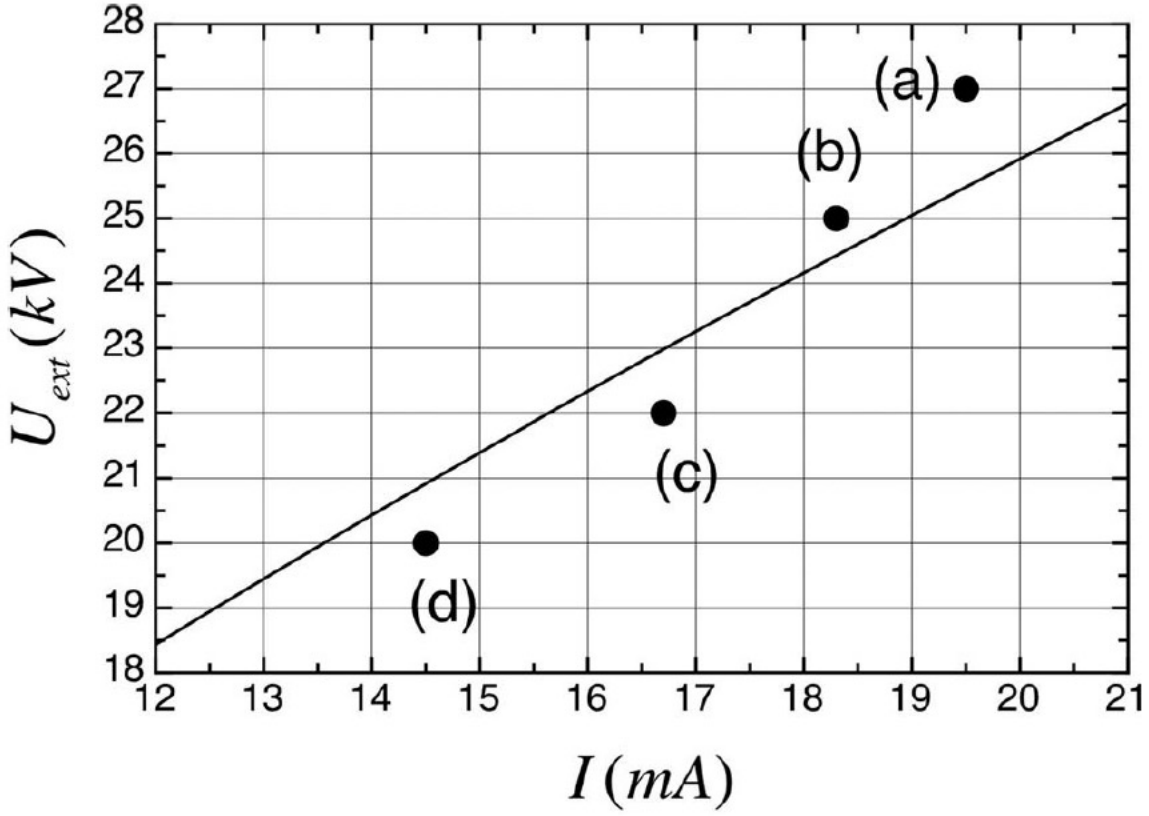

$$\eta_{opt} = 0.52.$$

$$U_{ext} = \left(\frac{I}{P_o \eta_{opt}}\right)^{2/3}$$

Extraction voltage versus H+ beam current for maximizing beam brightness. Dots: experimental results.

Repeller Electrode: Three Electrode Extraction

- Extraction electric field is attractive for neutralizing particles resulting in beam decompensation

- Repelling electrode (trapping electrode) is inserted upstream of the extraction electrode. This electrode creates a potential barrier to keep the neutralizing particles within the beam by preventing them to be attracted toward the ion source.

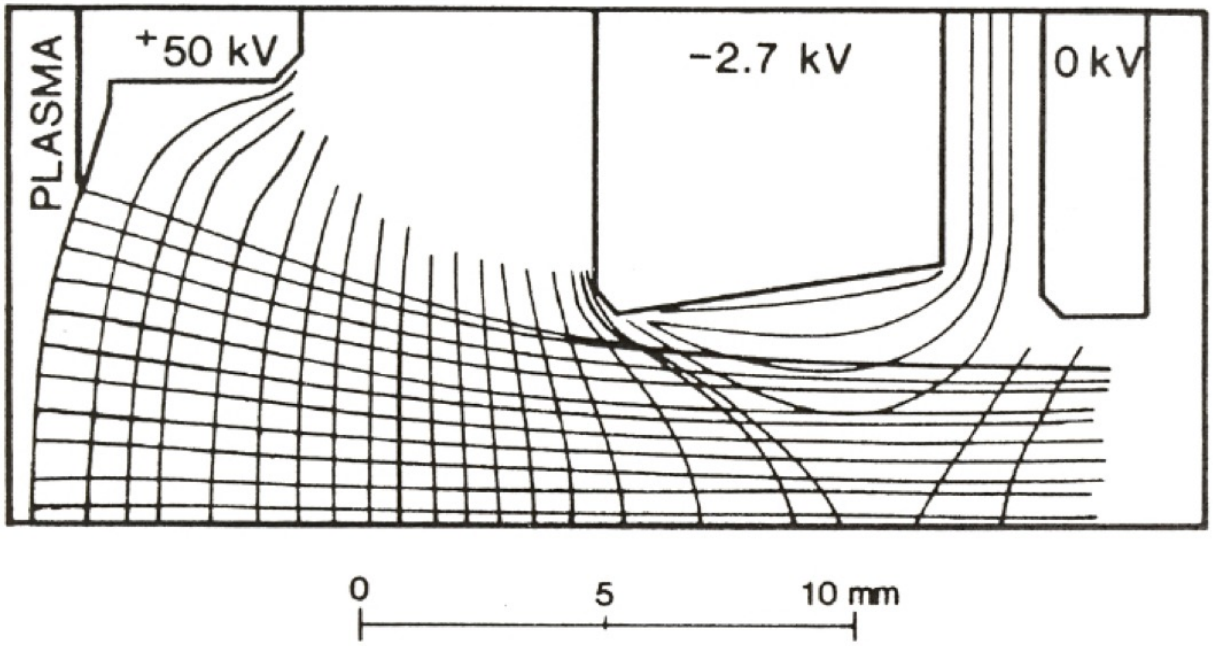

Three electrode beam extraction system (B.Piosczyk, FZ Karlsruhe).

Four-Electrode Extraction System

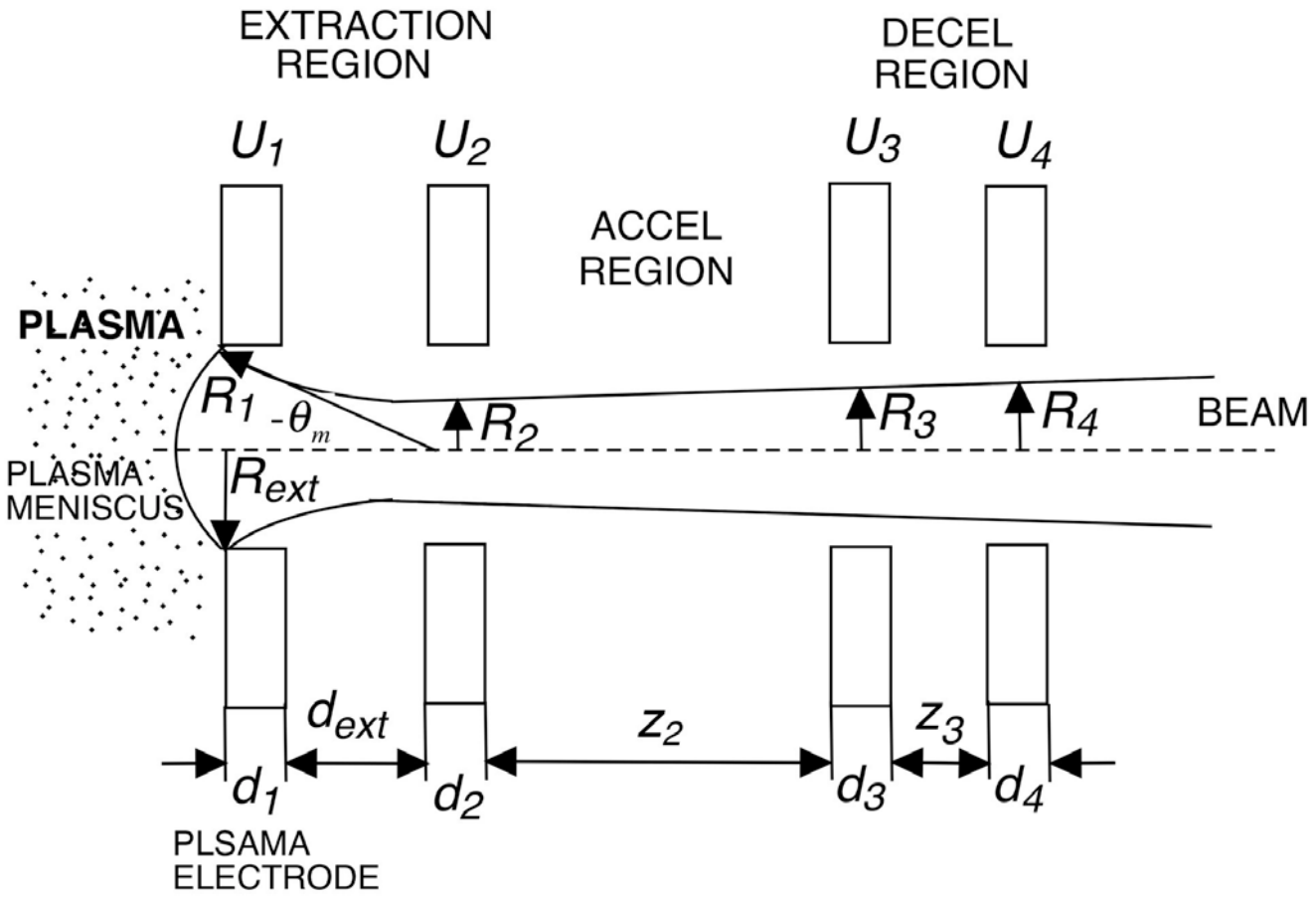

Four-Electrode Extraction System

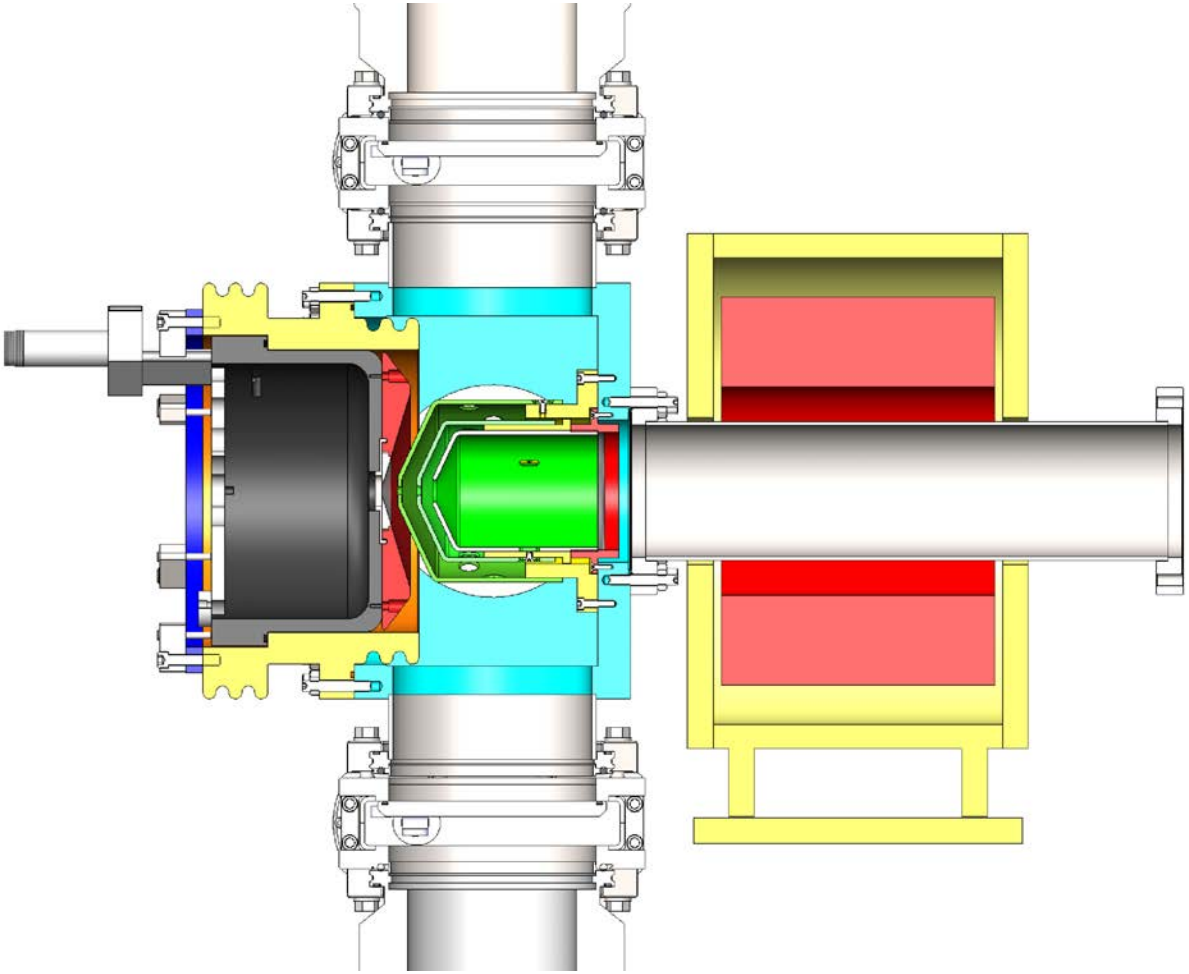

Layout of ion source and extraction system. Duoplasmatron source is on the left. Extraction electrodes are in the center and the 1st LEBT solenoid is on the right. Pumps are above and below electrodes.

Divergence of the Beam in 4-Electrode Extractor (J.Kim et al, J.Appl. Physics, 49(2) (1978), p.517)

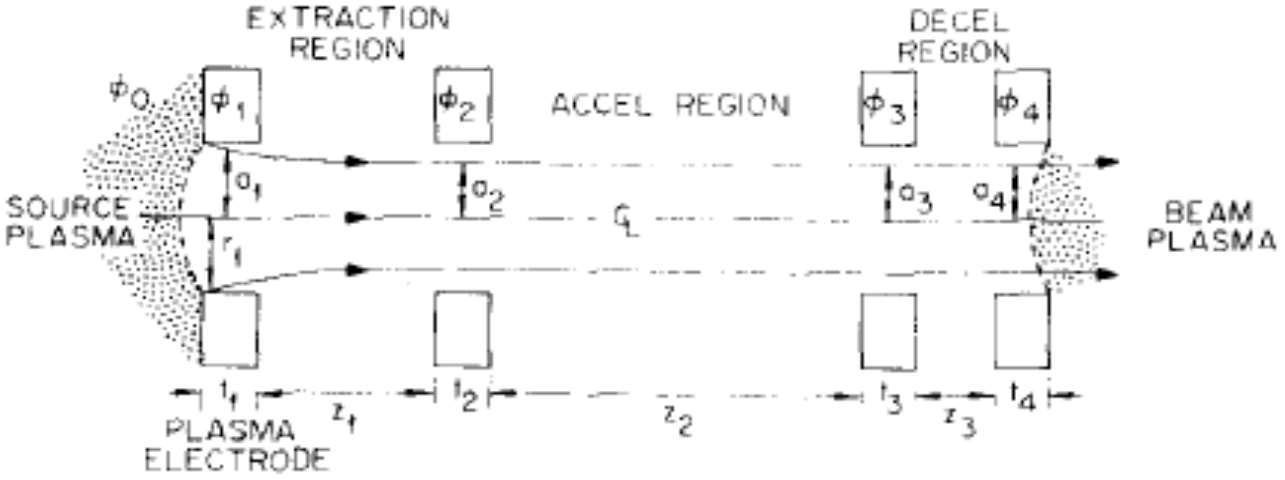

FIG. 1. Schematic of a two-stage four-electrode accelerating column with definitions of some relevant parameters and nomenclature.

$$\theta = 0.62S\left[\frac{P}{P_0} - 0.40\left(\frac{a_2}{a_1}\right)\frac{\Gamma^2}{f(1+\Gamma)} + 0.53\left(\frac{a_2}{a_1}\right) - 1\right]$$

$$+ 0.31S\left(\frac{P}{P_0}\right)\left[1 + \left(\frac{t_1}{t_2}\right) + 0.35\left(\frac{a_1}{a_2}\right)\right.$$

$$\left.\times\left(f + \frac{z_3 + t_2 + t_3}{z_1}\right)(1 + 0.50\Gamma)^{-1.5}\right].$$

where P is the perveance in the extraction gap, $P = I/V_{ext}^{3/2}$ and P_0 is the Child-Langmuir[7] space-charge-limited perveance for the one-dimensional diode of length z_1 with no electrons, $P_0 = (\frac{4}{9}\pi)(a_1^2/z_1^2)\epsilon_0(2e/M)^{1/2}$, where ϵ_0 is the permittivity of the vacuum.

Parameters of High-Intensity LEBT

Location	Particle, Energy	Type	Beam current, mA	Rms beam emittance (π mm mrad)	Chopper
SNS	H^-, 65 keV	2 Einzel lenses	35	0.22/0.18	40 kV Electrode chopper
J-Park	H^-, 50 keV	2 Solenoids	35	0.22	Induction cavity
BNL	H^-, 35 keV	2 Solenoids	100	0.4	
FNAL	H^-, 35 keV	2 Solenoids	45	0.3	Einzel lens chopper
LANSCE	H^-, 80 keV	2 solenoids	17	0.2	Electrostatic deflector
CERN Linac4	H^-, 45 keV	2 solenoids	40	0.25	Electrostatic deflector
JHF 1996	H^-, 50 keV	2 solenoids	16	0. 1	
ISIS	H^-, 65 keV	3 solenoids	60	0.55	
ESS	H^+, 75 keV	2 solenoids	55	0.2	

Electrostatic LEBT

Pro:

• no transient time for space charge compensation

• no repelling electrode for the neutralizing particle trapping is needed- design of electrostatic LEBTs are simplified

• the beam lines are compact, which tends to minimize the beam losses by charge exchange

Con:

• no space charge compensation (neutralizing particles are attracted or re- pulsed by the electric field induced by the focusing elements).

• vulnerable to beam losses that can lead to high voltage breakdowns and beam trips

• Einzel lenses intrinsically induce optical aberrations that creates beam halo and emittance growth

• Electrostatic LEBTs are intensity limited. Beam divergence and size will increase rapidly with its intensity (especially for current of several tens of mA). Its seems difficult to operate the LEBT with a higher current than the design current without expecting beam losses or dramatic emittance growth.

SNS LEBT and Parameters of the Beam

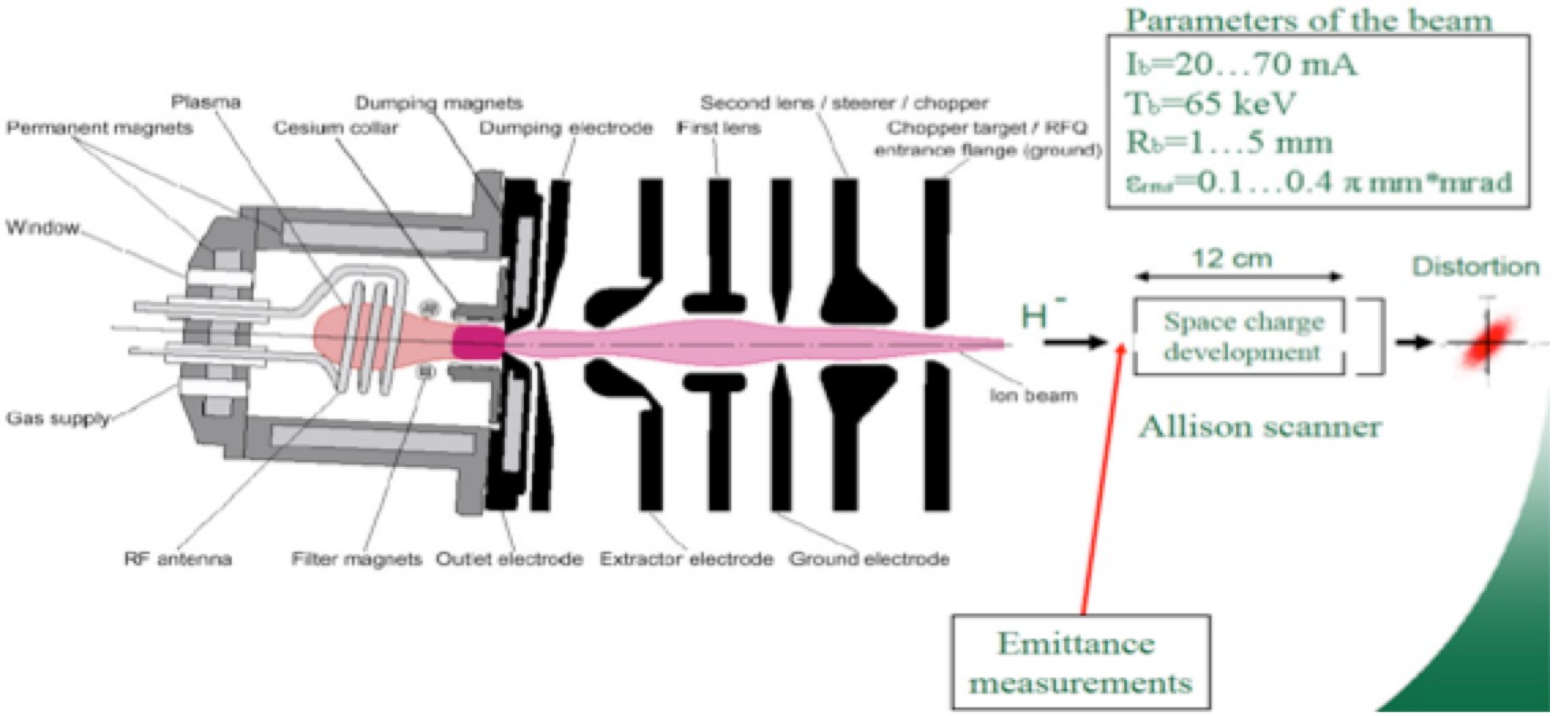

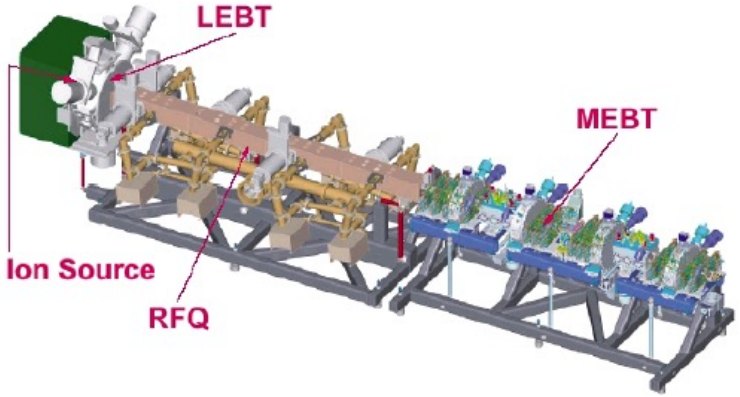

Figure 1. The 9-m long SNS front-end beamline.

SNS Injector Beam Parameters

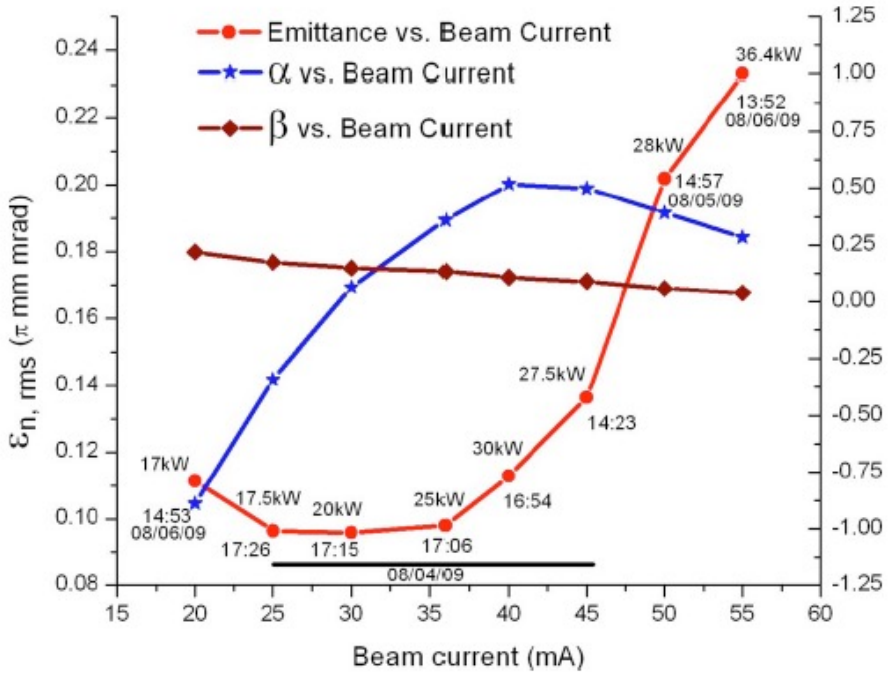

FIG. 5. (Color online) Emittance and twiss parameters dependence on the beam intensity.

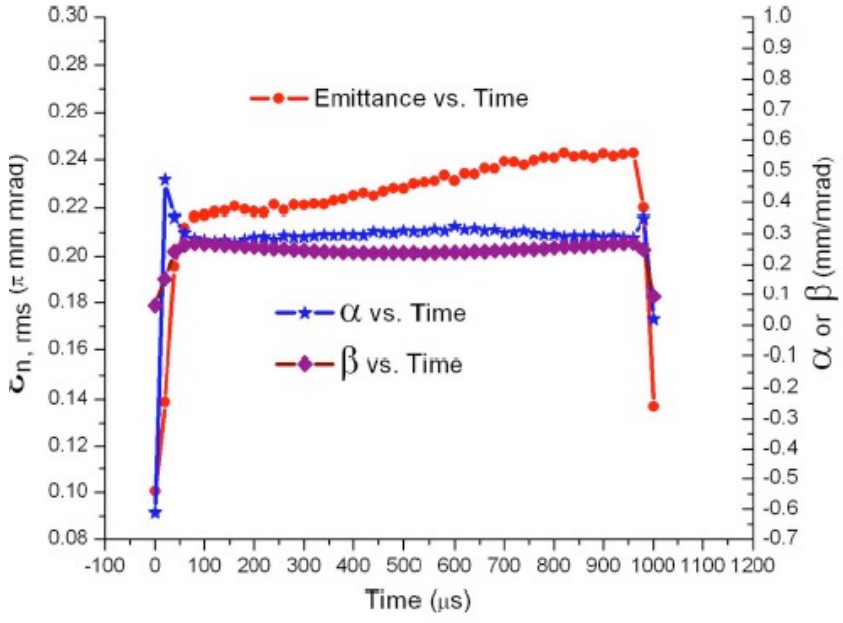

IG. 8. (Color online) Evolution of the emittance and twiss parameters over ıe 1.0 ms beam pulse duration.

SNS Injector Beam Parameters

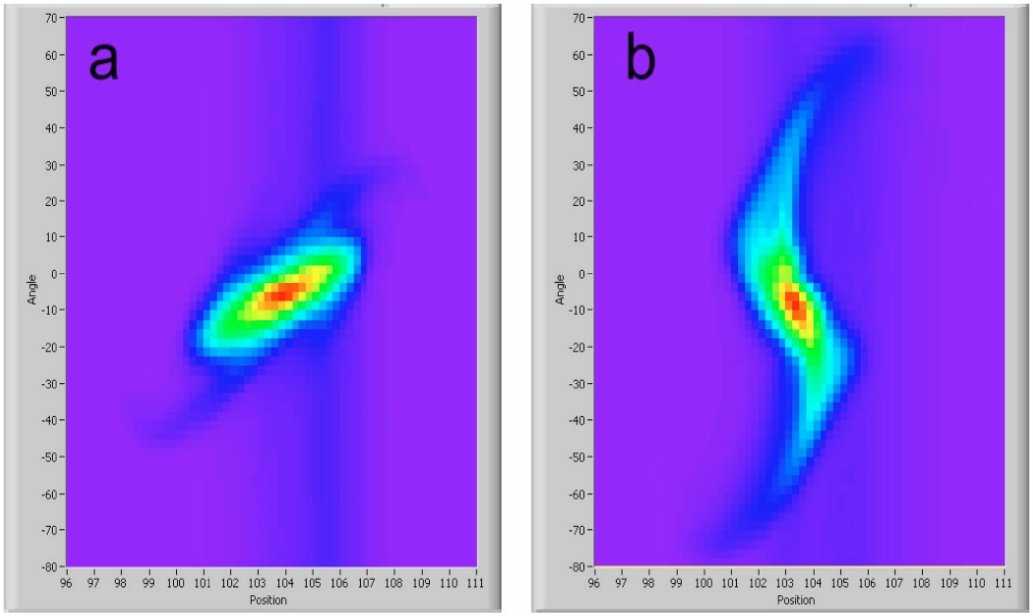

FIG. 6. (Color online) Phase-space plots of (a) 20 and (b) 55 mA beams.

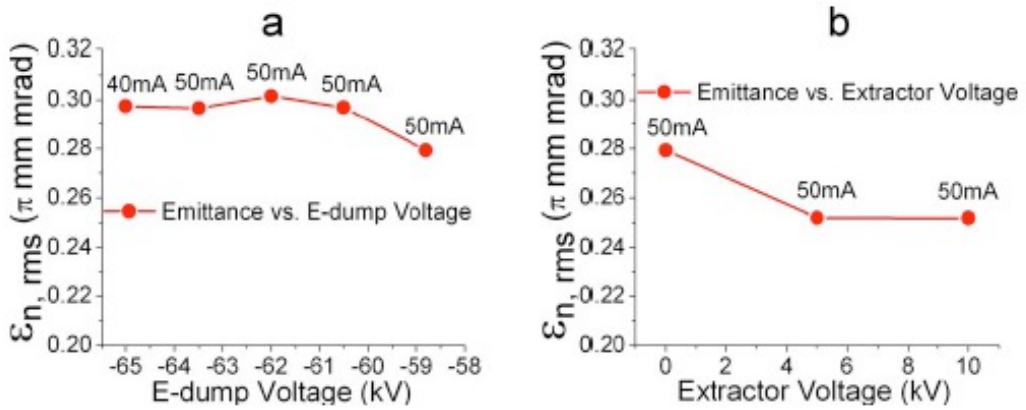

FIG. 7. (Color online) Emittance dependences on (a) e-dump voltage with the extractor at ground and (b) extractor voltage with the e-dump set at −58.8 kV.

Magnetostatic LEBT

Pro:

- beam is neutralized by the ionization on the residual gas
- smaller emittance growth due to nonlinear space charge forces than that in electrostatic LEBT
- beam emittance can be improved with a higher pressure in the beam line
- for positive ion beam, an additional source of neutralizing particles exists: secondary electrons are produced when a beam hits the beam pipes
- magnetic lenses have less spherical aberrations than electrostatic lenses with the same focal length

Con:

- In a magnetic LEBT the rise time of the pulsed beams is dominated by the space charge compensation transient time (several tens of μs)
- a fast chopping system have to be inserted to reach a rise time in the order of the hundreds of ns.

Layout of New LANSCE 35 keV H^+ Injector

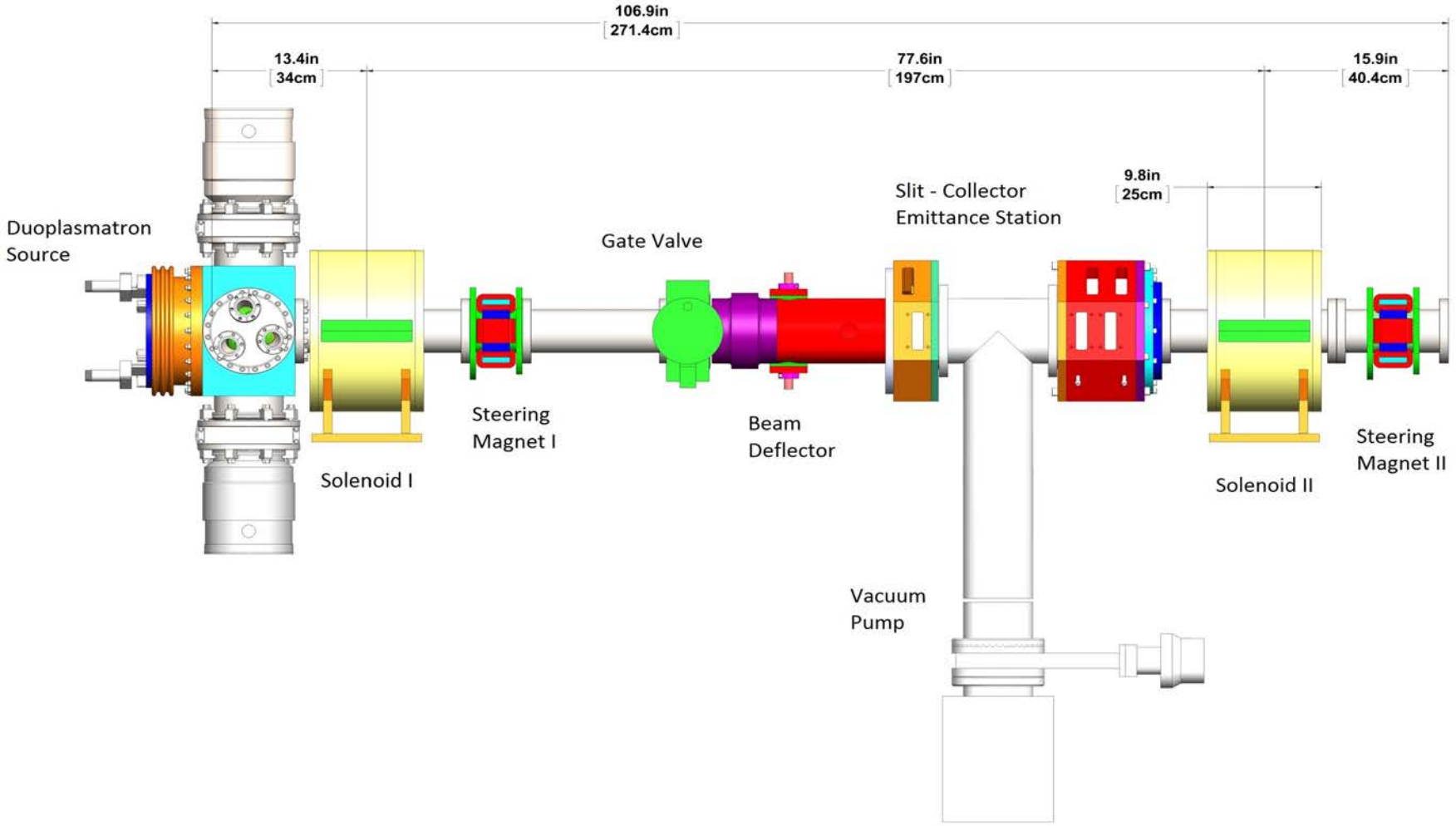

80 keV H^- LANSCE Beam Transport

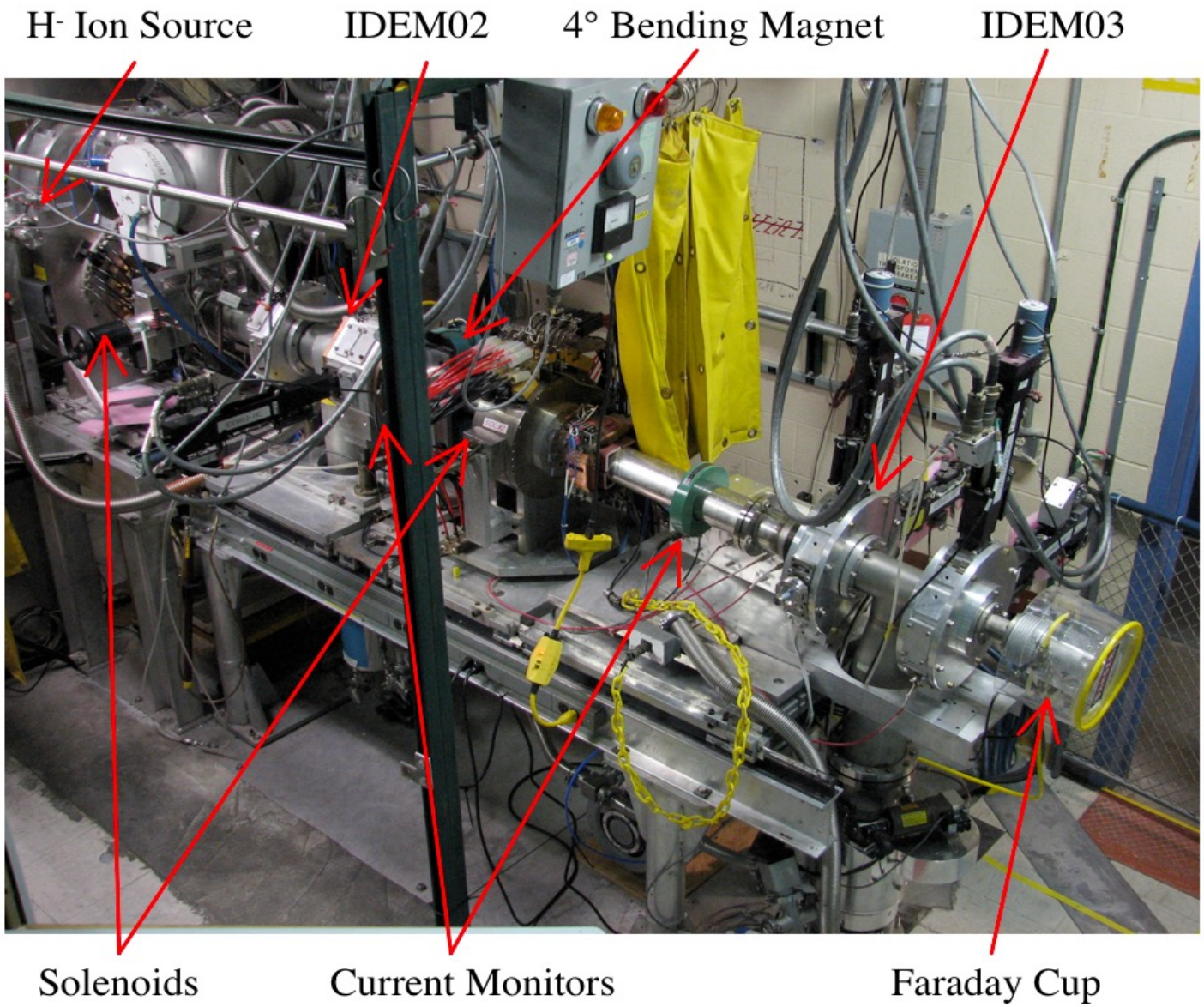

Interaction of the Beam with Residual Gas

Due to presenece of residual gas atoms or molecluse in transport channel, there is a constant interaction of beam particles with atoms or molecules of residual gas. Particle-residual gas interaction processes can be divided by elastic (single and multiple Coulomb scattering) and inelastic processes (ionization, electron capture, electron lost) where projectile particle loses it's energy.

Every process is characterized by cross section (similar to geometrical cross section of interacting particles) which depend on type of interacting particles and energy of incoming particles.

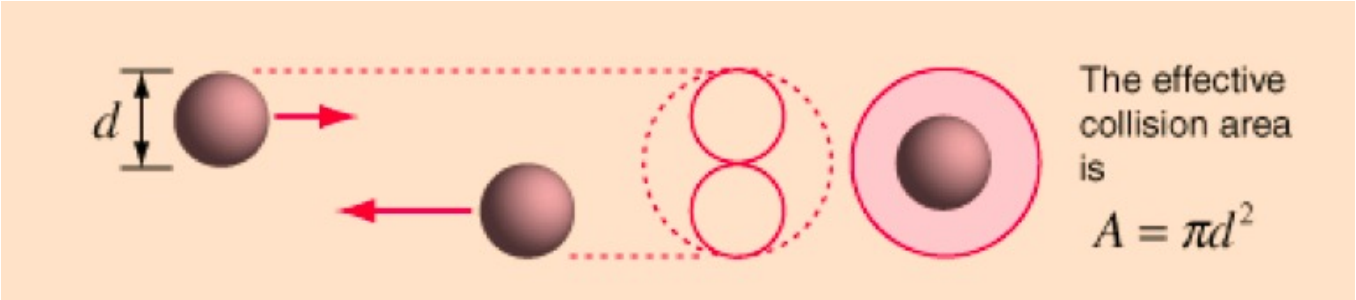

Cross Section

Cross section of the process is the ratio of rate of event per unit time $\frac{dN}{Ndt}$ to flux density of interacting particles $n_g v$, where n_g is the density and v is velocity:

$$\sigma = \frac{dN}{Ndt}\frac{1}{n_g v}$$

Particularly, losses of beam current I in the target of thickness dz with density of n_g atoms per m^3 are proportional to I, n_g, and dz:

$$dI = -I\sigma n_g dz$$

with the solution $I = I_o \exp(-\sigma n_g z) = I_o \exp(-\frac{t}{\tau})$

where beam lifetime is expressed as $\tau = \frac{1}{\sigma n_g v}$

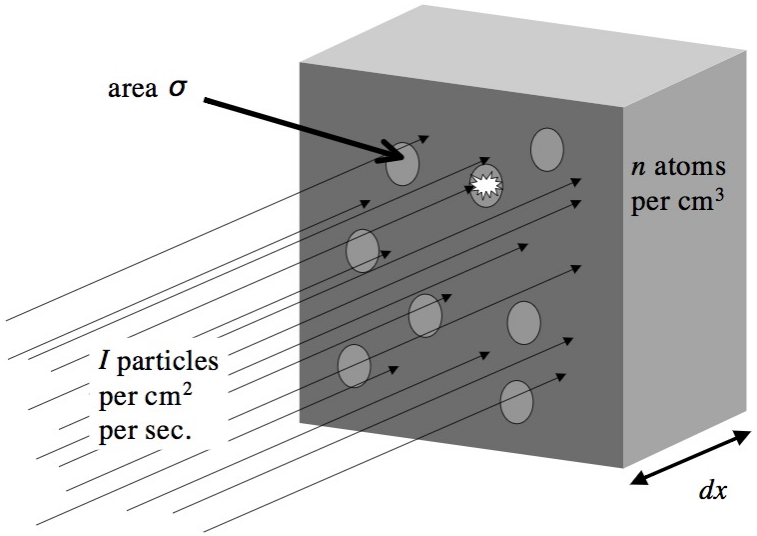

On definition of cross section.

Ionization of Residual Gas

Important phenomenon of low-energy beam interaction with residual gas is ionization of residual gas resulting in creation of electron-ion pairs, which neutralize space charge of primary beam.

Time required for ionization of residual gas by the incoming beam with velocity of βc

$$\tau_N = \frac{1}{n_s \sigma_i \beta c}$$

n_s is the density of scattering gas centers, σ_i is the ionization cross section.

Number of molecules per unit volume at pressure p and temperature T determined from the ideal gas law:

$$n_g = \frac{p}{kT}$$

Boltzman constant

$k = 1.38 \times 10^{-23}$ J·K^{-1}

Density of scattering centers for residual gas containing 2 atoms per molecule (H_2)

$$n_s = 2n_g$$

Ionization Cross Section: Thomson Model

Direct ionization is a results of the interaction of an incident particle having energy ε with a valence electron of neutral atom or molecule. Ionization happens when the energy transferred to the valence electron exceeds the ionization potential *I*. The process definitely includes quantum effects, but can be estimated from simple classical Thomson model of the atom. Ionization cross section (Thomson formula):

$$\sigma_i = \frac{1}{(4\pi\varepsilon_0)^2}\frac{\pi e^4}{\varepsilon}\left(\frac{1}{I}-\frac{1}{\varepsilon}\right)$$

Thomson formula in general case should be multiplied by number of valence electrons Z_v. When ε = 2*I,* the Thomson cross section has a maximum:

$$\sigma_o = \frac{Z_v}{(4\pi\varepsilon_o)^2}\frac{\pi e^4}{4I^2}$$

Maximum cross section is close to geometrical atomic cross section: for molecular nitrogen $\sigma_o = 10^{-16}$ cm^2 , for argon $\sigma_o = 3\text{x}10^{-16}$ cm^2 .

Ionization Cross Section: Thomson Model (cont.)

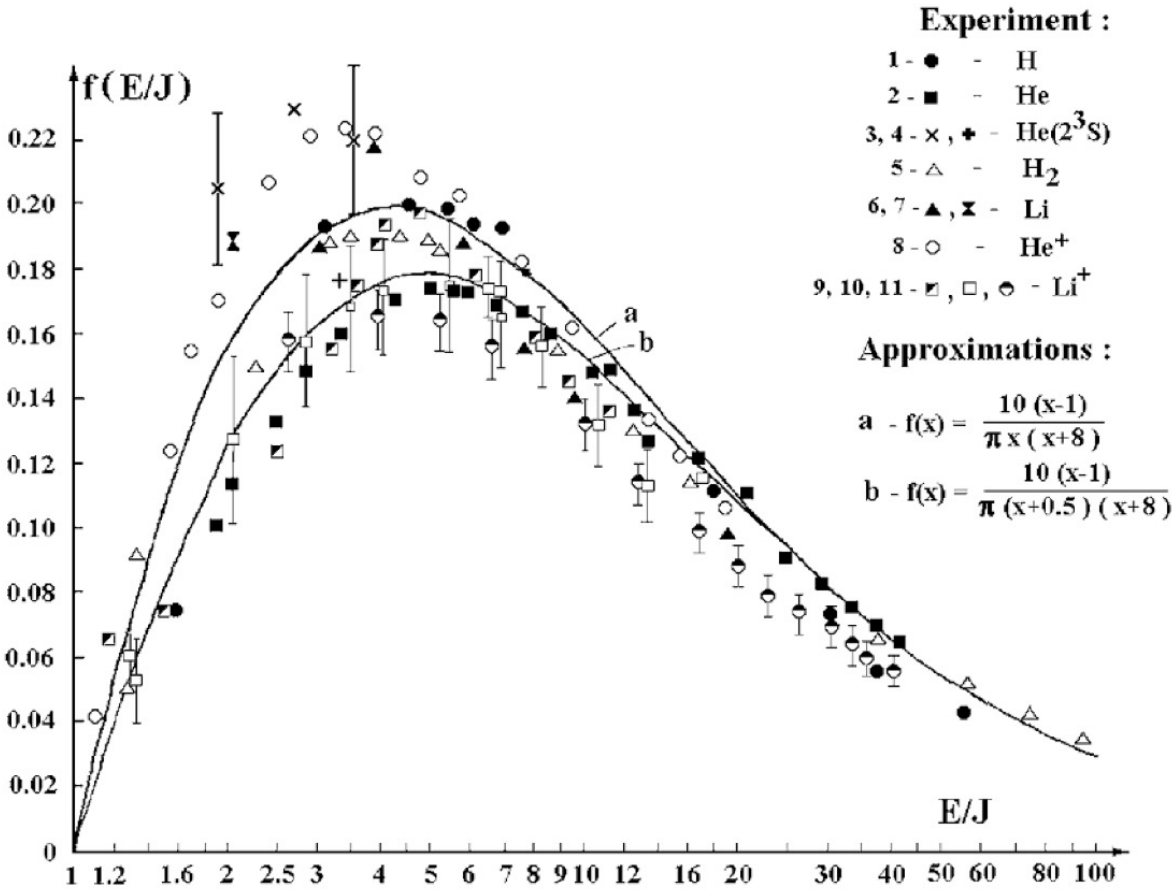

Figure 2.11 The reduced cross sections of ionization of atoms and ions by electron impact with valence *s* electrons versus the reduced electron energy. Experiment: 1 – [95]; 2 – [96]; 3 – [97]; 4 – [98]; 5 – [99]; – [103]; 11 – [104]; 12 – [105]. Approximation $f(x) = 10(x-1)/[\pi x(x+8)]$ is given by the solid curve and approximation $f(x) = 10(x-1)/[\pi(x+0.5)(x+8)]$ is represented by the dashed curve.

Ionization Cross Sections of H^+ on Different Gases

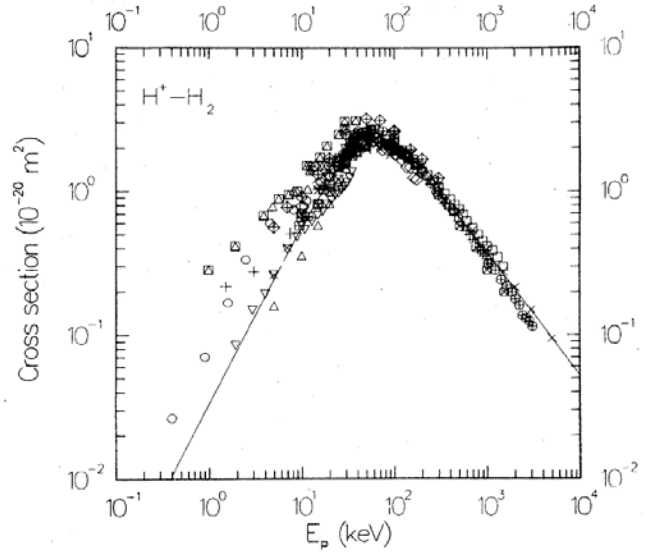

FIG. 13. Cross sections for ejection of electrons in $H^+ + H_2$ collisions. The solid curve is the recommended fit. Experimen-

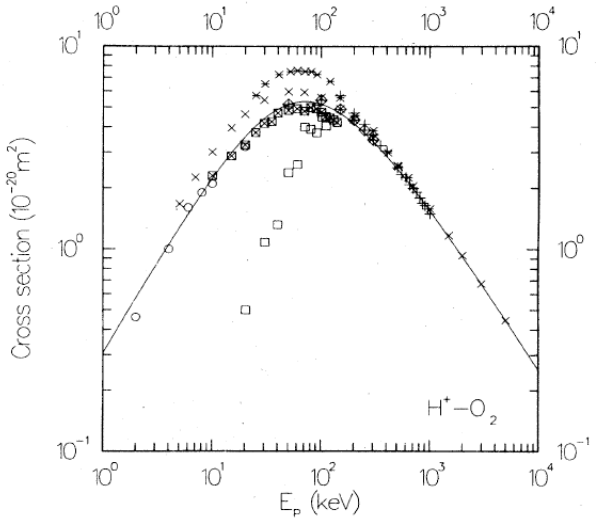

FIG. 16. Cross sections for ejection of electrons in $H^+ + O_2$ collisions. The solid curve is the recommended fit. Experimen-

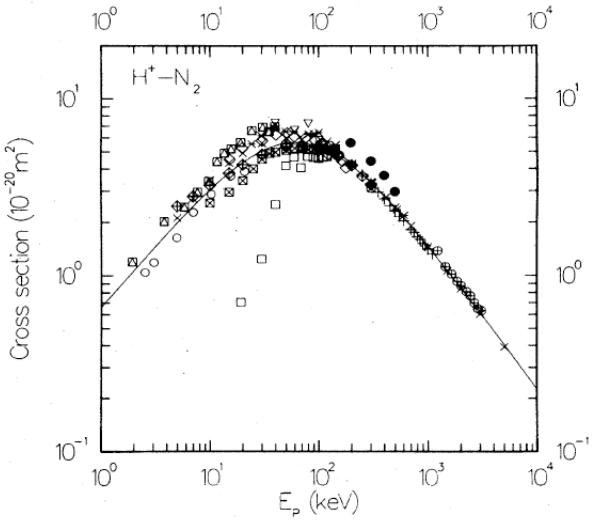

FIG. 14. Cross sections for ejection of electrons in $H^+ + N_2$ collisions. The solid curve is the recommended fit. Experimen-

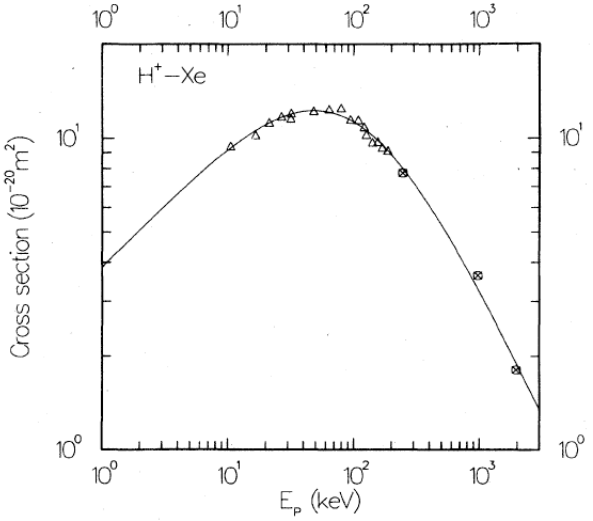

FIG. 11. Cross sections for ejection of electrons in $H^+ + Xe$ collisions. The solid curve is the recommended fit. Experimental data: △, Fedorenko *et al.* (1960); ⊠, Toburen (1974).

Space Charge Neutralization: 80 keV H^- Beam in H_2 Residual Gas with Pressure of P = 3.5 x 10^{-6} Torr

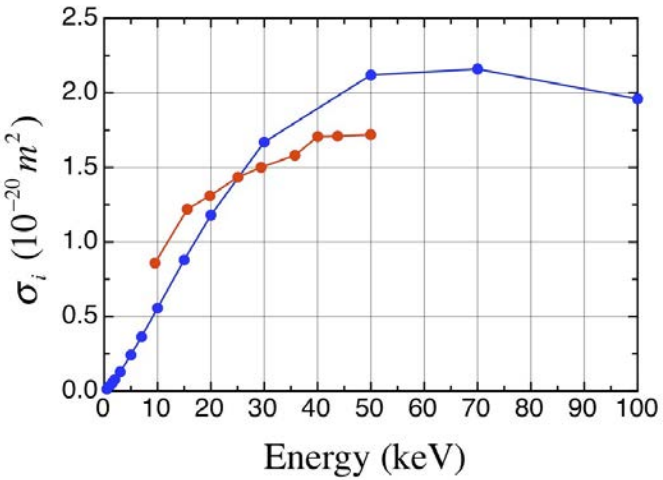

Density of H_2 molecules under the pressure of $p = 3.5 \cdot 10^{-6} Torr$ $(4.6 \cdot 10^{-4}$ Pascal)

$$n_g = \frac{p}{kT} = 1.1 \cdot 10^{17} \frac{1}{m^3}$$

Ionization Cross Section for 80 keV $\sigma_i = 2.1 \cdot 10^{-20} m^2$

Neutralization time

$$\tau_N = \frac{1}{2 n_g \sigma_i \beta c} = 57\,\mu s$$

Ionization cross-section of H_2 by H^- (red, Ref. [1]) and H^+ (blue, Ref [2]) collisions.

Space charge neutralization factor is determined by a ratio of effective beam current to full beam current:

$$\eta = 1 - \frac{I_{eff}}{I_o}$$

[1] Ya.M.Fogel, A.G.Koval, Y.Z.Levchenko, Zh. Eksp. Teor. Fiz., 38, 1053 (1960) [Sov. Phys. JETP 11, 760 (1960)].
[2] M.E.Rudd, Y.-K.Kim, D.H.Madison, J.W.Gallagher, Reviews of Modern Physics, 57, No.4, 965 (1985).

Space charge neutralization dependence on time

$$\eta = 1 - \exp(-\frac{t}{\tau_N})$$

Measured Space Charge Neutralization of H^- Beam within Pulse Length (H_2 Residual Gas with Pressure of P = 3.5 x 10^{-6} Torr)

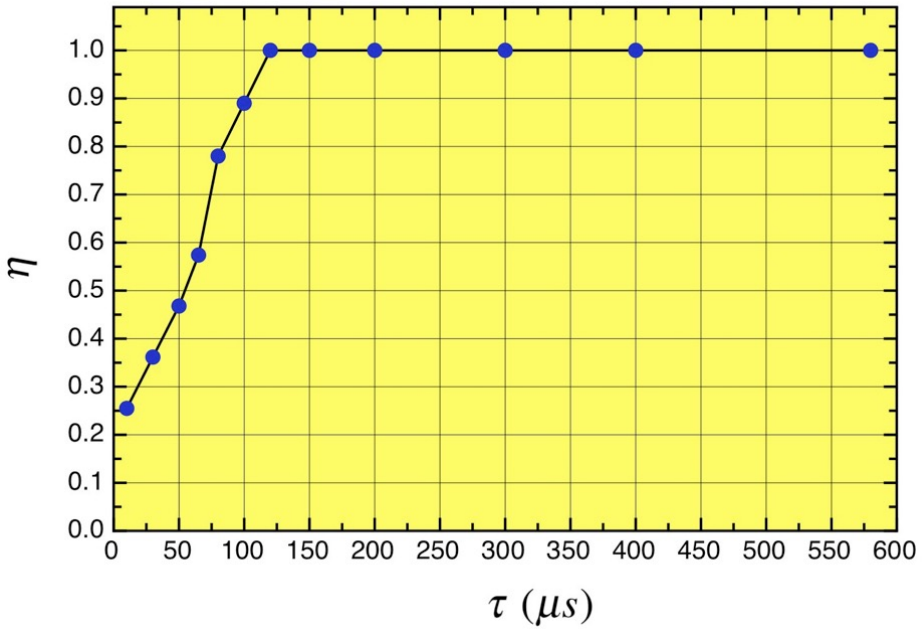

Space charge neutralization of 80 keV H^- beam as a function of beam pulse length.

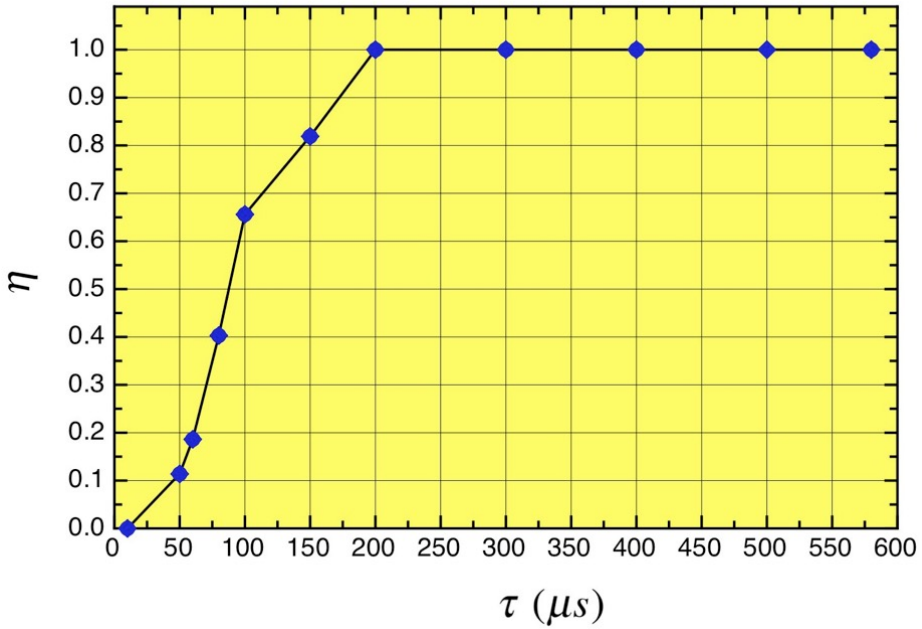

Space charge neutralization of 35 keV H^- beam as a function of beam pulse length.

Effect of Space Charge Neutralization on Beam Parameters

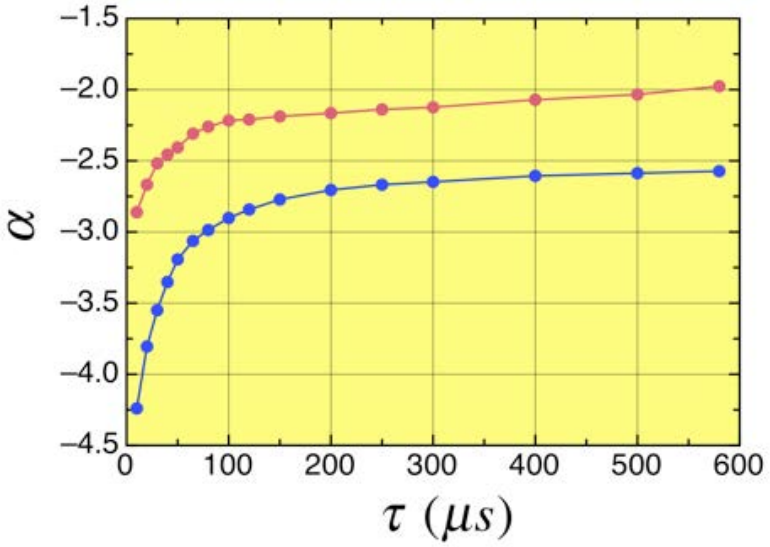

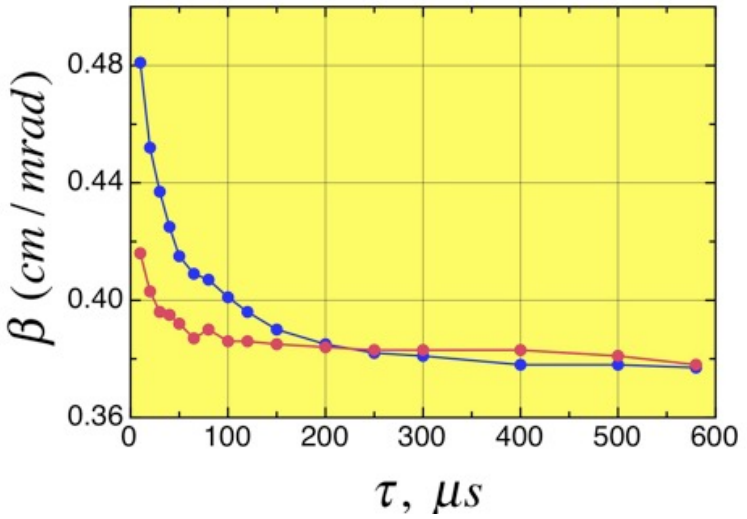

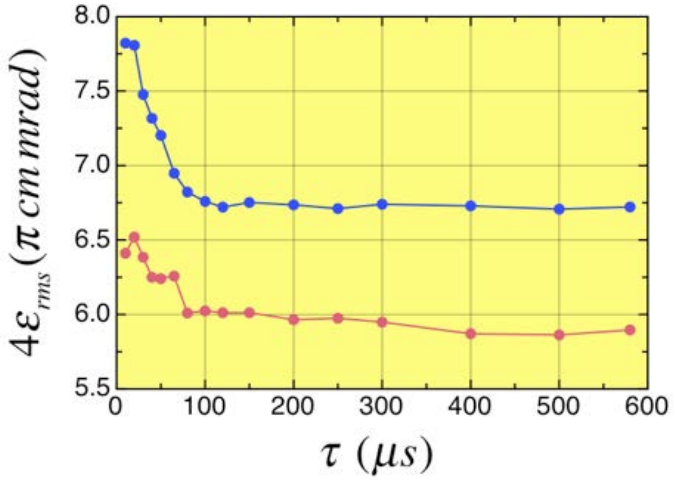

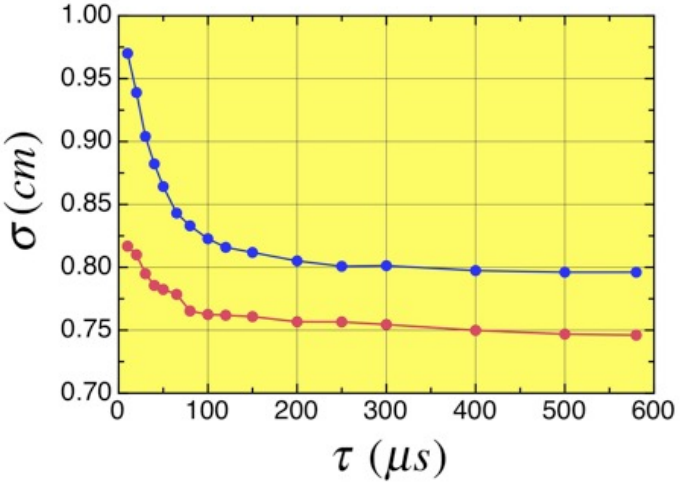

Variation of 80 keV H- beam parameters during pulse length.

Effect of the Beam Space Charge Neutralization in Residual Gas on 750 keV H^- Beam Parameters

(Left)Measured vertical beam emittance at TBEM3 and (right) BEAMPATH simulations at different values of beam pulse length (simulations performed with current I = 15 mA for t = 50-100 ms and with current I = 0 for $\tau \geq 150$ μs.)

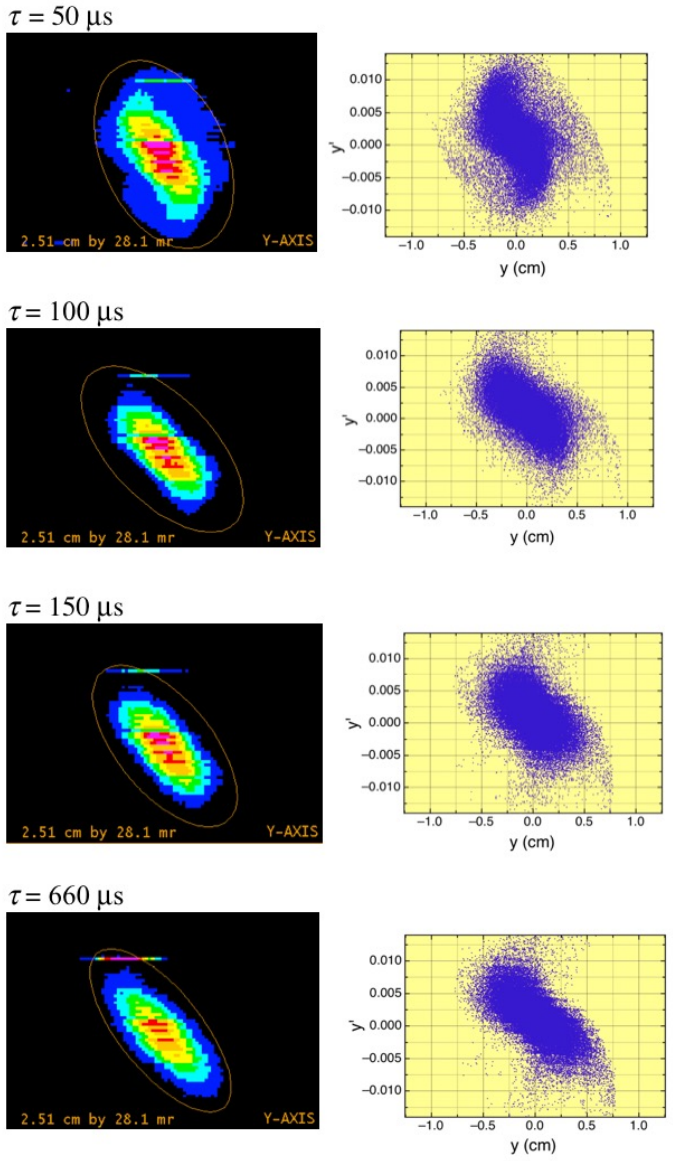

750 keV H- Beam Space Charge Neutralization on Residual Gas

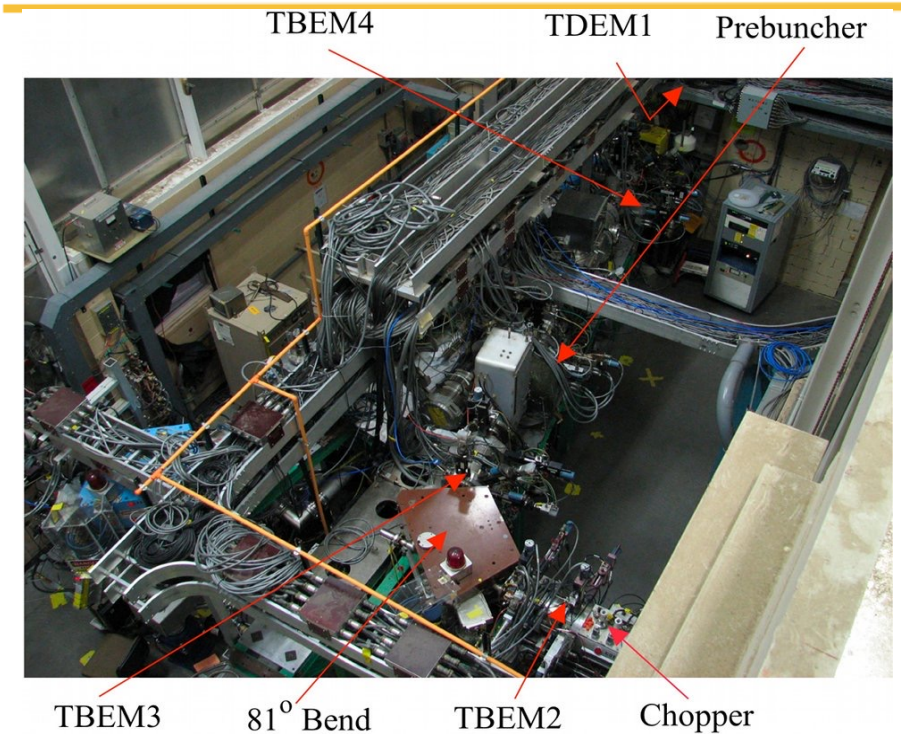

Layout of 750-keV H- Low Energy Beam Transport of LANSCE

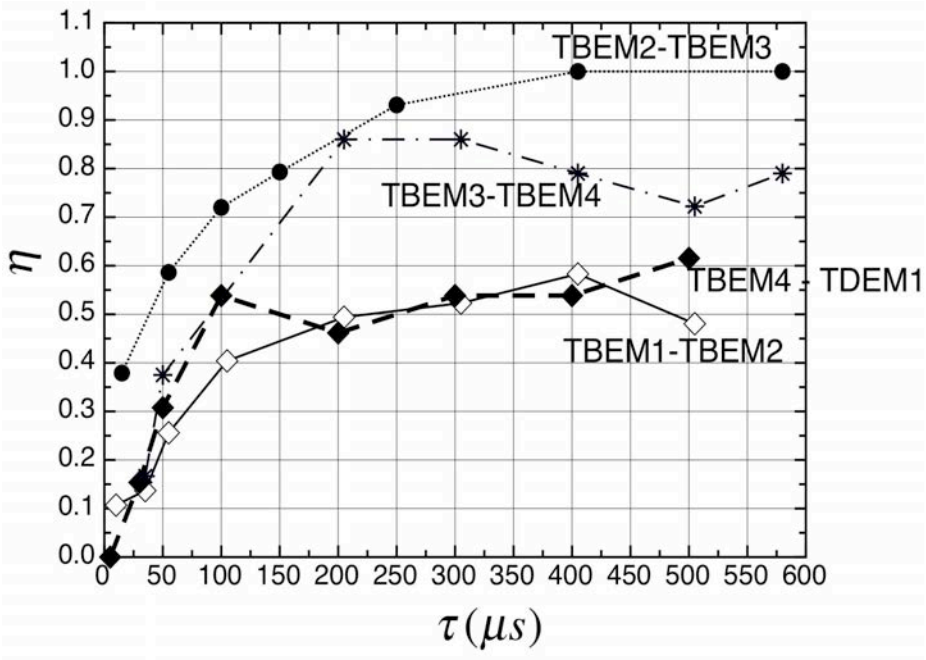

Space charge neutralization of 750 keV H- beam as a function of pulse length along the channel . Layout of 750-keV H- Low Energy Beam Transport of LANSCE.

Low Pressure (Vacuum) Measuring Devices

Tubulated hot-cathode ionization gauge.

Electrons emitted from the filament move several times in back and forth movements around the grid before finally entering the grid. During these movements, some electrons collide with a gaseous molecule to form a pair of an ion and an electron. The number of these ions is proportional to the gaseous molecule density multiplied by the electron current emitted from the filament, and these ions pour into the collector to form an ion current. Since the gaseous molecule density is proportional to the pressure, the pressure is estimated by measuring the ion current.

Important parameter of IGs is sensitivity whch indicate that each gas component contributes to total pressure with certain weight:

$$S = \frac{p_{gauge}}{p_{true}}$$

IG is usually calibrated with sensitivity S=1 for N_2.

Table Gas Sensitivity (T.Anderson, Accelerator Vacuum 101)

Gas	H2	CH4	H2O	CO	N2	C2H6	O2	Ar	C3H6	CO2
Sens	0.46	1.4	1.12	1.05	1.0	2.6	1.01	1.29	3.6	1.4

Residual Gas Analyzer

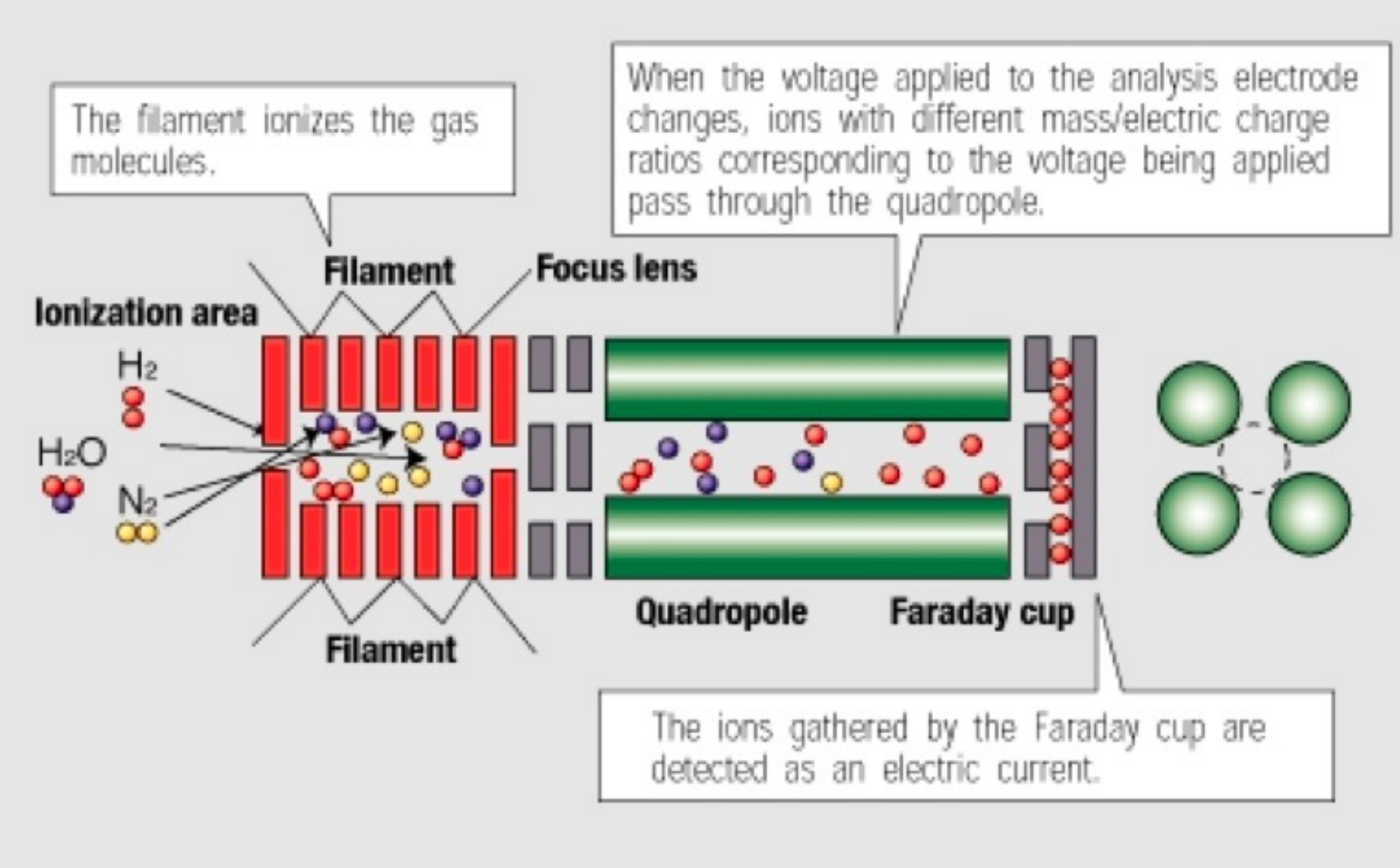

Residual Gas Spectrum

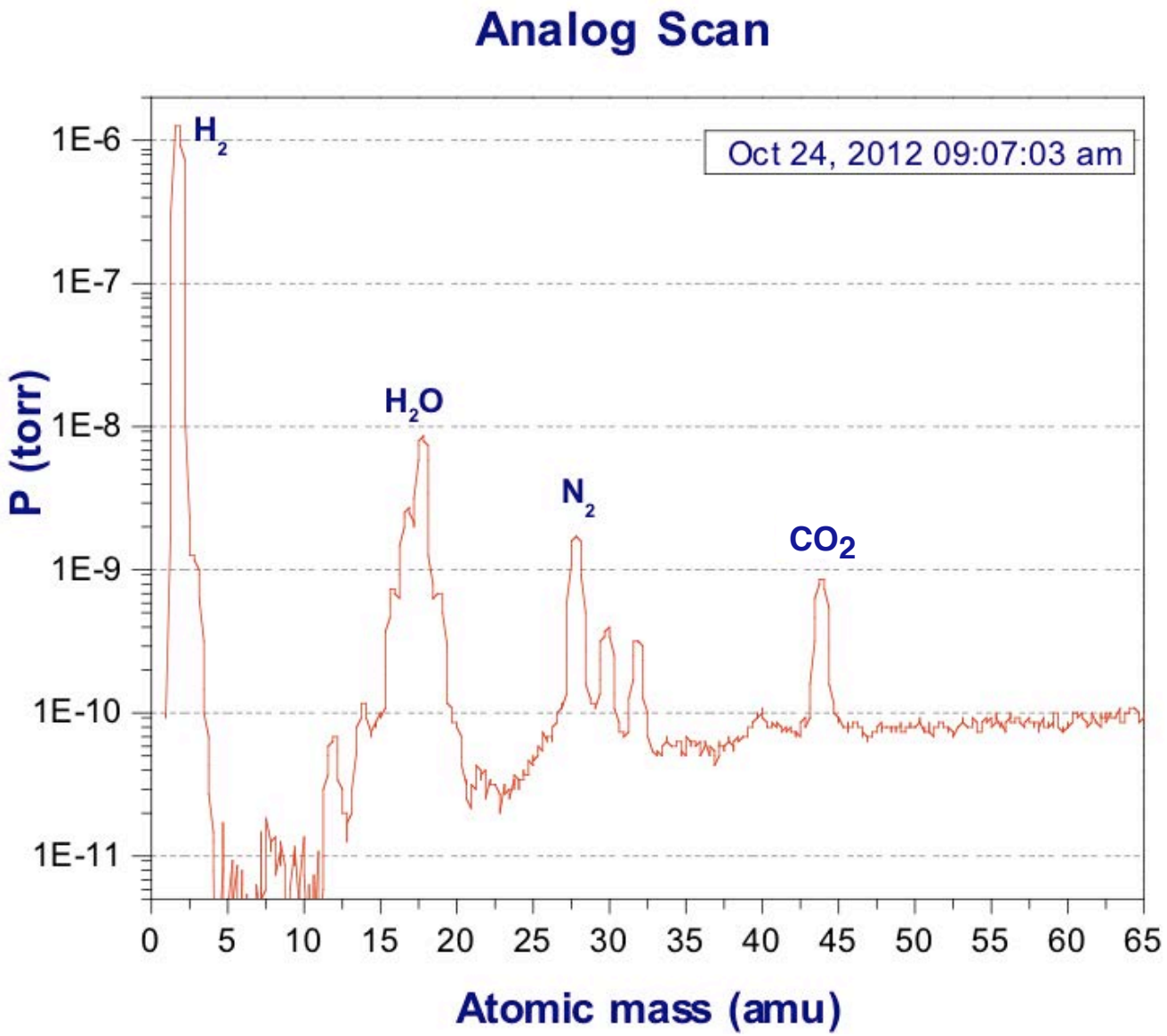

Pressure Units

Pressure units

V·T·E	Pascal	Bar	Technical atmosphere	Standard atmosphere	Torr	Pounds per square inch
	(Pa)	(bar)	(at)	(atm)	(Torr)	(psi)
1 Pa	≡ 1 N/m^2	10^{-5}	1.0197×10^{-5}	9.8692×10^{-6}	7.5006×10^{-3}	1.450377×10^{-4}
1 bar	10^5	≡ 10^6 dyn/cm^2	1.0197	0.98692	750.06	14.50377
1 at	0.980665×10^5	0.980665	≡ 1 kp/cm^2	0.9678411	735.5592	14.22334
1 atm	1.01325×10^5	1.01325	1.0332	≡ p_0	≡ 760	14.69595
1 Torr	133.3224	1.333224×10^{-3}	1.359551×10^{-3}	1.315789×10^{-3}	≈ 1 mm_{Hg}	1.933678×10^{-2}
1 psi	6.8948×10^3	6.8948×10^{-2}	7.03069×10^{-2}	6.8046×10^{-2}	51.71493	≡ 1 lb_f/in^2

Neutralization Time (μs) for 35 keV H^+ Beam in Different Gases

$$\tau_n = \frac{1}{\sigma_i \, n_{gas} \, v}$$

Gas	Ionization Cross Section (10^{-20} m^2)	10^{-5} Torr
H_2	1.67	36
He	0.494	243
Ne	1.09	110.3
N_2	5.0	11.9
O_2	4.41	13.6
Ar	5.11	23.5
Kr	7.24	16.6
Xe	11.9	10.1
CO	5.78	20.8

Improvement of 66 mA 95 keV H^+ SILHI Source Beam Emittance by Heavy Gas Injection in LEBT (Rev. Sci. Instr., 71, 3, p. 1413, 2000)

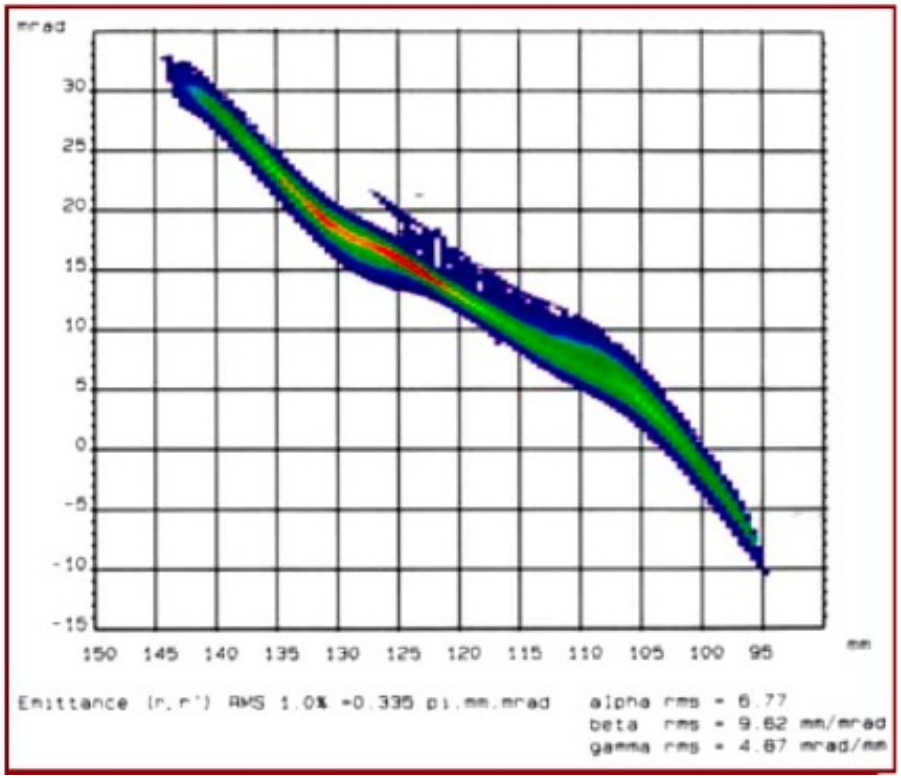

FIG. 2. ε rms norm$=0.33\,\pi$ mm mrad for a 66 mA 95 keV H^+ beam ($P_{\text{real}}=4.3\times10^{-5}$ Torr).

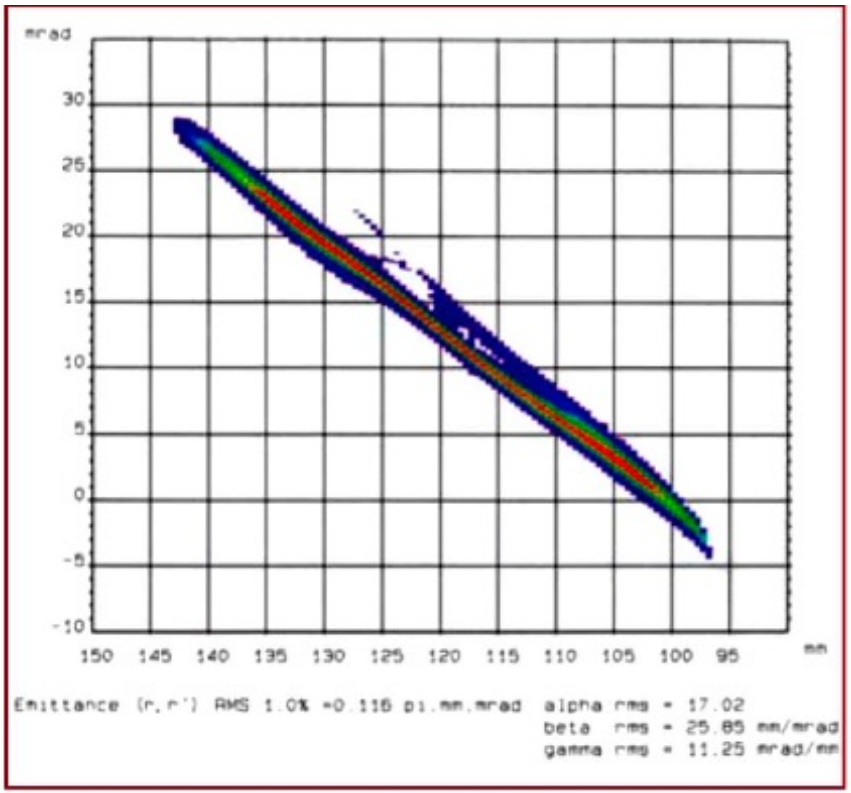

FIG. 3. ε rms norm$=0.11\,\pi$ mm mrad (r,r') for a 66 mA 95 keV H^+ beam with Kr injection ($P_{\text{real}}=5.2\times10^{-5}$ Torr).

Cross Section for Stripping H^- in Different Gases (Atomic Data for Controlled Fusion Research, ORNL-5206)

Single stripping cross-section σ_{-10} of 750 keV H^- in different gases

Gas	Cross section, cm^2
H_2	$7 \cdot 10^{-17}$
He	$5 \cdot 10^{-17}$
N_2	$3 \cdot 10^{-16}$
O_2	$4 \cdot 10^{-16}$

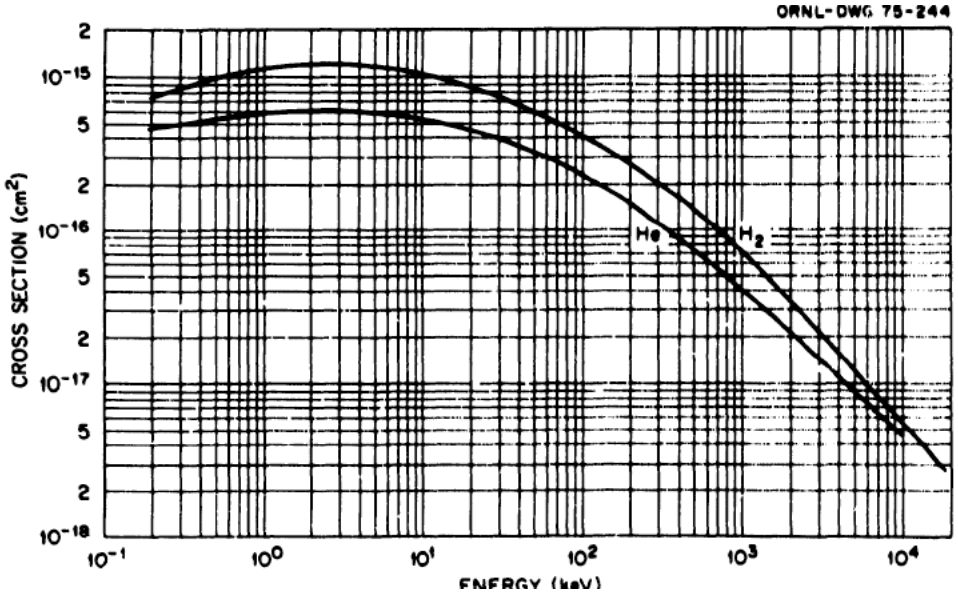

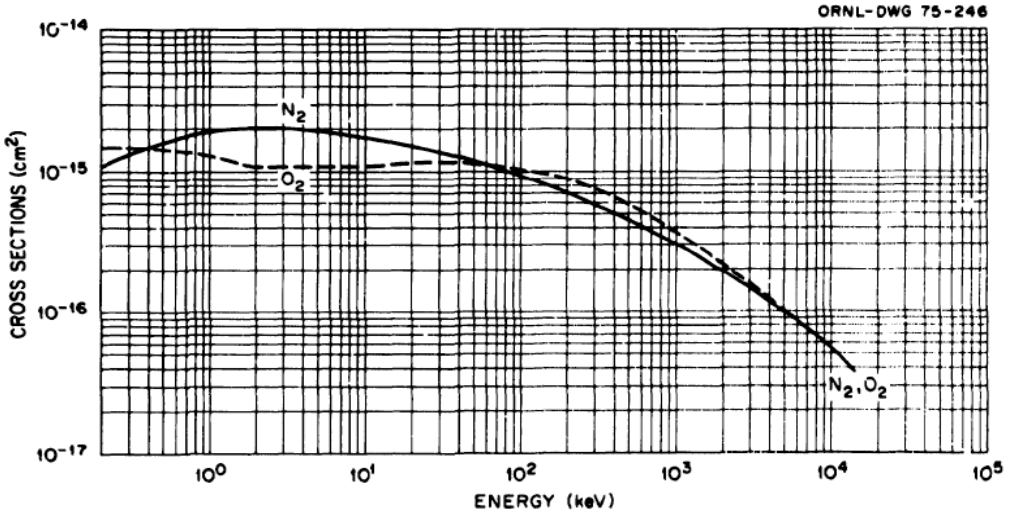

750 keV H^- Beam Performance Under Different Vacuum Conditions

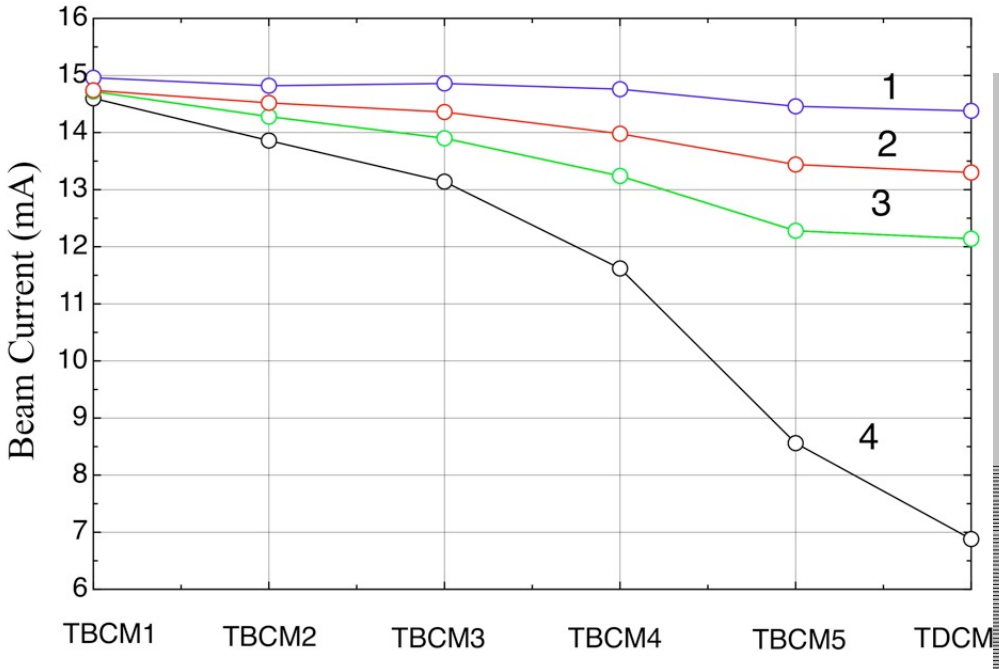

Beam transmission through LEBT as a function of vacuum conditions:
(1)4.6e-07 Torr,
(2)7.4e-06 Torr,
(3)1.3e-05 Torr,
(4)4.9e-05 Torr.

$7 \cdot 10^{-7}$ *Torr*

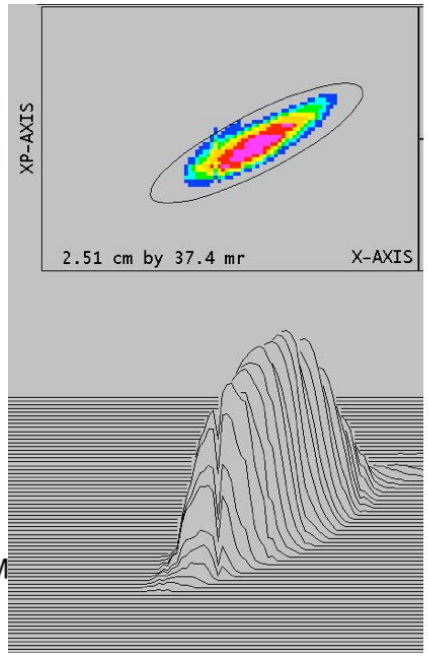

$3 \cdot 10^{-5}$ *Torr*

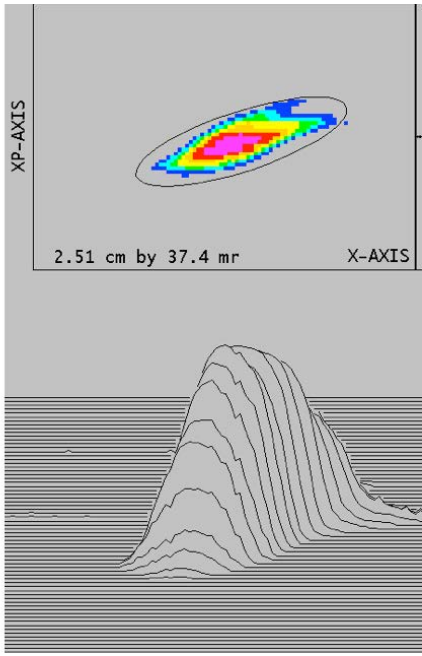

TDEM1 emittance scan with (left) nominal vacuum of 7e-07 Torr and (right) with vacuum of 3e-05 Torr.

Design of Magnetostatic LEBT

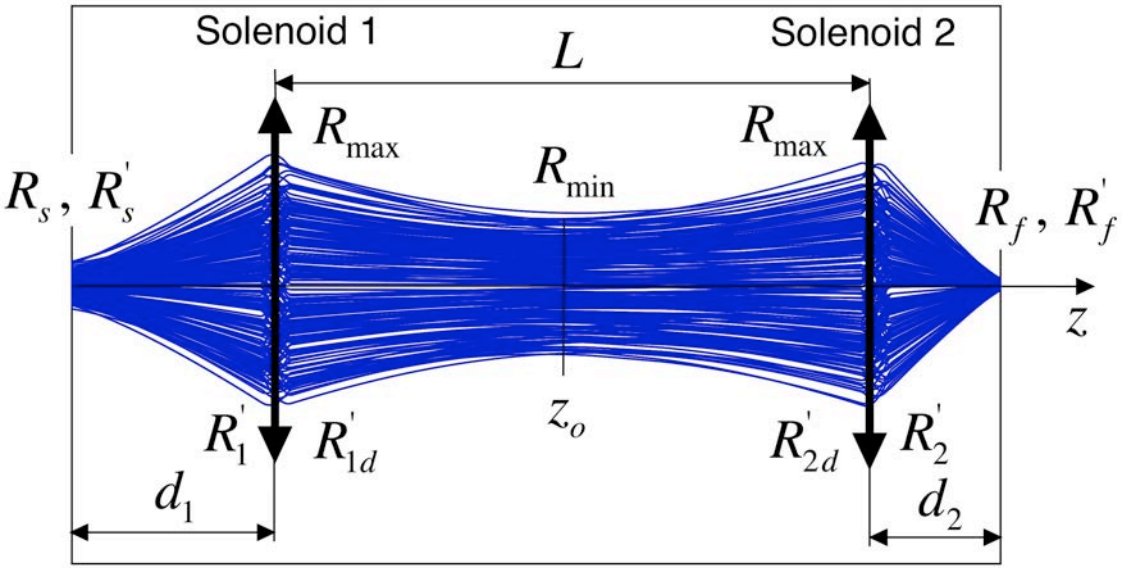

Initial Data:

Beam Current I_o

Space charge neutralization factor η

Effective beam current $I = I_o(1-\eta)$

Unnormalized beam emittance ε

Initial envelope parameters R_s, R_s'

Final envelope parameters R_f, R_f'

Distance between solenoids L

To Be Determined:

Solenoid Geometry and Fields

Distances d_1, d_2

Y.B. et al, NIM-A 753 (2014) 1-8

Minimization of Beam Size in LEBT

Consider beam with negligible current, but with finite value of beam emittance (emittance-dominated beam). Evolution of beam radius R along drift space z between solenoids as a function of initial radius R_o and slope of the envelope R_o' is given by integration of envelope equation assuming $I = 0$:

$$\frac{R}{R_o} = \sqrt{(1 + \frac{R_o'}{R_o} z)^2 + (\frac{\text{э}}{R_o^2})^2 z^2} \tag{5.1}$$

From the symmetry point of view it is clear, that matched beam has a minimum size, or waist, $R_{min} = R_o$ in the middle point of the drift space between lenses, and maximum size R_{max} inside focusing elements. At the waist point, $R_o' = 0$. Therefore from Eq. (5.1)

$$R_{\max}^2 = R_{\min}^2 + (\frac{\text{э}L}{2R_{\min}})^2 \tag{5.2}$$

Equation $\partial R_{\max} / \partial R_{\min} = 0$ determines minimal value of R_{max} as a function of beam emittance and distance between lenses

$$\frac{\partial R_{\max}}{\partial R_{\min}} = \frac{1}{\sqrt{R_{\min}^2 + (\frac{\text{э}L}{2R_{\min}})^2}} [R_{\min} - \frac{1}{R_{\min}^3} (\frac{\text{э}L}{2})^2] = 0 \tag{5.3}$$

Minimization of Beam Size in LEBT (Con.)

Solution of Eq. (5.3) is

$$R_{\min}(0) = \sqrt{\frac{\text{ə}L}{2}} \qquad R_{\max}(0) = \sqrt{\text{ə}L} \tag{5.4}$$

which coincides with periodic solution of matched beam with zero current at phase advance of $\mu_o \approx \pi/2$. Eq. (5.4) determines the minimum value of R_{max} at given value of beam emittance and given distance between solenoids L.

Consider now space-charge dominated regime, where beam emittance is negligible. Analysis of beam dynamics in drift space determines the condition for transporting beam with maximum current through drift space restricted by aperture R_{max} and distance L:

$$R_{\max} = \frac{L}{1.082}\sqrt{\frac{I}{I_c(\beta\gamma)^3}}\ , \qquad R_{\min} = \frac{R_{\max}}{2.35} \tag{5.5}$$

In more general case, when both beam emittance and beam current are not negligible, precise value of R_{max} is determined by variation of the value of R_{min} at the middle point between solenoids, $z = z_{o,}$ and searching for the smallest value of the beam size at the center of solenoids R_{max} via an exact solution of the envelope equation in drift space between solenoids.

Determination of Lens Parameters and Distances d_1, d_2

After determination of the minimal value of R_{max}, the distances d_1, d_2 are defined by integration of envelope equation in drift space

$$\frac{d^2R}{dz^2} - \frac{э^2}{R^3} - \frac{P^2}{R} = 0$$

to establish points where the beam radius evolves from initial value of R_o to R_{max} :

$$z = \frac{R_o^2}{2\,э}\int_1^{(\frac{R_{\max}}{R_o})^2} \frac{ds}{\sqrt{[1+(\frac{R_o R_o^{'}}{э})^2]s + (\frac{PR_o}{э})^2 s\ln s - 1}} . \qquad (5.7)$$

In Eq. (5.7), the values of R_o, $R_o^{'}$ correspond to either R_s, $R_s^{'}$ or R_f, $R_f^{'}$. Envelope equation has the first integral:

$$(\frac{dR}{dz})^2 = (\frac{dR}{dz})_o^2 + (\frac{э}{R_o})^2(1-\frac{R_o^2}{R^2}) + P^2\ln(\frac{R}{R_o})^2$$

which determines divergence of the beam as a function of initial beam parameters, beam current, and beam emittance. Slopes of beam envelopes at solenoids $R_1^{'}$, $R_2^{'}$ can be found from the first integral of envelope equation in drift space:

$$R^{'} = \sqrt{(R_o^{'})^2 + (\frac{э}{R_o})^2[1-(\frac{R_o}{R})^2] + \frac{2I}{I_c(\beta\gamma)^3}\ln(\frac{R}{R_o})^2} . \qquad (5.8)$$

Determination of Lens Parameters and Distances d_1, d_2

The values of R'_{1d}, R'_{2d} are determined by the first integral assuming $R_o = R_{\min}$, $R'_o = 0$. Then, focal lengths of solenoids f_1, f_2, are determined by the total change in the slope of the beam at each solenoid:

$$f_1 = \frac{R_{\max}}{\left|R'_{1d}\right| + \left|R'_1\right|}, \qquad f_2 = \frac{R_{\max}}{\left|R'_{2d}\right| + \left|R'_2\right|}. \tag{5.9}$$

After that, the magnetic field within each solenoid is determined from thin lens approximation as

$$B_o = \frac{2mc\beta\gamma}{q\sqrt{f\,D}}. \tag{5.10}$$

Minimization of Emittance Growth in Lens due to Spherical Aberrations

The emittance growth due to spherical aberrations is estimated as:

$$\frac{э}{э_o} = \sqrt{1 + K\left(\frac{C_\alpha R^4}{f\, э_o}\right)^2}$$

where the coefficient K = 0.05…0.5 depends on the beam distribution. Let us restrict the emittance growth due to spherical aberrations to a value of 10%. Assuming that the beam has a waterbag distribution (K = 0.114), the spherical aberration coefficient C_α is restricted to be

$$\frac{C_\alpha R^4}{f\, э_o} < 1.35 \quad \text{or} \quad C_\alpha < 1.35\,\frac{f\, э_o}{R^4}$$

The field distribution within a solenoid is well approximated as $B(z) = \dfrac{B_o}{1 + \left(\frac{z}{d}\right)^4}$

where B_o is the maximum field in solenoid, and d is the filed profile characteristic length. The spherical aberration coefficient C_α can be expressed in terms of a characteristic parameter d as $C_\alpha = \dfrac{5}{12 d^2}$.

Then, the characteristic length of field distribution, d, has to be larger than

$$d > \sqrt{\frac{5}{12 C_\alpha}}$$

Example of Solenoid Design

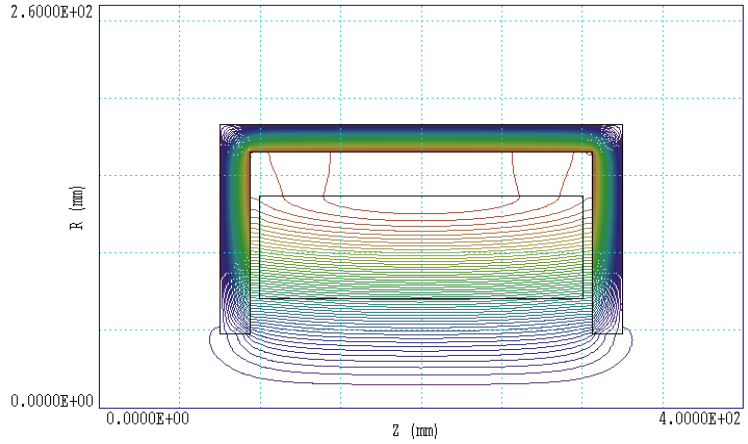

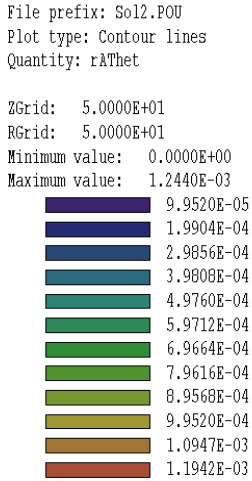

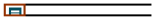

Physical length	25 cm,
Effective length *D*	17.63 cm,
Aperture radius	5.4 cm,
Coil current density	3.1 Amps/mm^2
Maximum current density required for cooling	10 Amps/mm^2

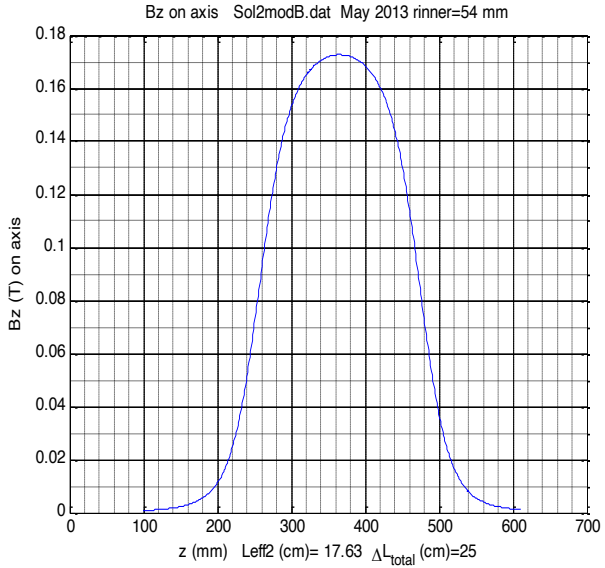

Solenoid and axial field distribution.

Separation of Beam Components in LEBT

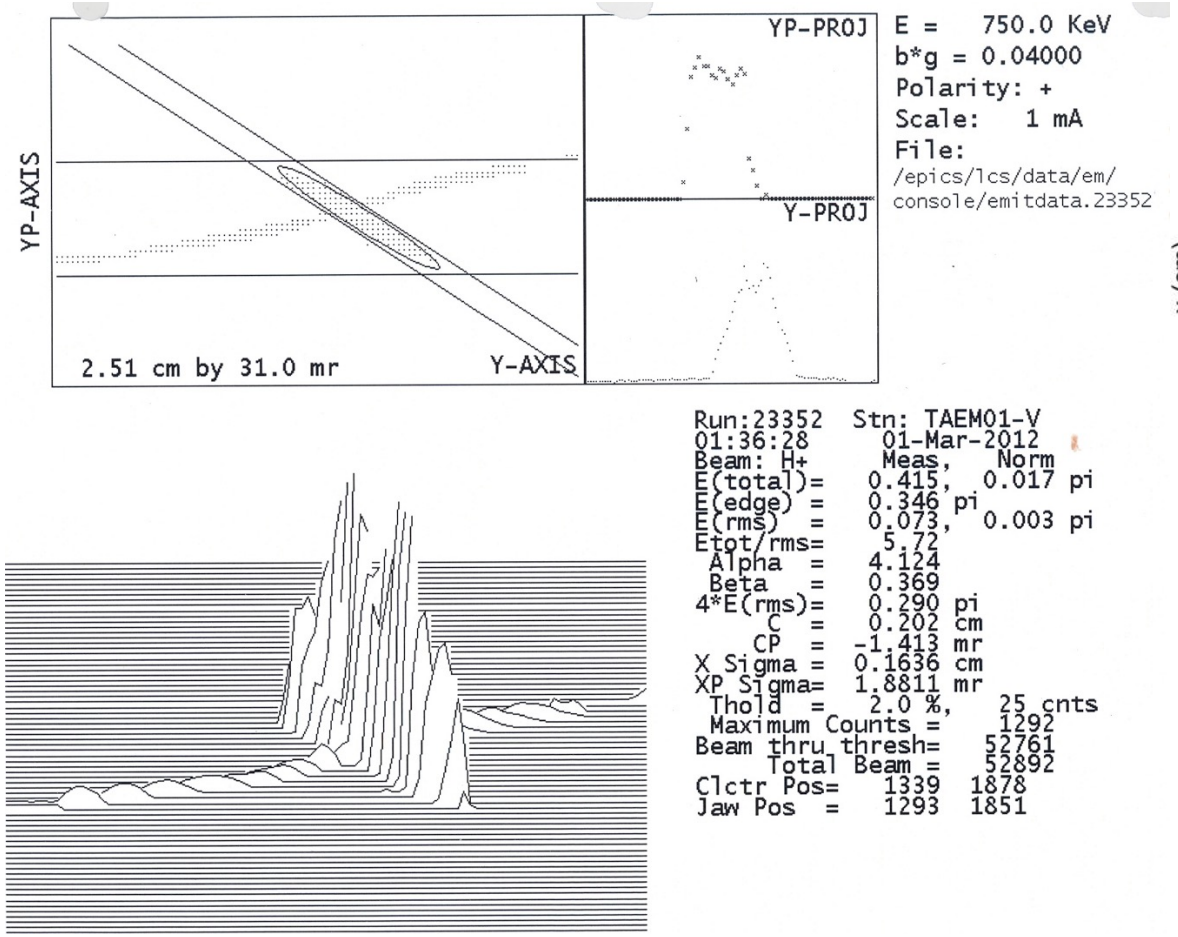

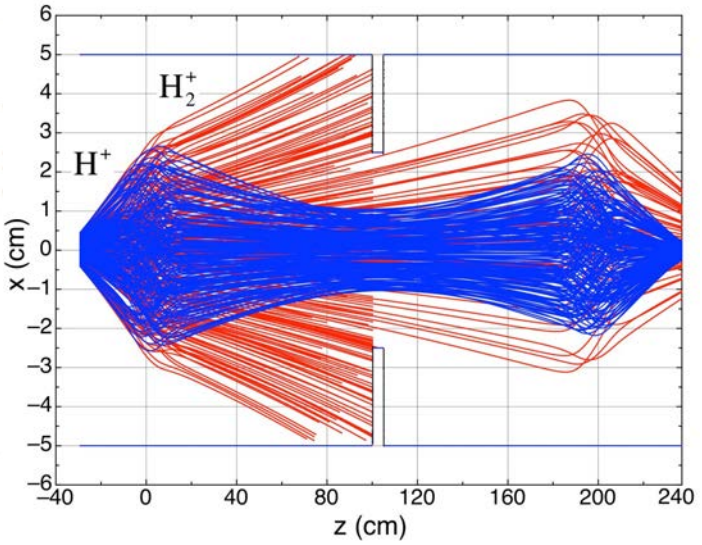

Dynamics of 2- component beam in LEBT with collimator

Measured H^+ transverse phase space at 750 keV for the LANSCE duoplasmatron source. H_2^+ beam is also observed. Beam current is 15.9 mA. Ratio of $\varepsilon_{total} / \varepsilon_{rms} = 5.7$. Straight lines are used to restrict phase space area where beam emittance is determined.

Bending Magnet for Removing Electrons from H- Beam

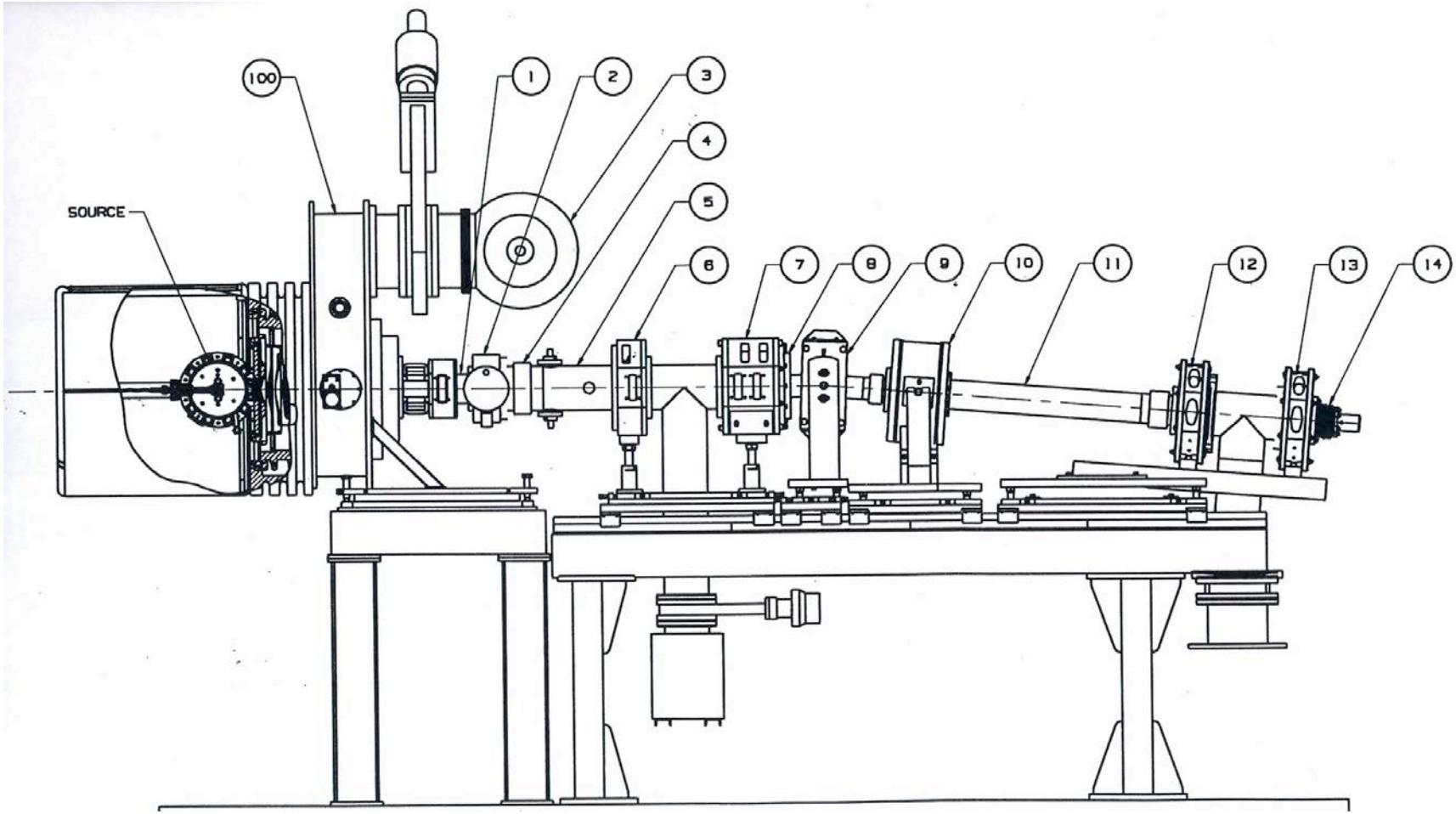

The separation angle between two beam components after a dipole bending magnet with bending angle, *a,* is given by:

$$\Delta\alpha = \alpha(1 - \frac{q_1}{q_2}\frac{p_2}{p_1})$$

Wien Filter

In a Wien filter, a crossing *E x B* field is used to separate the beams. The primary beam is not deflected because of the balance between the electric and magnetic Lorentz force:

$$\int \vec{F}_{defl} dz = q \int (\vec{E} + \vec{v} \times \vec{B}) dz = 0 \qquad (32)$$

The fields in the Wien filter are selected to cancel out for the primary, desired beam but act as a filter for other beam components, where the conditions of Eq. (32) are not met. The separation angle between 2 components after a Wien filter with field $E_{Wien} = \beta_1 c B_{Wien}$ is

$$\Delta\alpha = \frac{E_{Wien} L_{Wien} q_2}{m_2 \gamma_2 (\beta_2 c)^2} \left(1 - \frac{\beta_1}{\beta_2}\right) \quad . \qquad (33)$$

Wien Filter

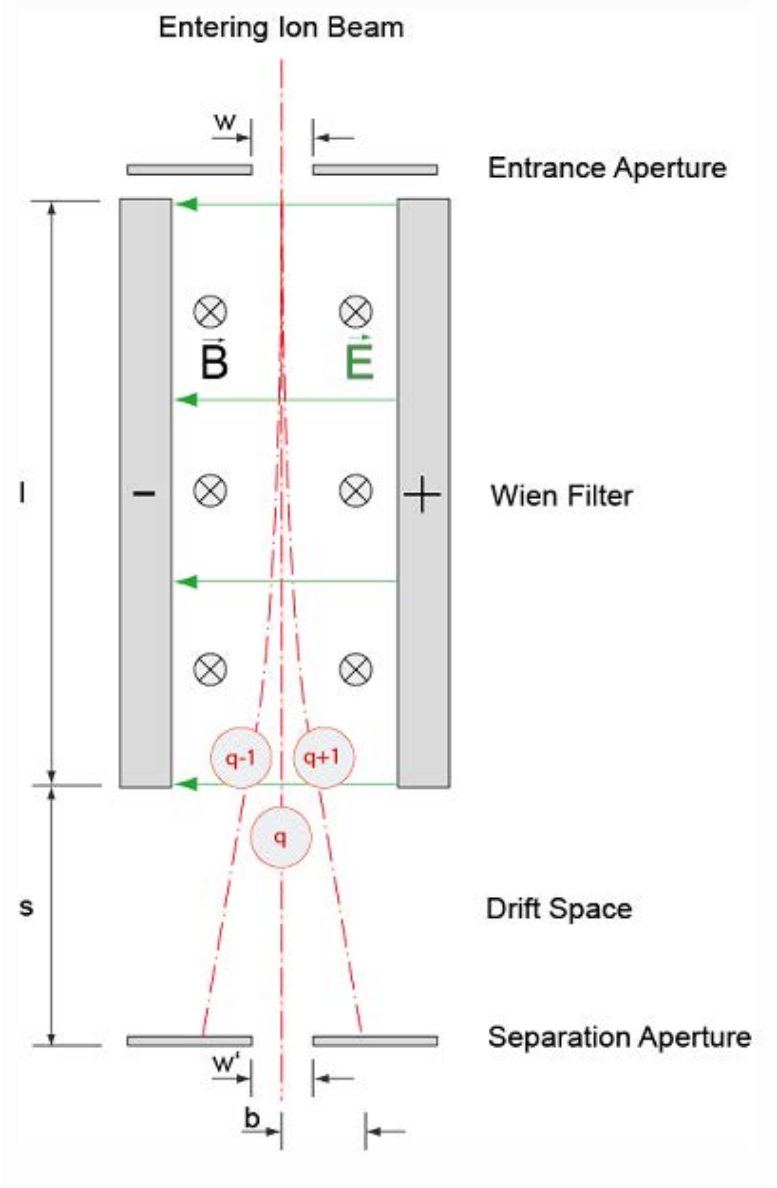
Entering Ion Beam
w
Entrance Aperture
B
E
l
−
+
Wien Filter
q-1
q+1
q
s
Drift Space
Separation Aperture
w'
b

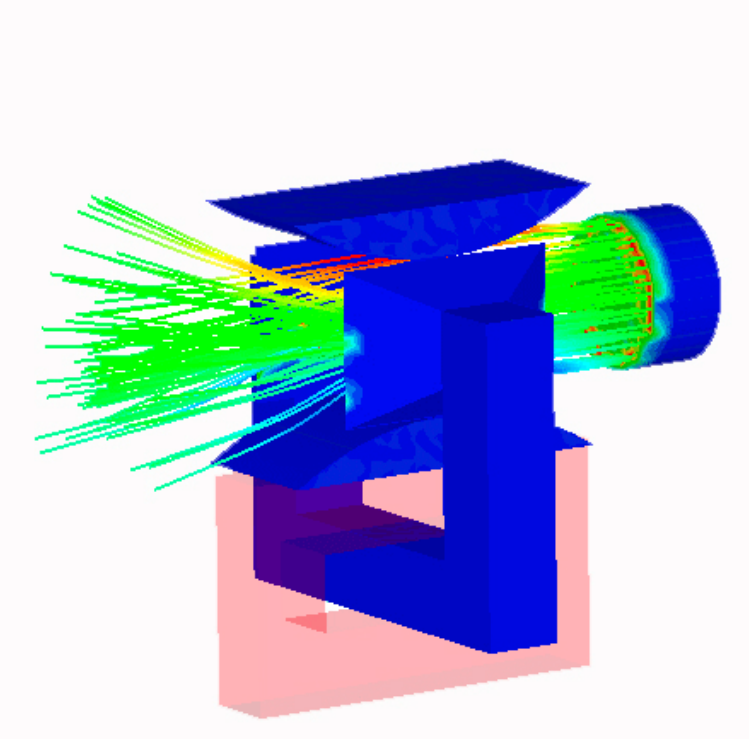

Mismatch Effect in Wien Filter

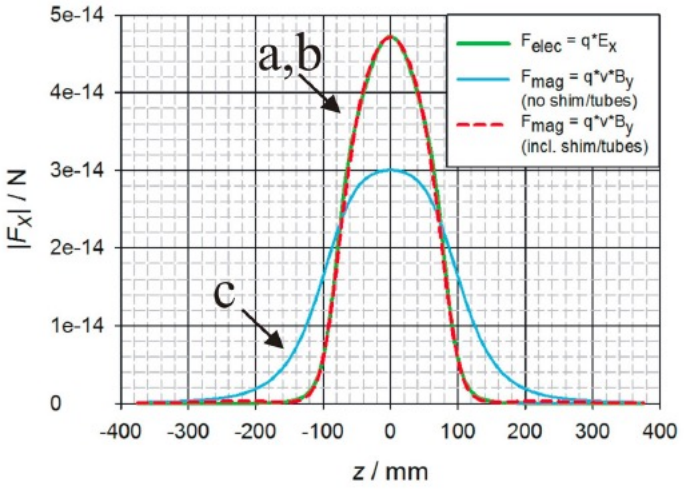

Figure 4: Calculated deflecting forces for on-axis particles (Curve a,b: matched case, c: without shimming).

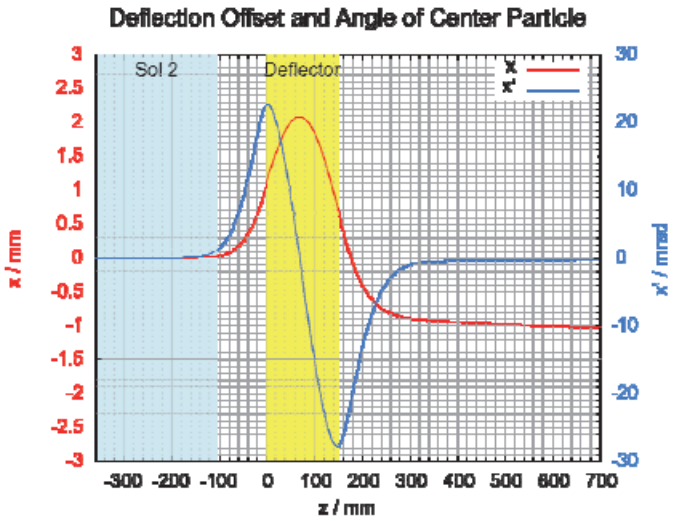

Figure 2: Horizontal movement of the center particle along the chopper axis z for the locally mismatched case.

The beam can pass the chopper without deflection, if the Wien condition is satisfied along the system:

$$\int \vec{F}_{defl}\, dz = \int q \cdot (\vec{E} + \vec{v}_p \times \vec{B})\, dz = 0 \quad (1)$$

But a local mismatch between both fields can still lead to a transverse offset. This effect will be minimized by installing shims and shorting tubes at the dipole while the electric deflector will utilize curved plates and shims. The calculated deflecting forces for on-axis particles travelling in longitudinal direction are presented in Fig. 4. Electric and magnetic fields were computed using CST EMS [6].

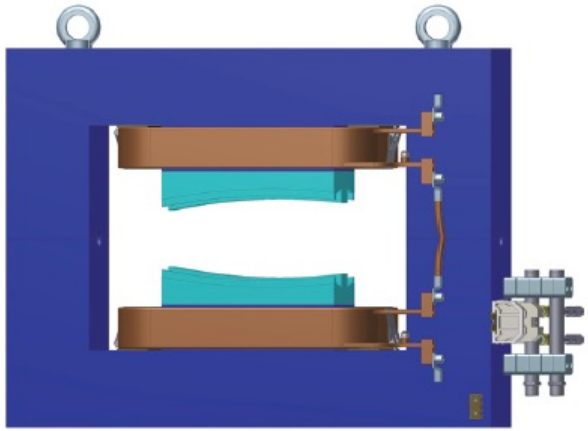

Figure 7: Drawing of chopper dipole with tilted and curved poles.

Beam Chopping

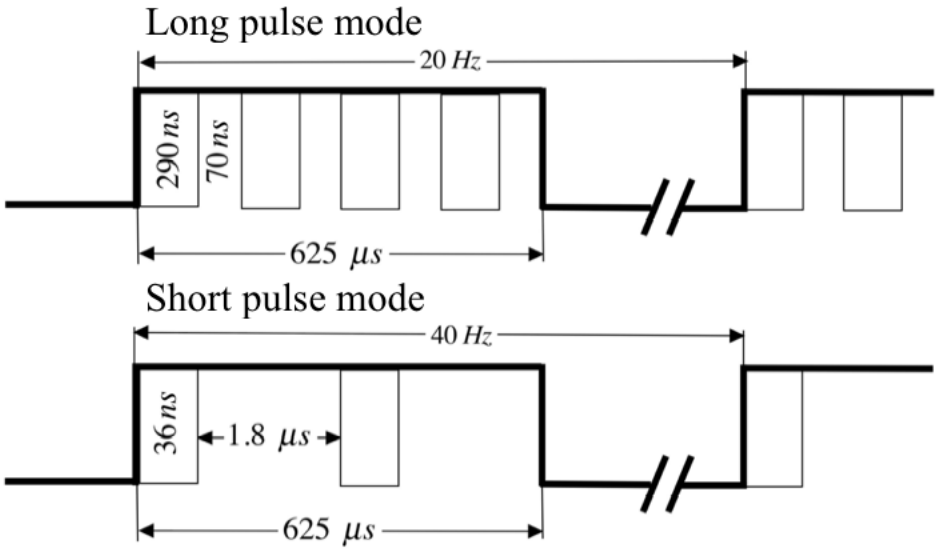

Pulse structure of LANSCE beam

$$I = \frac{Q}{T}$$

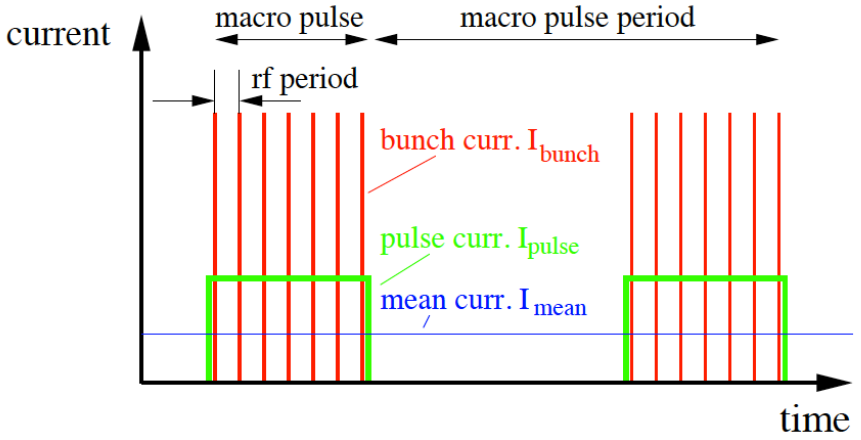

Time structure of different currents in LINAC (P.Forck, 2011)

LANSCE slow wave transmission line chopper

Injection of Long Pulse into Proton Storage Ring

PSR Layout

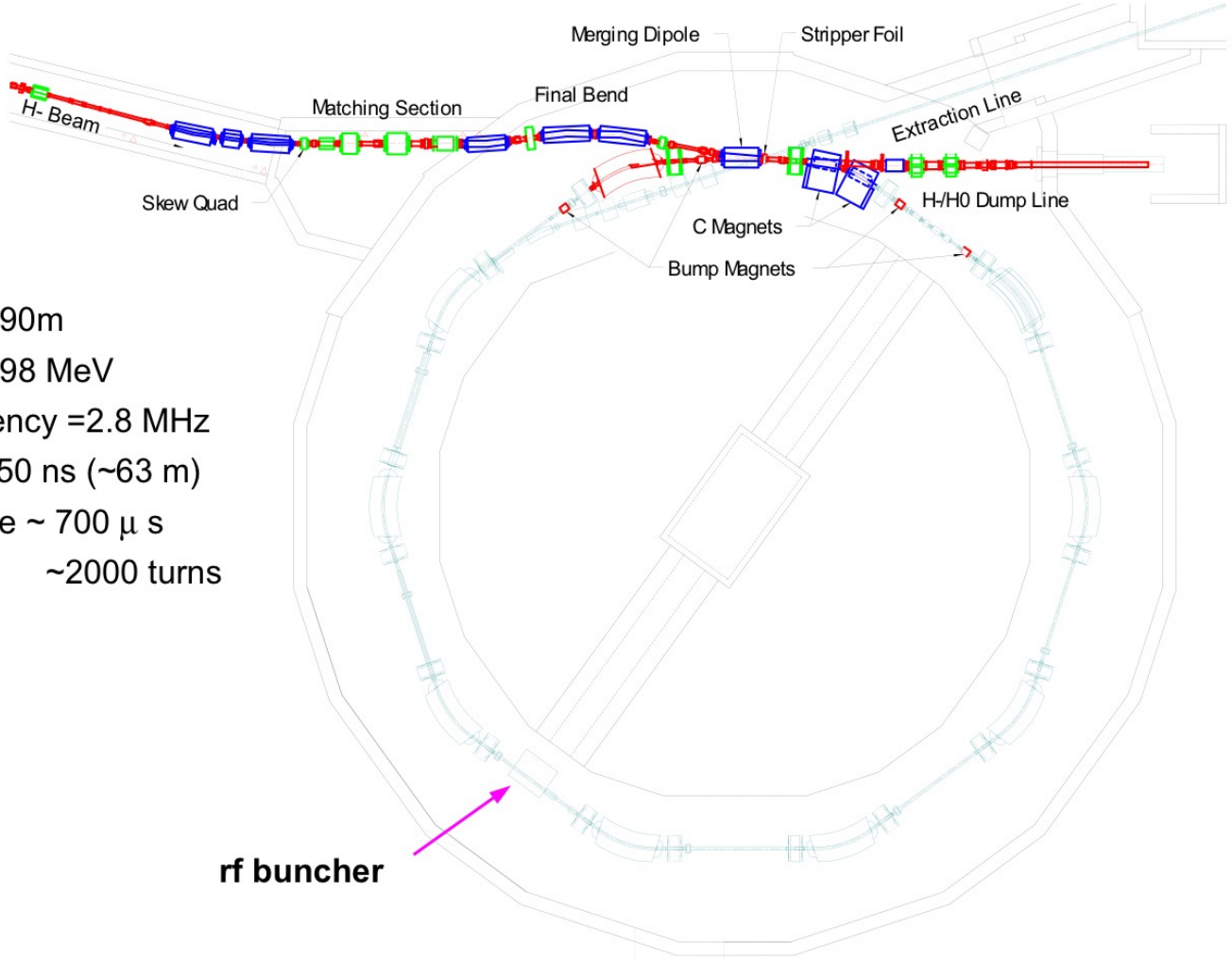

Circumference = 90m

Beam energy = 798 MeV

Revolution frequency =2.8 MHz

Bunch length ~ 250 ns (~63 m)

Accumulation time ~ 700 μ s

~2000 turns

Chopper pulse

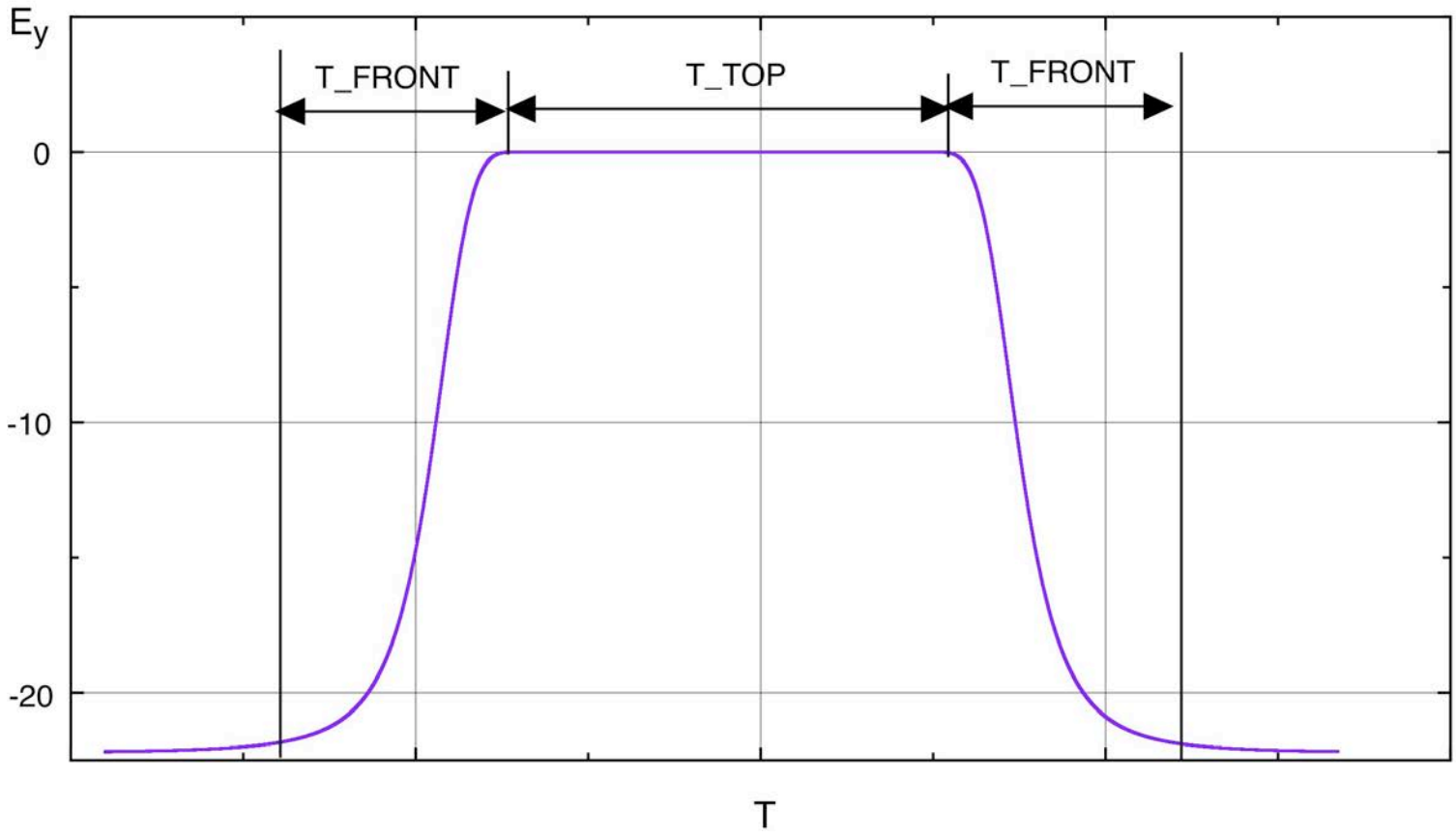

Short pulse beam

T_top = 20 ns
T_front = 10 ns

Long pulse beam

T_top = 280 ns
T_front = 10 ns

Increase of Beam Emittance due to Beam Chopping

1

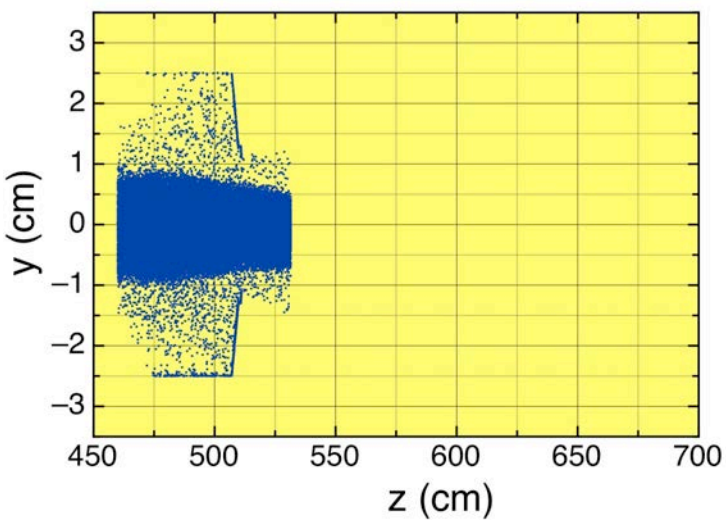

3

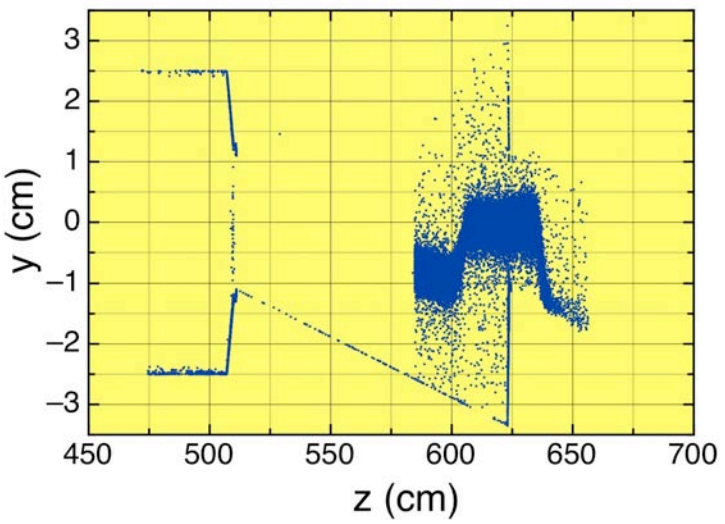

2

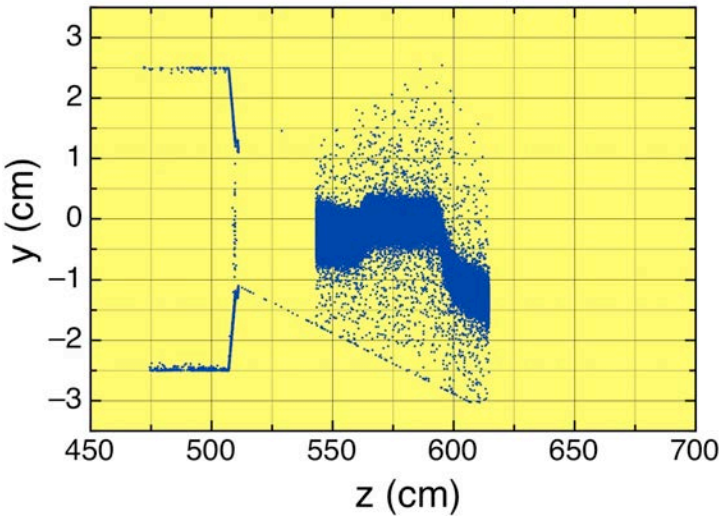

4

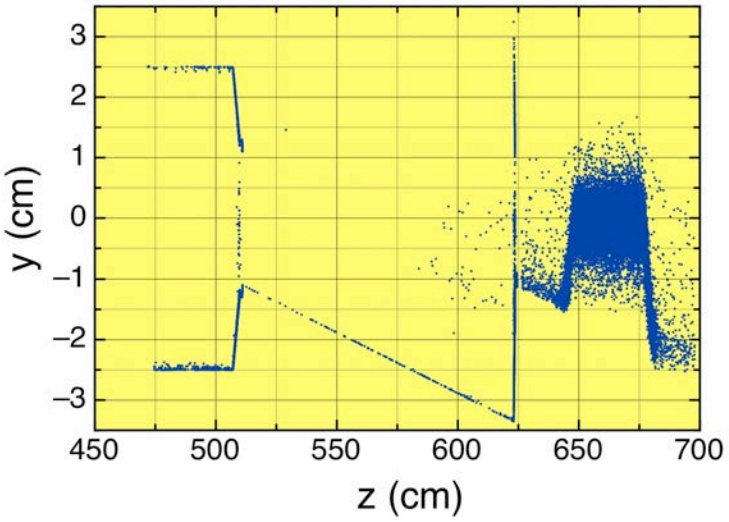

Effect of SNS Chopper on Beam Emittance

Transverse Emittance and Chopping

LEBT Chopper	RMS Horizontal, norm. mm*mrad	RMS Vertical, norm mm*mrad
On	0.40	0.22
Off	0.29	0.19

MEBT Horizontal Emittance (scales are the same)

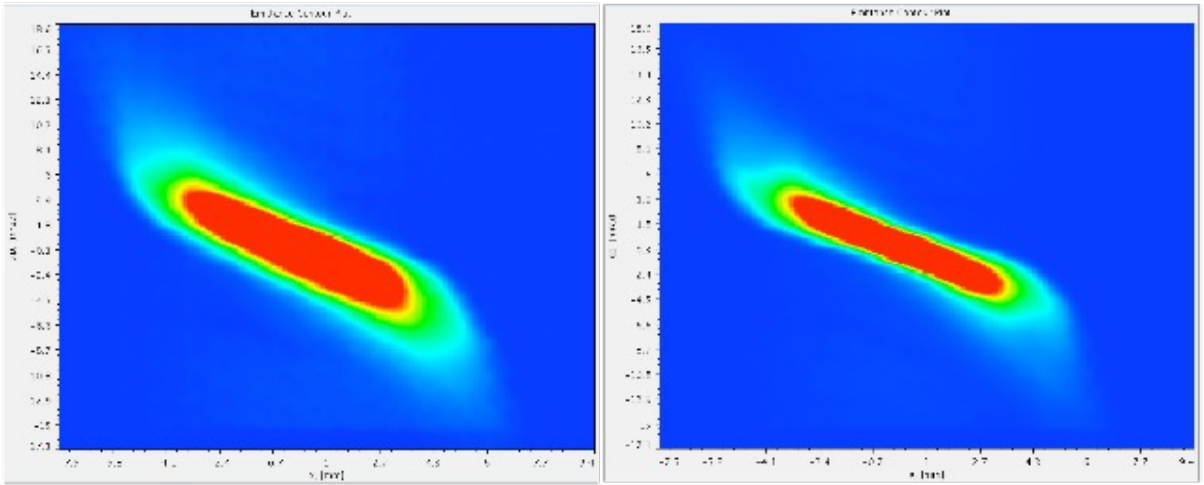

A.Shishlo (PAC2011).

Different Chopping Options for LEBT (C.Plostinar, ESS/AD/0022)

Table 1. LEBT and MEBT chopper parameters at CERN, J-PARC, RAL and SNS.

	CERN		J-PARC		SNS		RAL
Chopper Location	LEBT	MEBT	LEBT	MEBT	LEBT	MEBT	MEBT Only
Deflector Type	Electro-static	Electro-static	Induction Cavity	RF Cavity	Electro-static	Electro-static	Electro-static
Deflector Type Details	Deflecting plate	Meander Stripline	Beam Transformer	TE11 Mode	Einzel Lens	Meander Stripline	Stripline with Coaxial/ Stripline Delay
Beam Energy	45 keV	3 MeV	~50 keV	3 MeV	65 keV	2.5 MeV	3 MeV
Beam Pulse Length	0.4 ms		0.5 ms		1 ms		2 ms
Repetition Rate	50 Hz		25 Hz		60 Hz		50 Hz
Bunch Frequency	-	352.2 MHz	-	324 MHz	-	402.5 MHz	324 MHz
Rise Time	2 µs	2 ns	<50 ns	10 ns	<50 ns	10 ns	2 ns
Bunch by bunch chopping	-	Yes	-	No	-	No	Yes
Deflector Length	10 cm	2*40 cm	10 cm	17.2 cm	2.7 cm	2* 35 cm	2* 45 cm
Deflecting Voltage/Field	< 20 kV	+/- 600 V	+/-2.5 kV	1.6 MV/m	+/- 3 kV	2.5 kV	+/- 1.5 kV

As mentioned above, because of the rise and fall times of the chopper voltage in the LEBT (tens of ns), the beam will contain partially chopped bunches. These bunches have a trajectory which is to some extent rather uncertain and are likely to be lost along the linac. To mitigate this effect, CERN, J-PARC and SNS combine the “slow” chopper in the LEBT with a fast MEBT chopper.

A Two Stage Fast Beam Chopper For Next Generation High Power Proton Drivers (Michael A. Clarke-Gayther, STFC RAL, Didcot UK)

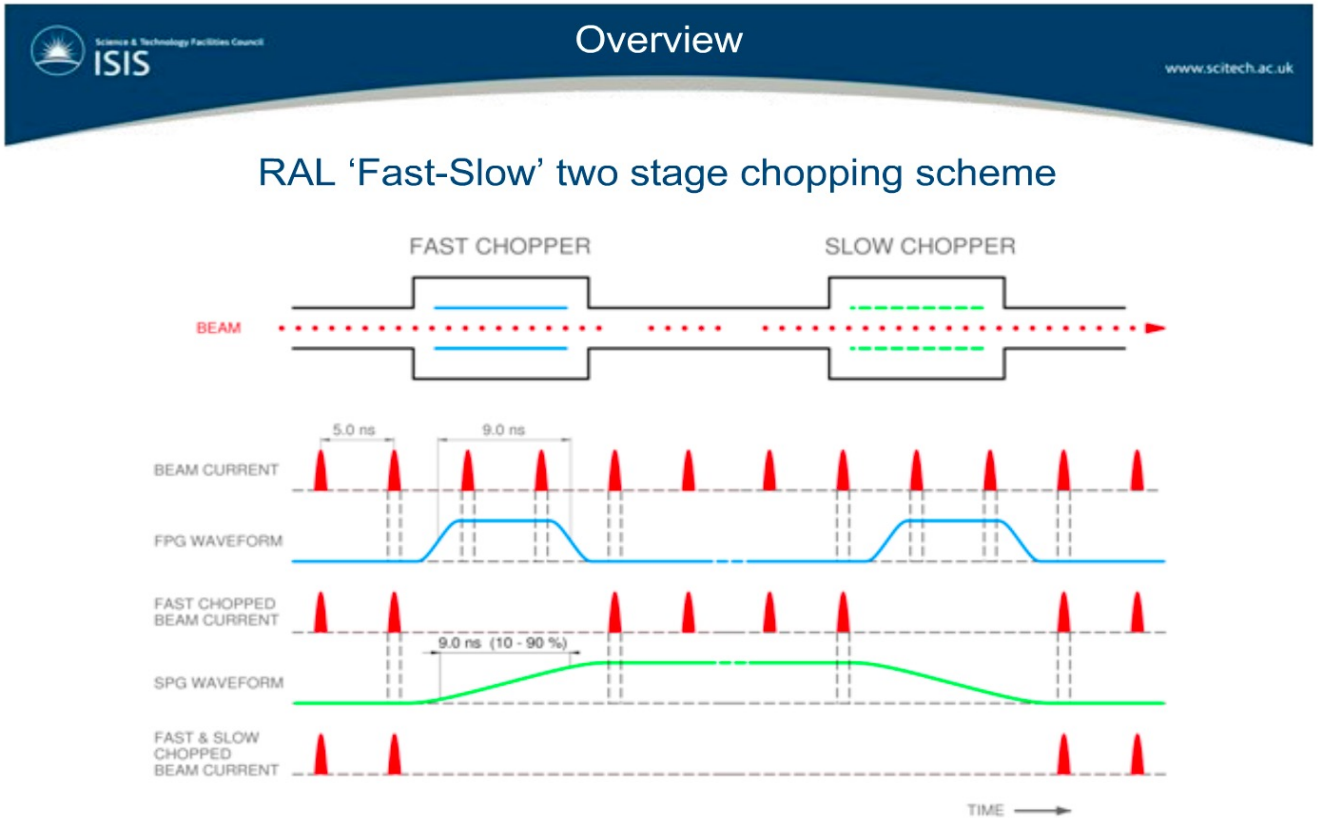

The upstream field is generated by a pair of AC coupled 'fast' transition time pulse generators (FPG) that output high voltage, dual polarity pulses into a 'slow-wave' transmission line electrode structure [2], where partial chopping of beam bunches is avoided by ensuring that the deflecting E-field propagates at the beam velocity. The

A Two Stage Fast Beam Chopper For Next Generation High Power Proton Drivers (Michael A. Clarke-Gayther, STFC RAL, Didcot UK)

ISIS Science & Technology Facilities Council

Overview

www.scitech.ac.uk

3.0 MeV MEBT Chopper (RAL FETS Scheme A)

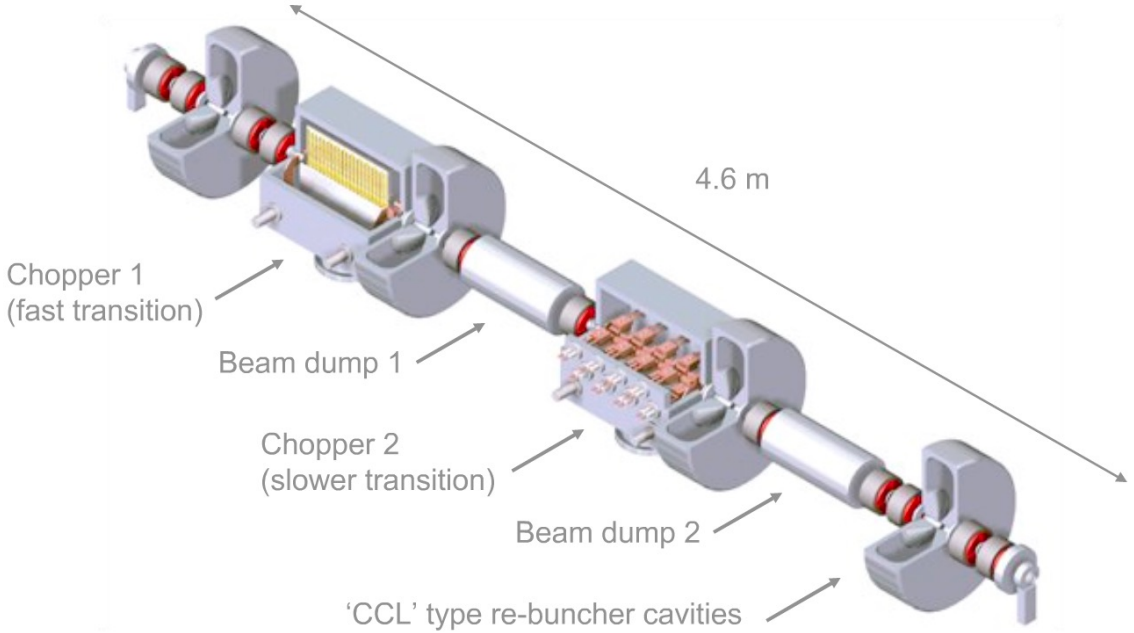

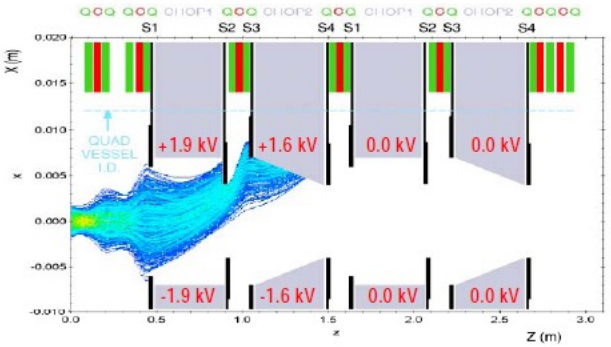

Figure 5: Fast chopping / Bunch 1-3 and 63-66 chopped.

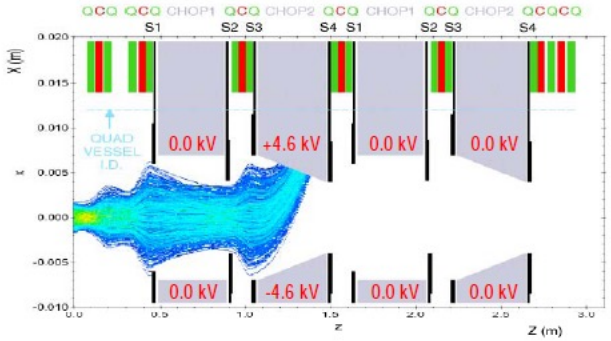

Figure 6: Slow chopping / Bunch 4-62 chopped.

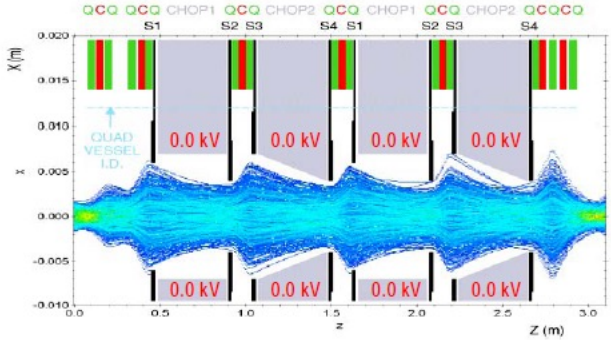

Figure 7: No chopping / Bunch 67-158 un-chopped.

CERN LEBT Pre-Chopper

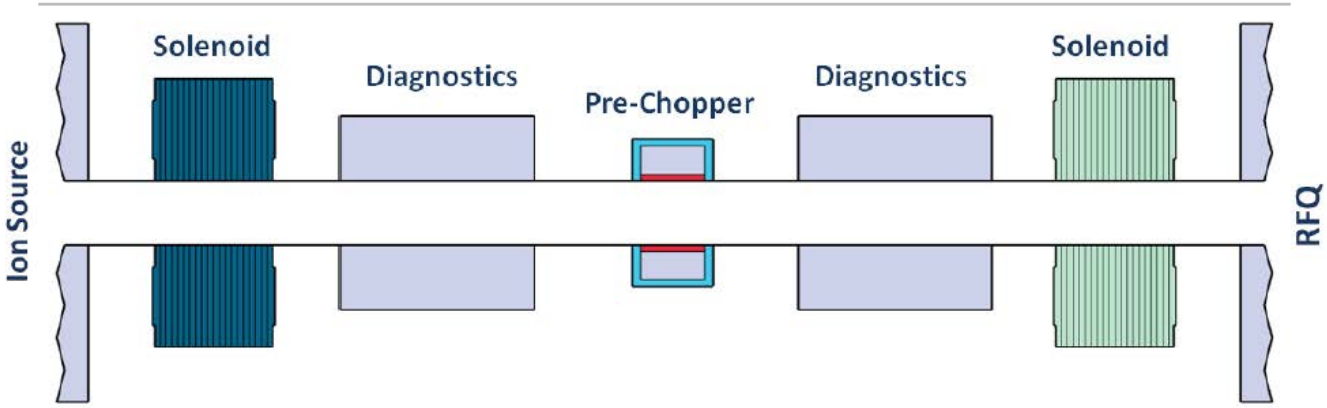

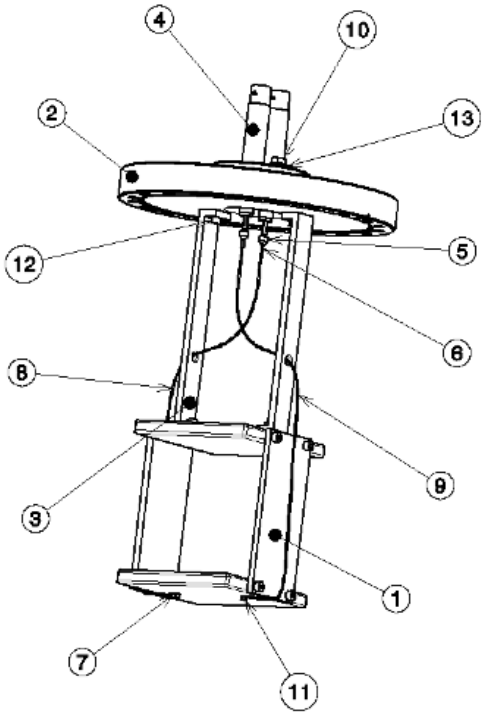

Figure 3: Schematic layout of the CERN Linac4 LEBT line.

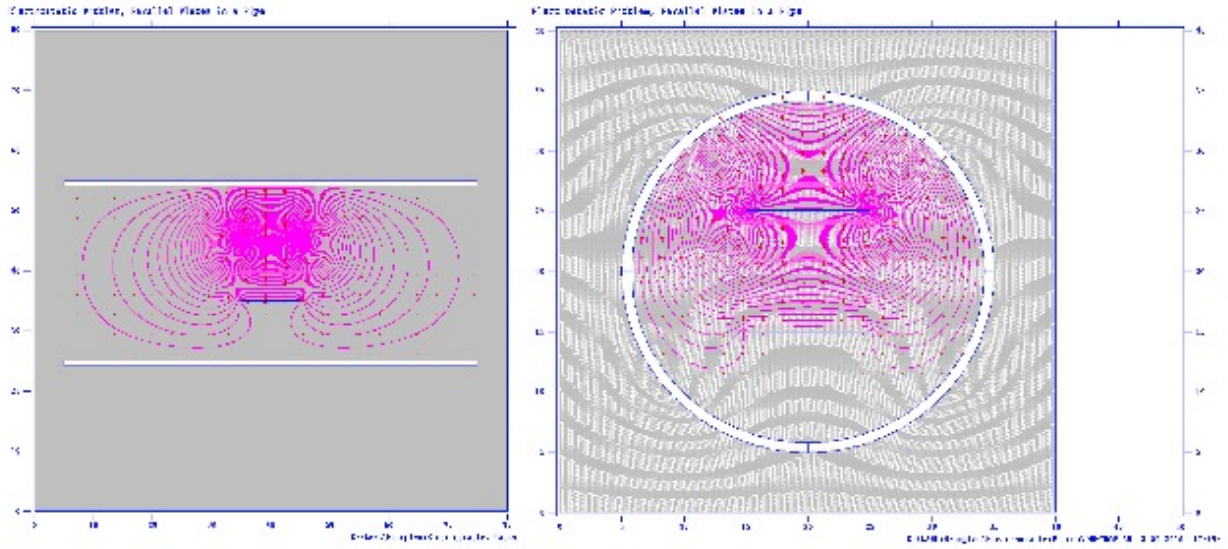

FNAL Einzel Lens Chopper

Einzel Lens Chopper

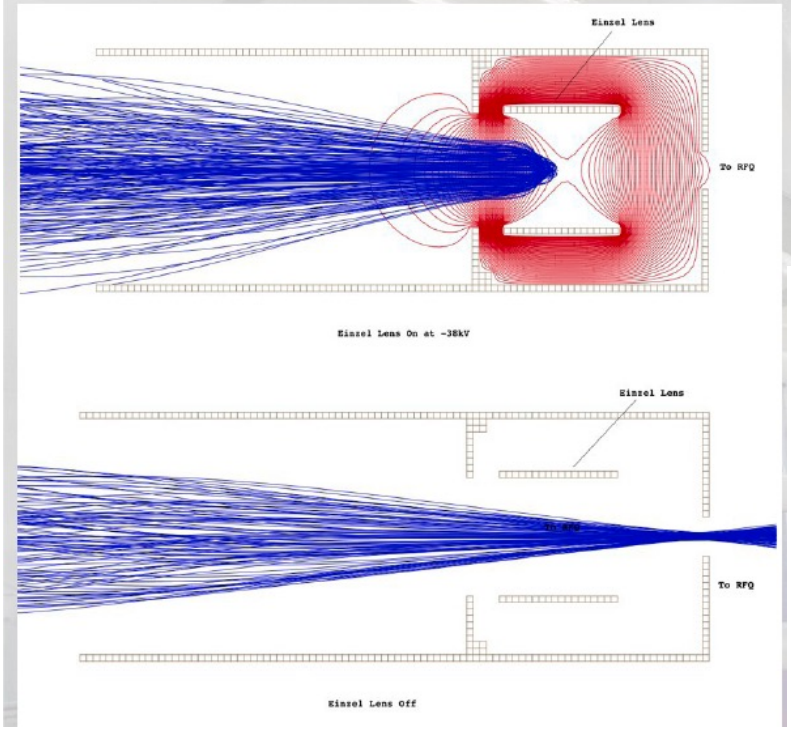

- Simulation using SIMION
- Optimized lens
  - 2” long
  - 1.75” diameter
  - -37 kV to stop 35keV

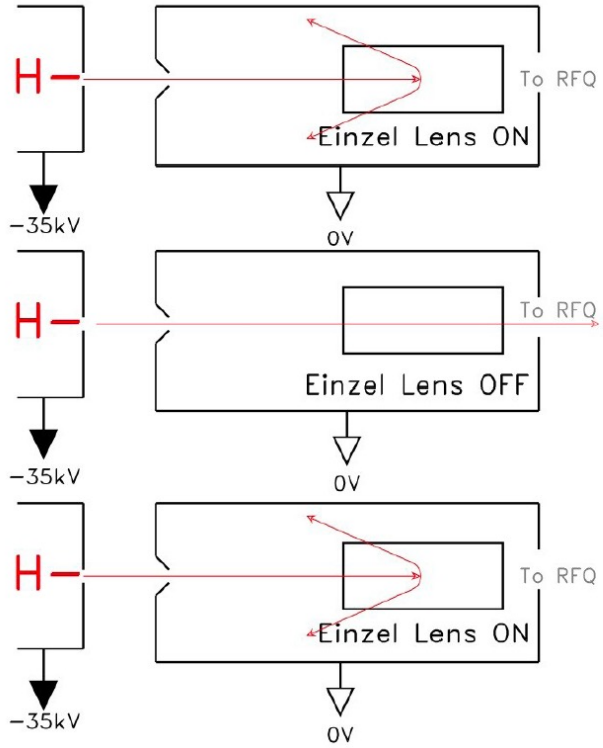

Einzel lens is on for ~40μs to deflect beam which until neutralization has taken place

Pulser and Einzel lens off for ~60μs

Einzel lens is turned on again to stop the H− beam

J-PARC RF Deflector

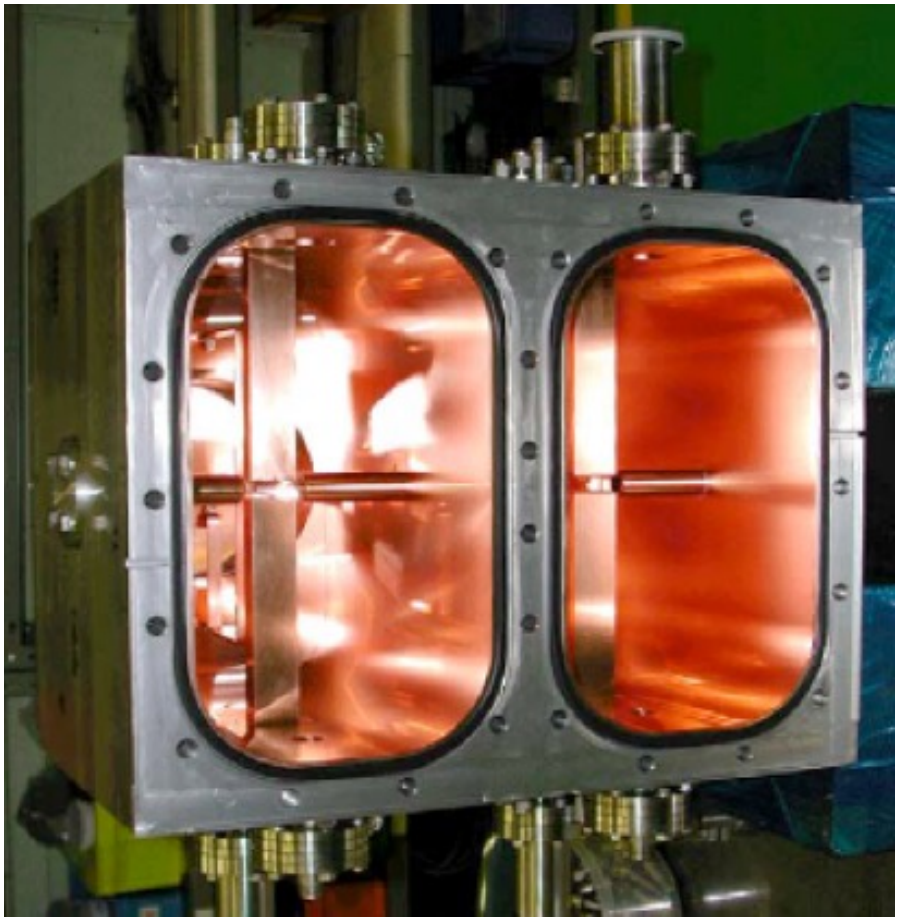

frequency	324 MHz
Q	~10
Cavity rise time	10ns
Power amplifier	Solid state, 36kW
Amplifier rise time	15ns
Max field	1.6MV/m
Gap length	20mm

Beam Matching in LEBT

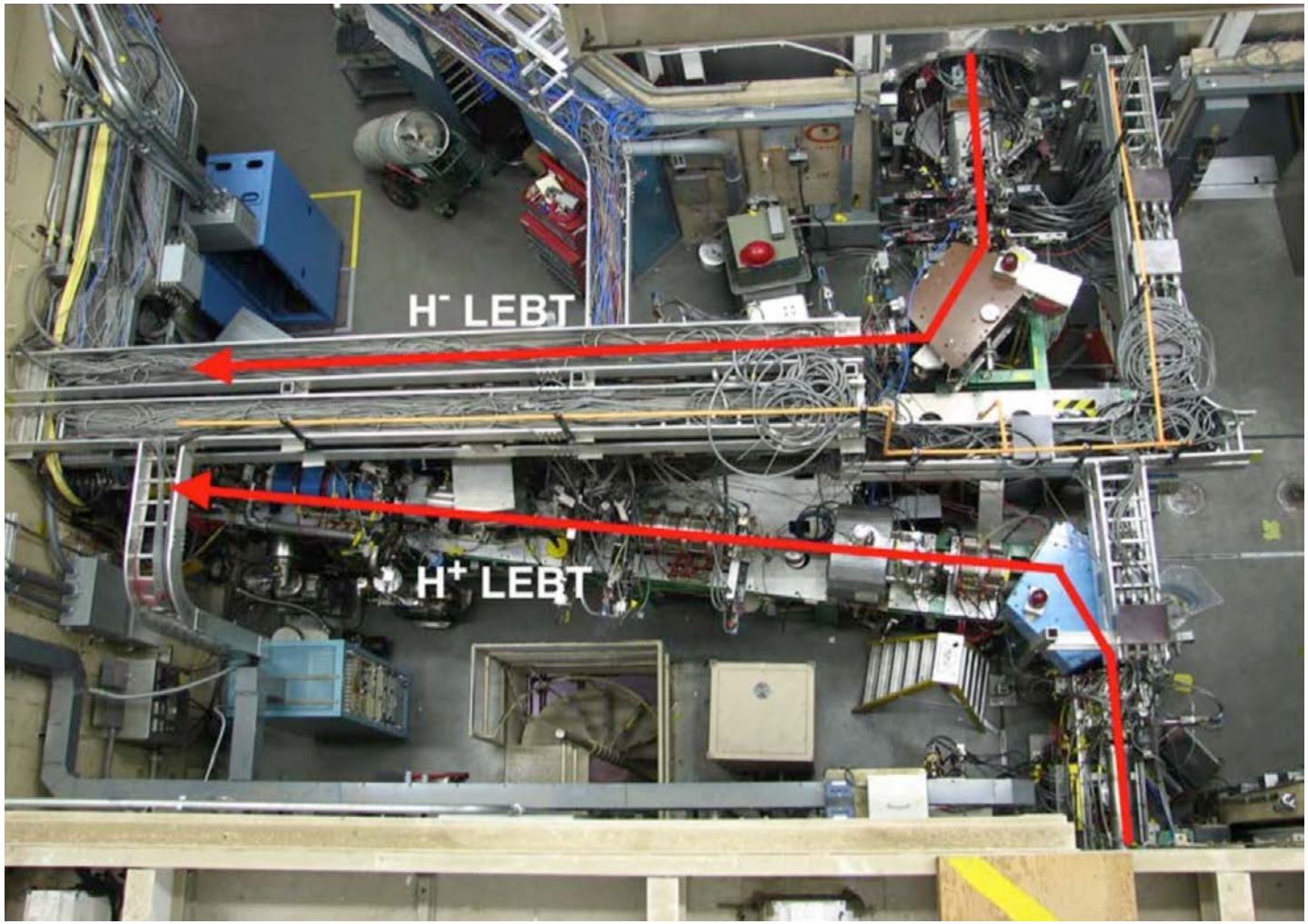

Top view of 750 - keV Low Energy Beam Transports (LEBT) of H^+ and H^- beams.

750 keV LANL Injector of H+ / H- Beams

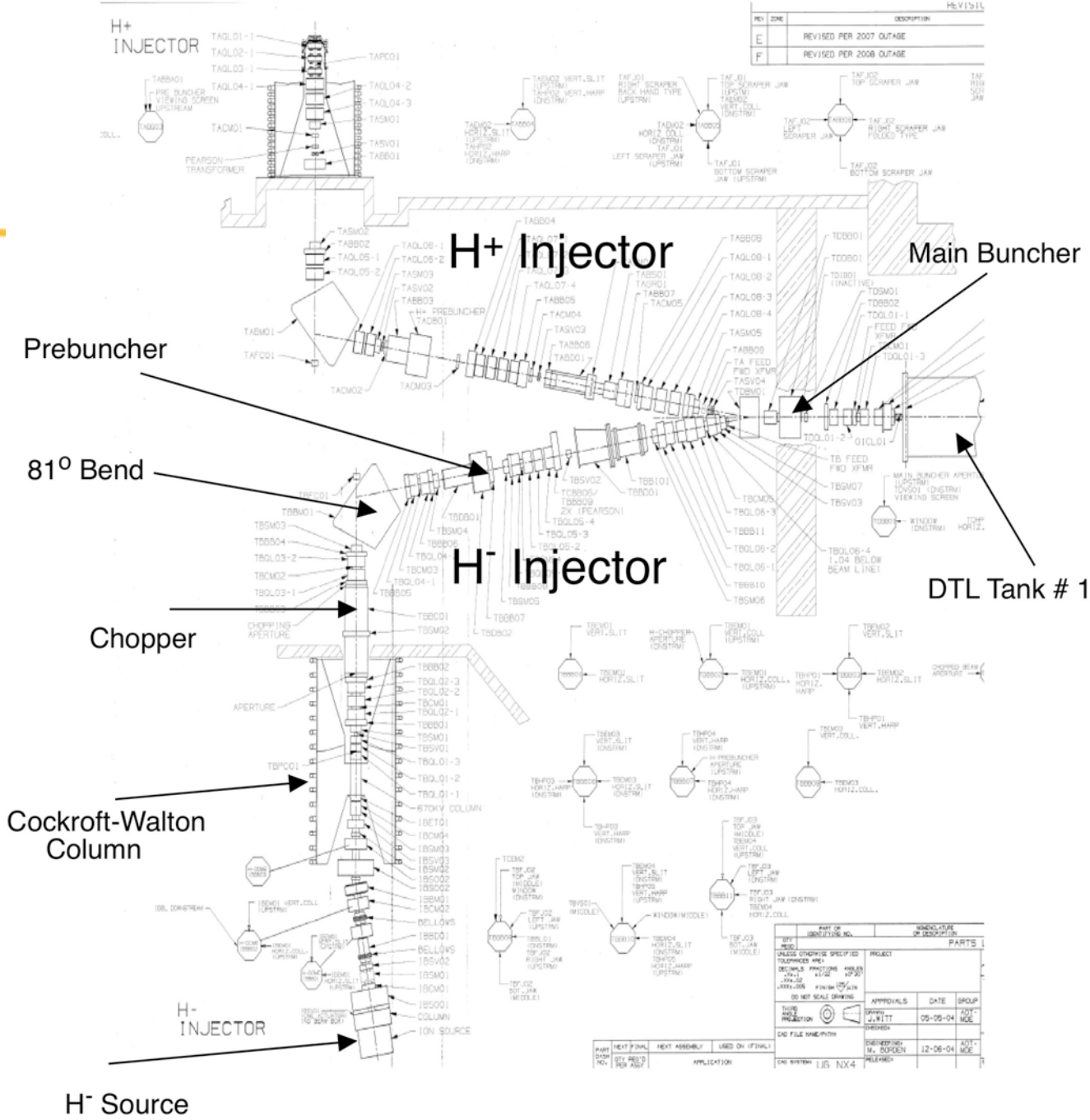

Matching of the H- Beam with 750 keV Low Energy Beam Transport

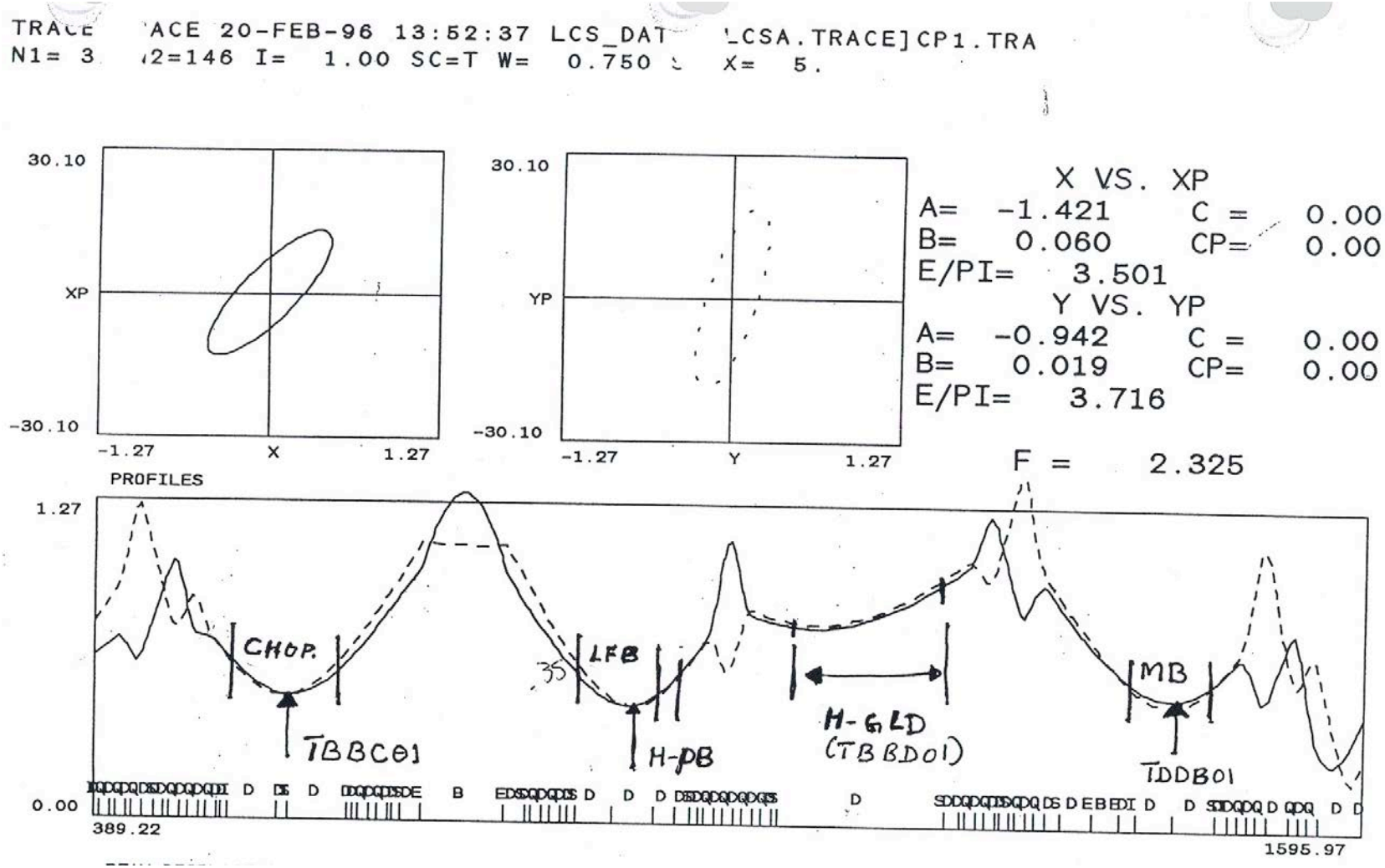

Matching of the H^+ Beam with 750 keV Low Energy Beam Transport

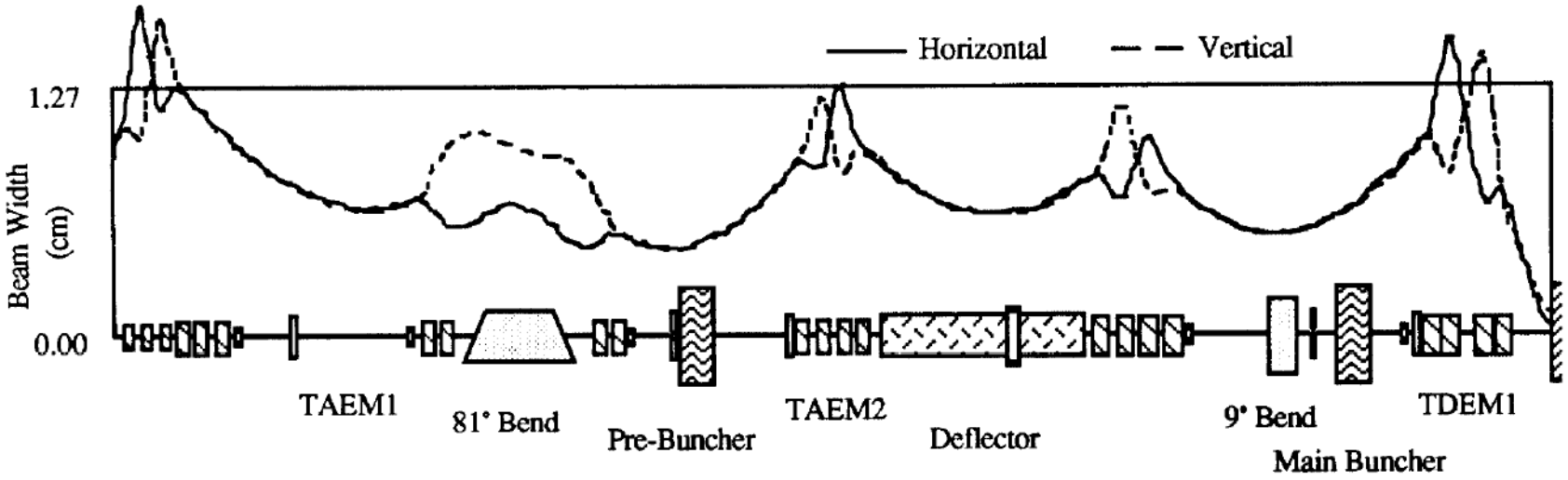

Emittance Scans for Beam Matching

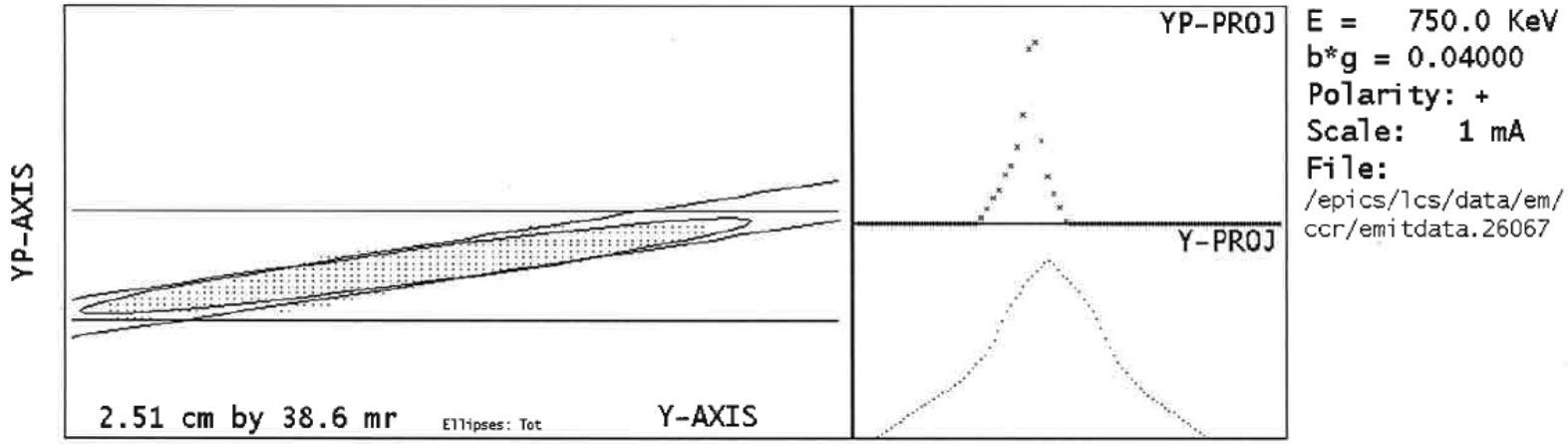

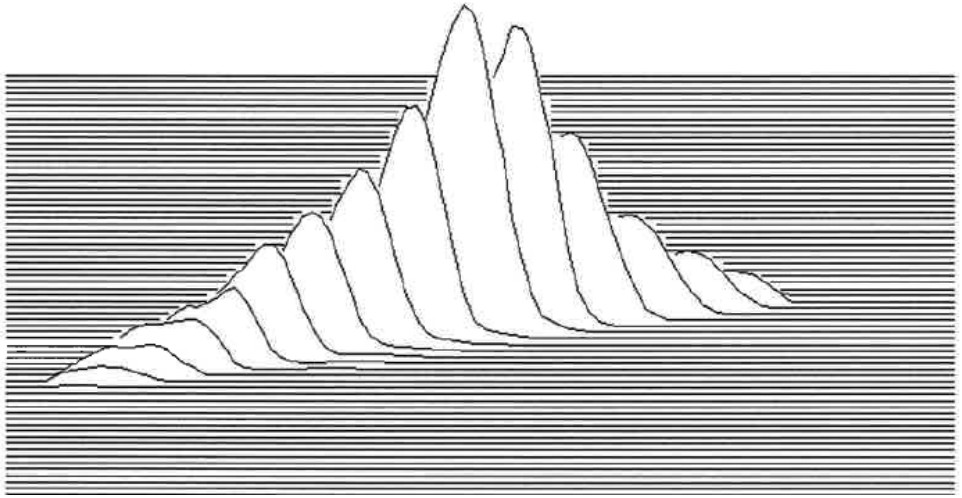

```
Run:26067  Stn: TDEM01-V
24:03:32     20-Jul-2015
Beam: H+      Meas,    Norm
E(total)=    1.712,   0.068 pi
E(edge) =    1.547 pi
E(rms)  =    0.195,   0.008 pi
Etot/rms=     8.79
 Alpha  =   -2.677
 Beta   =    0.699
4*E(rms)=    0.779 pi
  Cent  =   -0.137 cm
 CentP  =   -3.899 mr
X Sigma =   0.3688 cm
XP Sigma=   1.5082 mr
 Thold  =     0.5 %,     6 cnts
 Maximum Counts =      1324
Beam thru thresh=     80116
     Total Beam =     80417
Slit Pos =    1363   1953
Clctr Pos=    1380   1970
Slit Rate =     235, Nom.=     230
Clctr Rate=     234, Nom.=     229
E(ea) = 3.425,   0.137 pi
E(ea)/E(rms) =17.593
```

Beam Matching Using Envelope Code

Mismatch factor between expected and actual beam

$$F = \sqrt{\frac{1}{2}(R + \sqrt{R^2 - 4}) - 1}$$

$$R = \beta_{\exp}\gamma_s + \beta_s\gamma_{\exp} - 2\alpha_{\exp}\alpha_s$$

Average mismatch

$$\bar{F} = \frac{1}{2}(F_x + F_y)$$

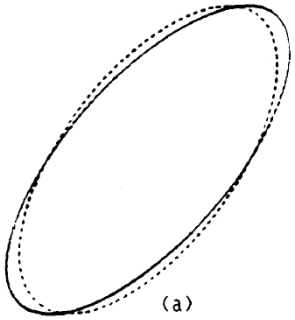

Use of Emittance Measurements

- Measure the beam Emittance and Twiss Parameters at one point.
- Using a simulation code we can then predict the trajectory of the beam envelope through a region to a point where the beam cannot be measured.

Measured **Predicted**

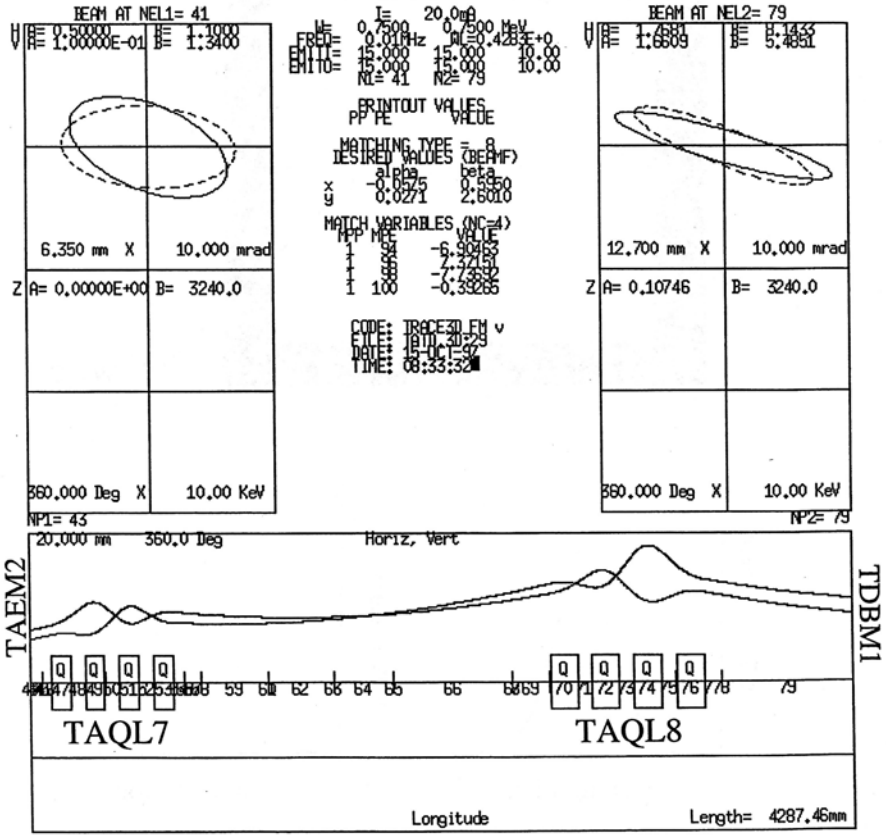

Beam Matching at the Entrance of LANL DTL

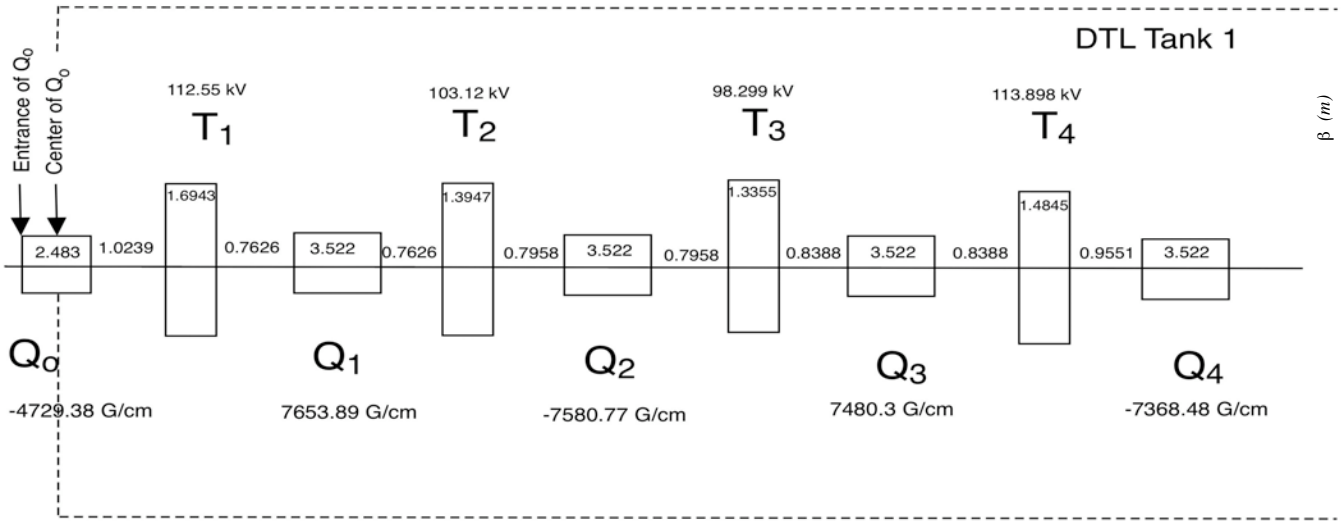

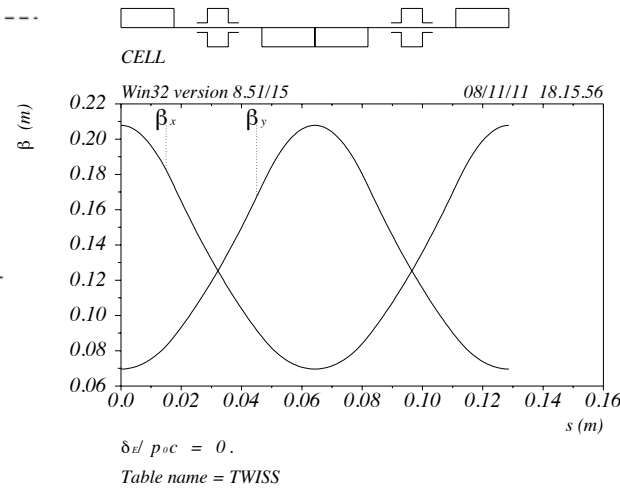

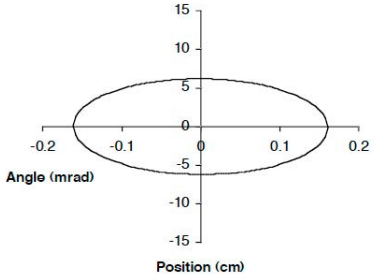

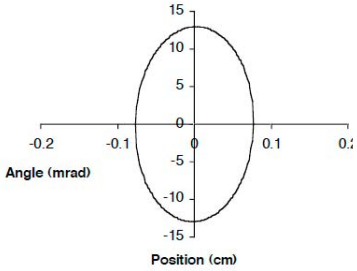

Matched beam ellipses at the entrance of DTL

Phase advance per cell $\mu_o = \frac{L}{2D}\sqrt{1-\frac{4}{3}\frac{D}{L}\frac{qG_mD^2}{m\gamma\beta c}} = 0.9749 \quad (55.8^o)$

Max value of beta-function $\beta_{\max} = \frac{L(1+\sin\frac{\mu_o}{2})}{\sin\mu_o} = 21.3\ cm$

Min value of beta-function $\beta_{\min} = \frac{L(1-\sin\frac{\mu_o}{2})}{\sin\mu_o} = 7.716\ cm$

Unnormalized acceptance $A = \frac{a^2}{\beta_{\max}} = \frac{a^2}{L}\frac{\sin\mu_o}{(1+\sin\frac{\mu_o}{2})} = 26.4\,\pi\,cm\,mrad$

Normalized acceptance $\varepsilon_{accept} = \beta\gamma A = 1.056\,\pi\,cm\,mrad$

Medium-Energy Beam Transports

1. Match and steer the beam from the RFQ into the Drift Tube Linac

2. Perform beam diagnostics with comprehensive set of beam instrumentation devices

3. Perform collimation of the transverse particle distribution

4. Perform additional beam chopping LEBT chopper

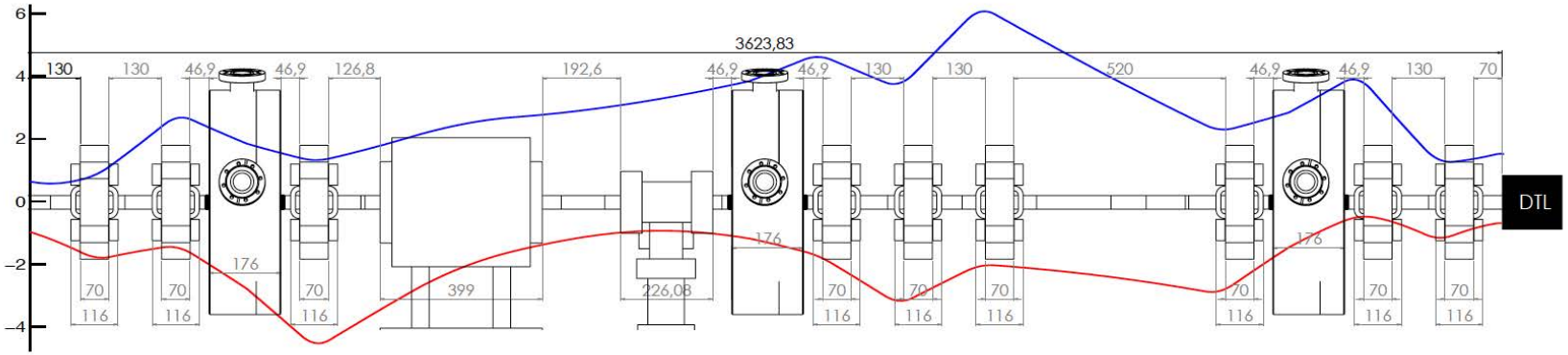

ESS medium energy beam transport layout, containing 10 quadrupoles, 3 bunchers, and 3 collimators (ESS Design Report).
Root

MEBT Collimator Scrappers

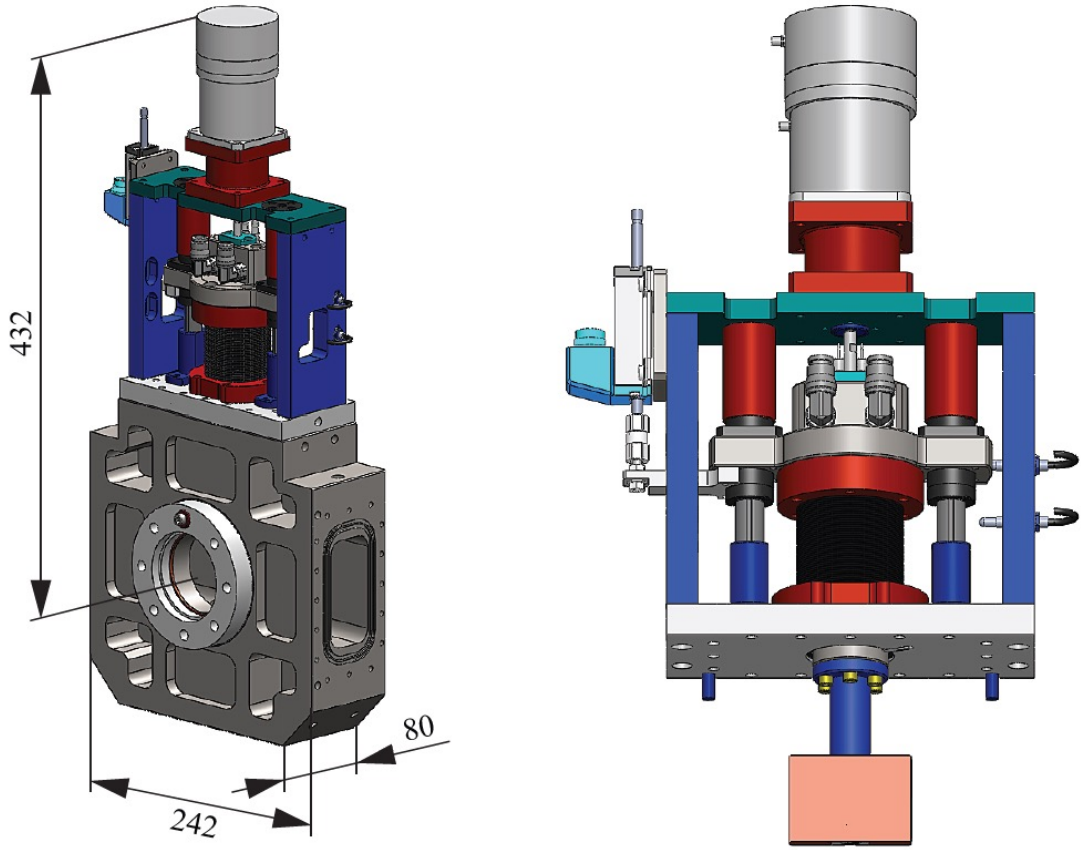

ESS MEBT Collimator Scrappers (ESS Design Report)

Medium-Energy Beam Transports

MEBT Chopper

SNS has two stage chopping system:

- LEBT chopper before RFQ: slow - rise time about 50 ns
- MEBT chopper (2.5 MeV): rise time is 15 ns, and it cleans the gap once again

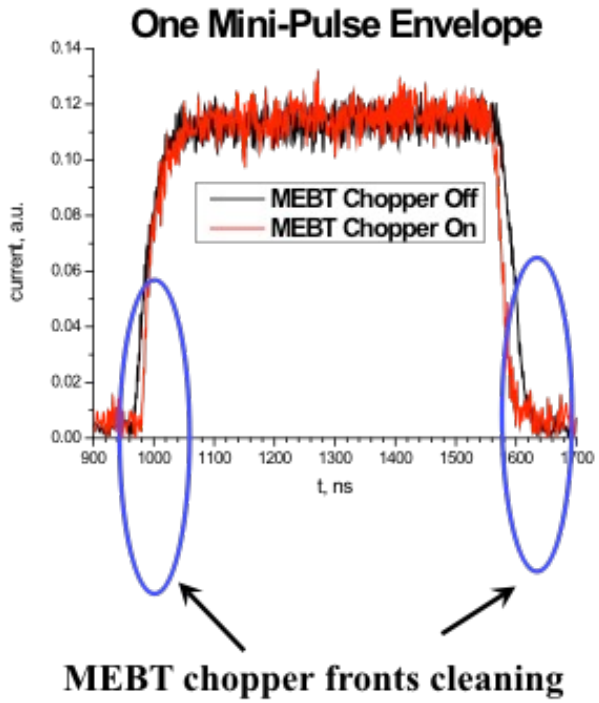

The original faster MEBT chopper (analog of Los Alamos PSR system) was damaged two times and was replaced.

We have a lot of partially chopped beam:

6 - 4% bunches have less than 50% of max charge.

No big effect on linac losses, but it improves extraction losses in the ring

A. Shishlo (PAC2011).

High Energy Beam Transports

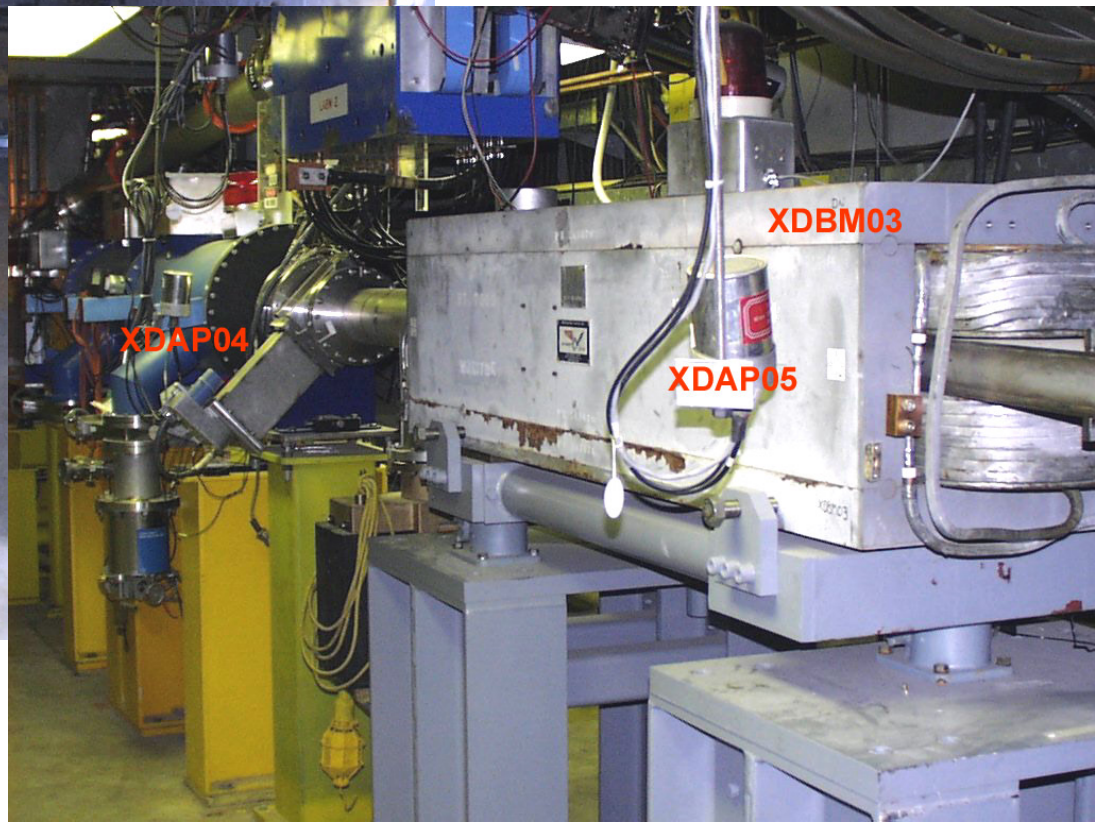

LANSCE High Energy Beam Lines

High Energy Beam Transports

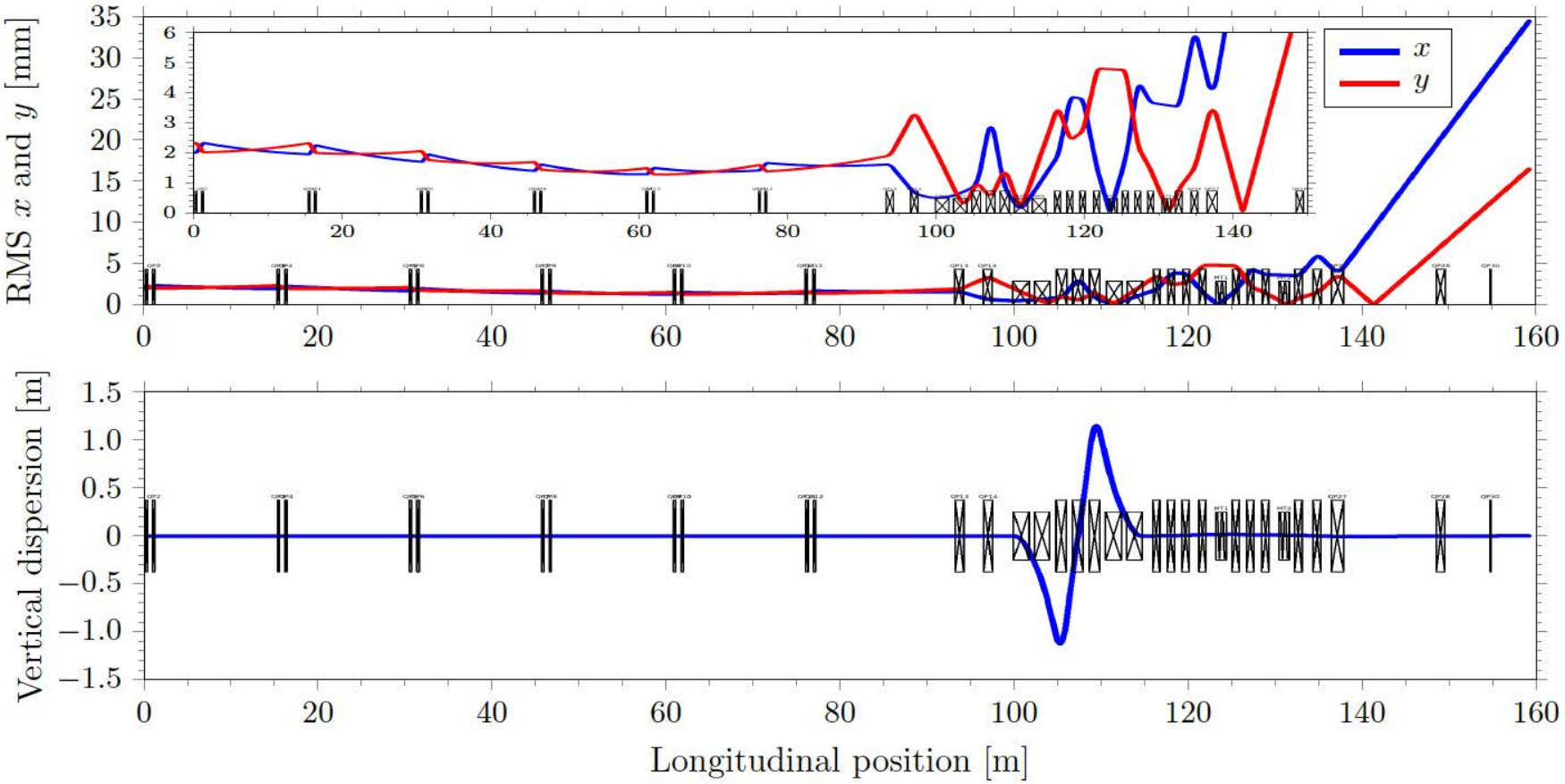

ESS beam size envelopes along the high energy beam transport

Emittance Measurement in a Dispersion Free Region

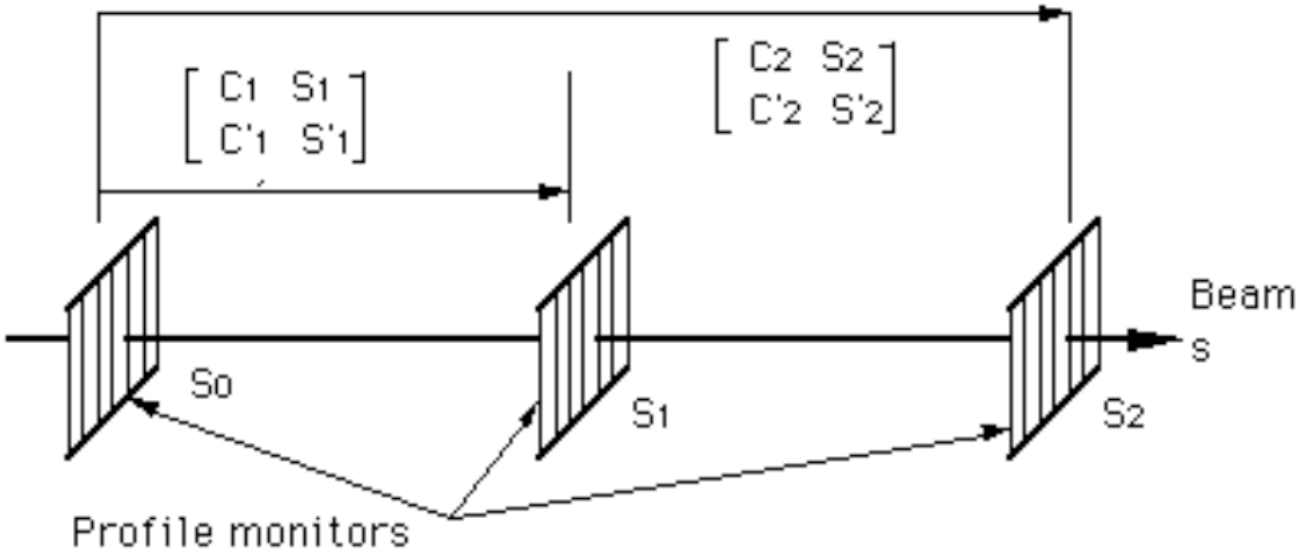

Beam Based Alignment

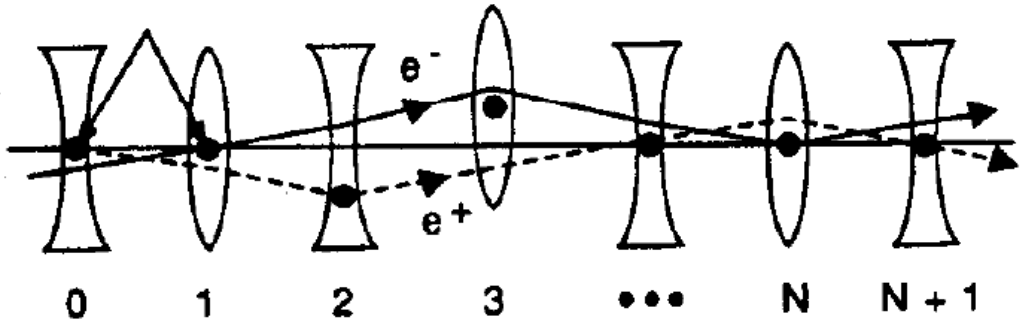

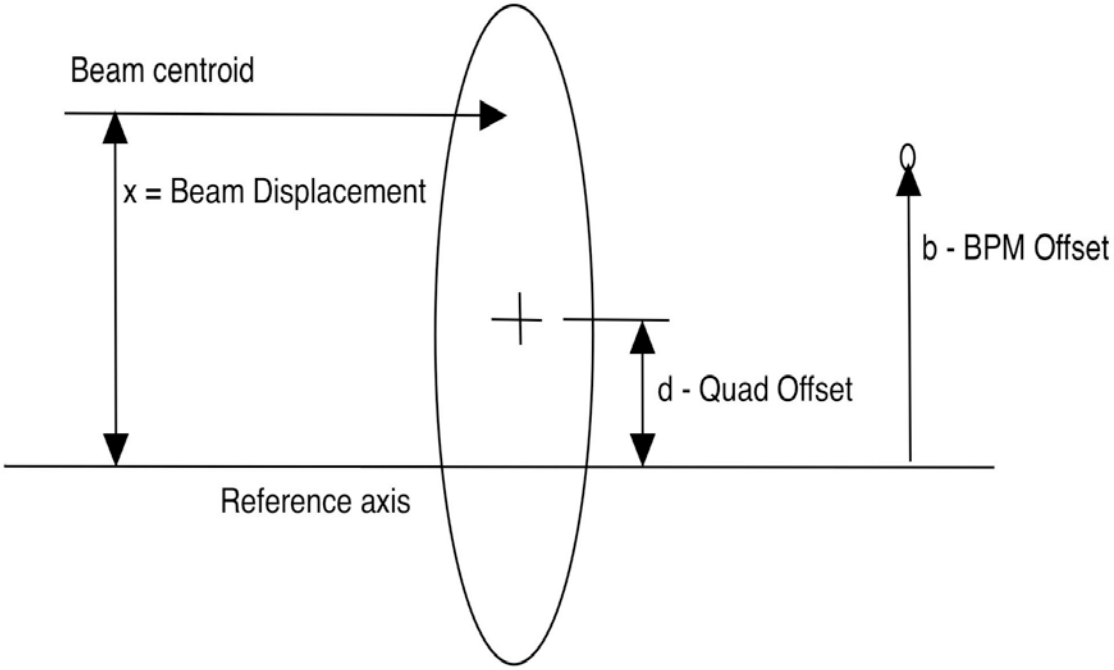

Displacements of beam centroid, quadrupole, and BPM.

Beam Based Alignment

Beam centroid displacement after transport through k elements [C.E.Adolpsen et al, SLAC-PUB-4902 (1989).]

$$\begin{pmatrix} x_k \\ x_k' \\ y_k \\ y_k' \\ z_k \\ \delta \end{pmatrix} = R_{o,k} \begin{pmatrix} x_o \\ x_o' \\ y_o \\ y_o' \\ z_o \\ \delta \end{pmatrix} + \sum_{j=1}^{k-1} (R_{j+1,k} - R_{j,k}) \begin{pmatrix} dx_j \\ 0 \\ dy_j \\ 0 \\ 0 \\ 0 \end{pmatrix}$$

where $R_{j,k}$ is the transfer matrix from element j to element k, and dx_j, dy_j are the offsets of element j. BPM and WS measurement of beam displacement are:

$$\Delta x_k = x_k - bx_k, \qquad \Delta y_k = y_k - by_k$$

where bx_k , by_k are the displacement of BPM or WS. Taking different quadrupole settings with BMP and WS measurements equal to number of elements, it is possible to determine offset of each element through solution of system of linear algebraic equations and then apply appropriate kick from steering magnet.

Beam Position Monitors and Steering Magnets

BPM: Collection of 4 electrodes (top, bottom, left, and right)
Electrodes pick up signal as the beam passes
Comparing signal of opposing electrodes yields the beam centroid position

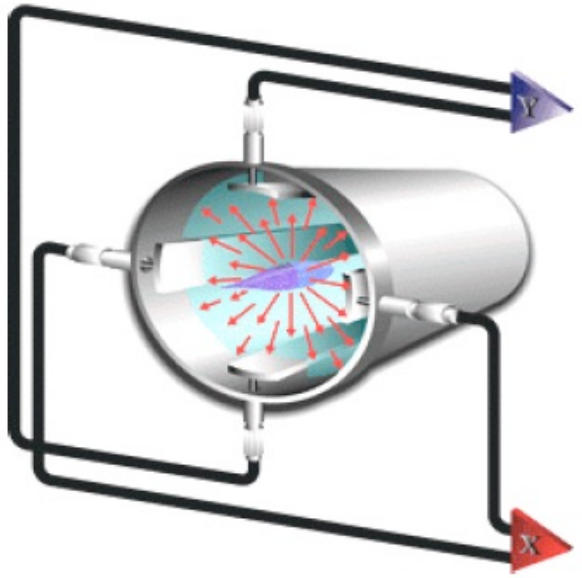

Steering magnet: Collection of 2 dipole magnets for beam alignment

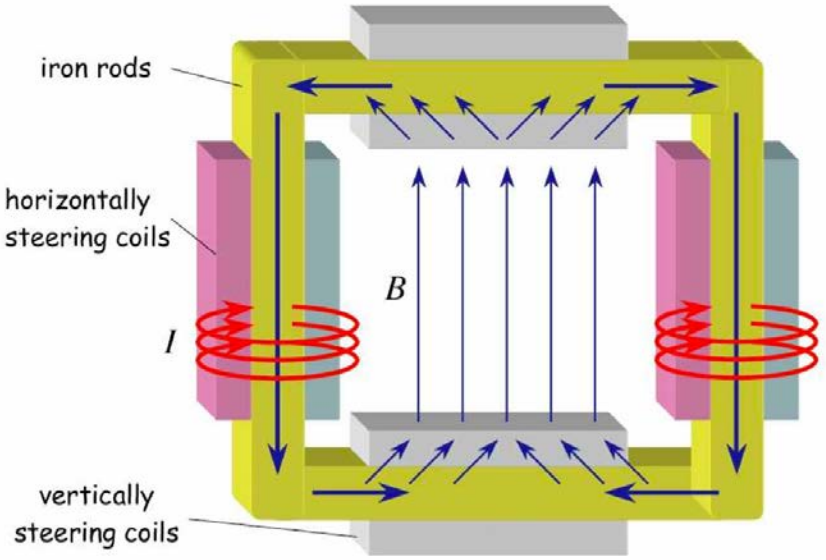

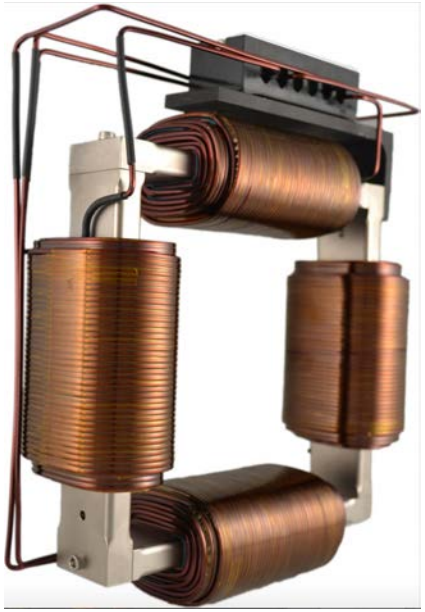

Injection of H^- Beam into Proton Storage Ring (PSR)

Beams at injection foil

New foil

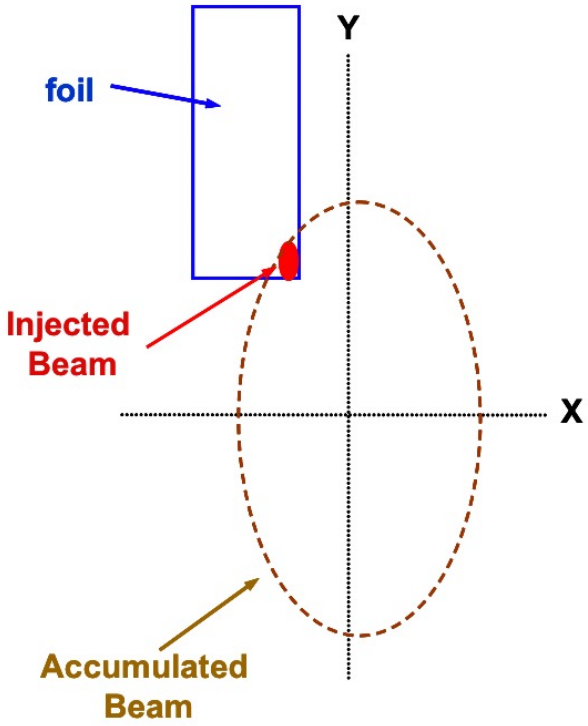

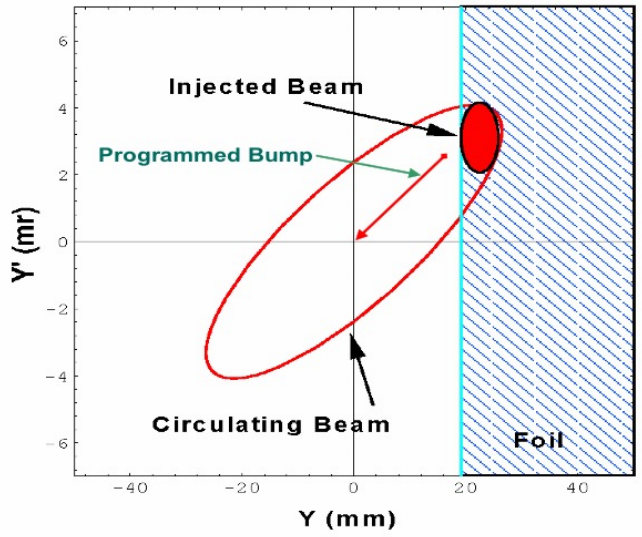

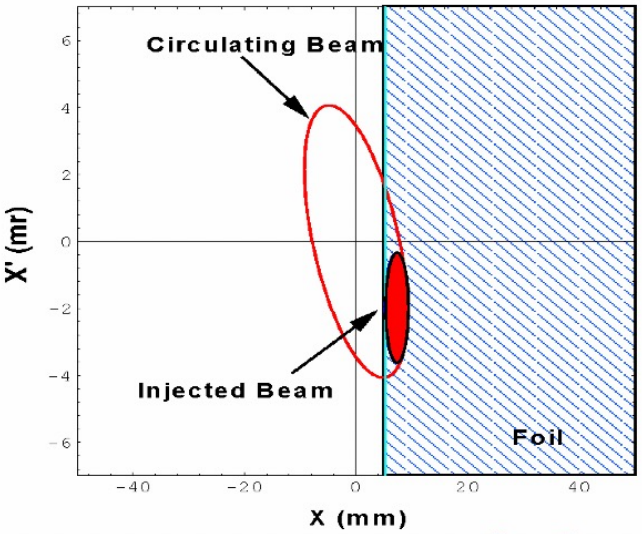

Foil Degradation

New Foil

Used Foil

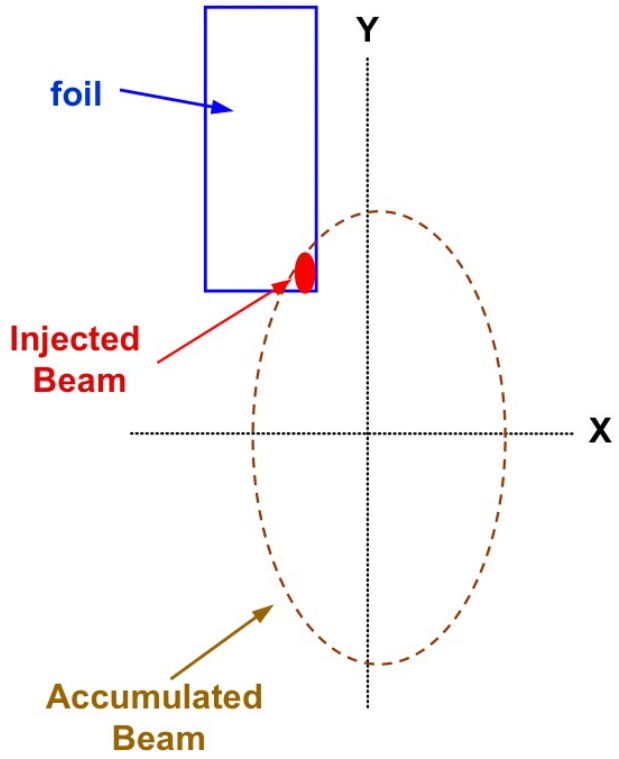

Foil edge for stripping distorts with time and becomes thicker leading to fewer excited states

Emittance Blow-Up Due To Thin Windows

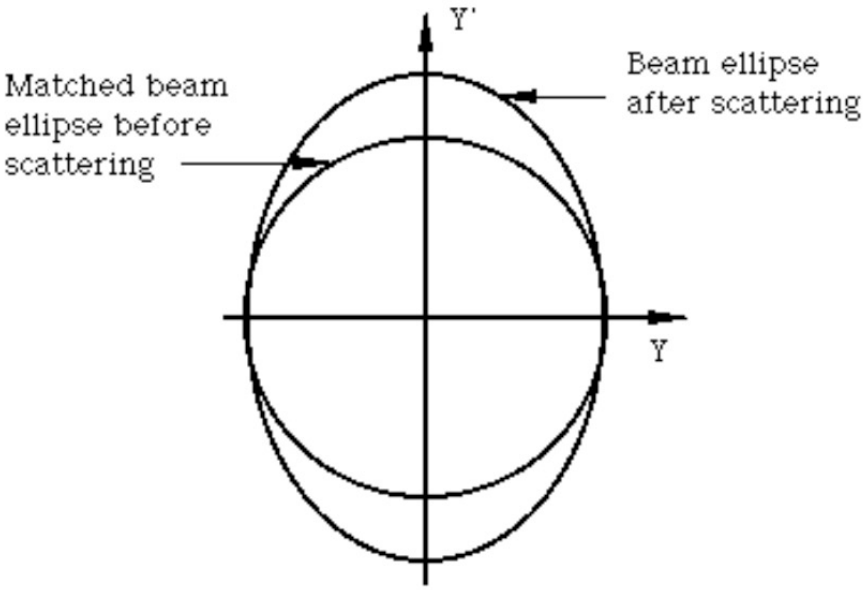

Emittance growth due to scattering (P.J. Bryant):

$$\varepsilon_2 = \varepsilon_1 + \frac{\pi}{2}\beta\langle\theta_s^2\rangle$$

Root mean square projected angle θ_s due to multiple Coulomb scattering in a window

$$\sqrt{\langle\theta_s{}^2\rangle} = \frac{0.0141}{\beta_c p[\mathrm{MeV}/c]} Z_{\mathrm{inc}} \sqrt{\frac{L}{L_{\mathrm{rad}}}}\left(1+\frac{1}{9}\log_{10}\frac{L}{L_{\mathrm{rad}}}\right) \quad [\mathrm{radian}]$$

where Z_{inc} is particle charge in units of electron charge, p is the particle momentum in MeV/c, $\beta_c = v/c$, L is thickness of scatter and L_{rad} is radiation length of material of the scatter.

Combination of 4 Quadrupoles as an Axial-Symmetric Lens (Russian Quadruplet)

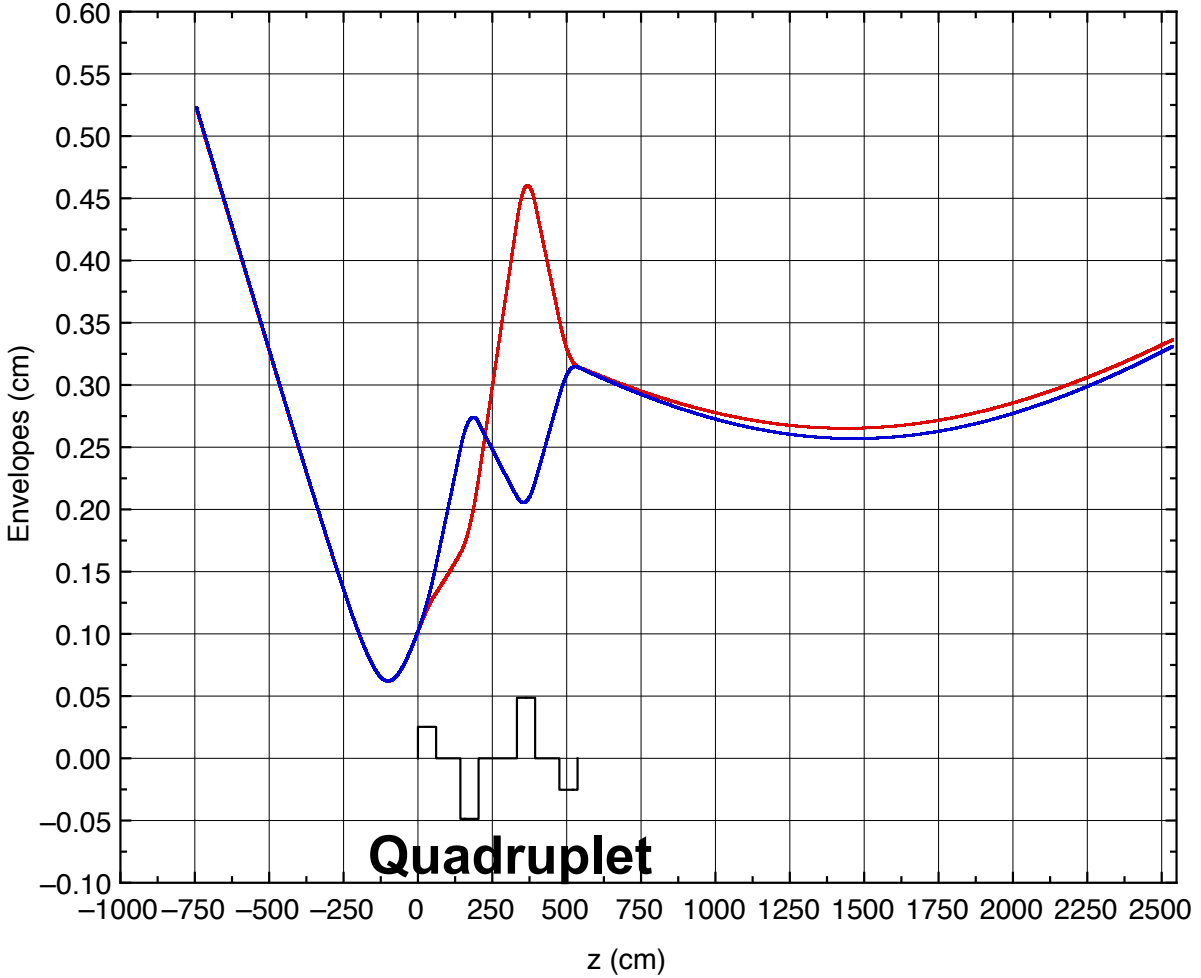

Combination of two identical Quadrupole Doublets:

- Order of quadrupoles in second doublet must be reversed with respect to first quadruplet
- Fields in similar quadrupoles are shifted by 90^{o}

(A. Dymnikov, S. Yavor,1963)

Uniform Irradiation of Large Targets

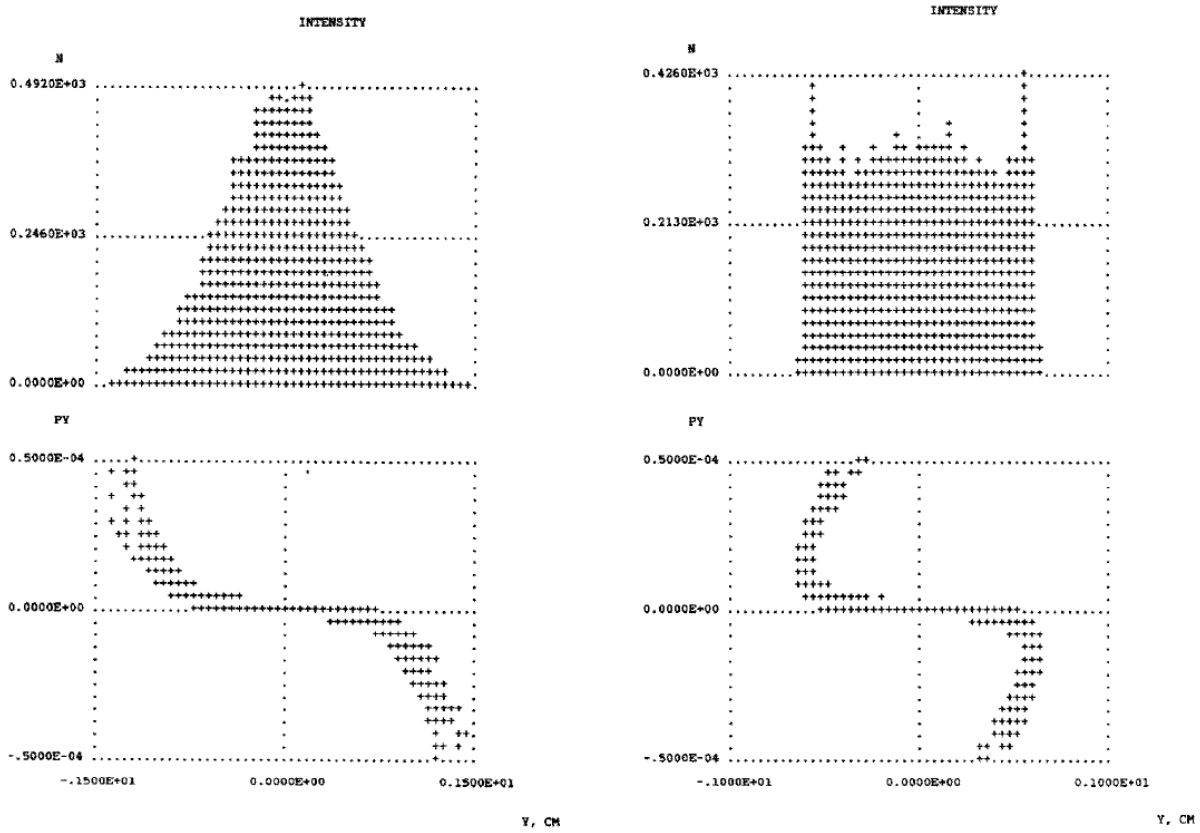

Beam intensity redistribution in the channel with higher order multipoles. Upper part illustrates particle distributions at the beginning (left) and at the end (right) of the transport channel, lower part shows the phase-space projections of the beam.

Initial and Final Beam Distributions in Nonlinear Expander

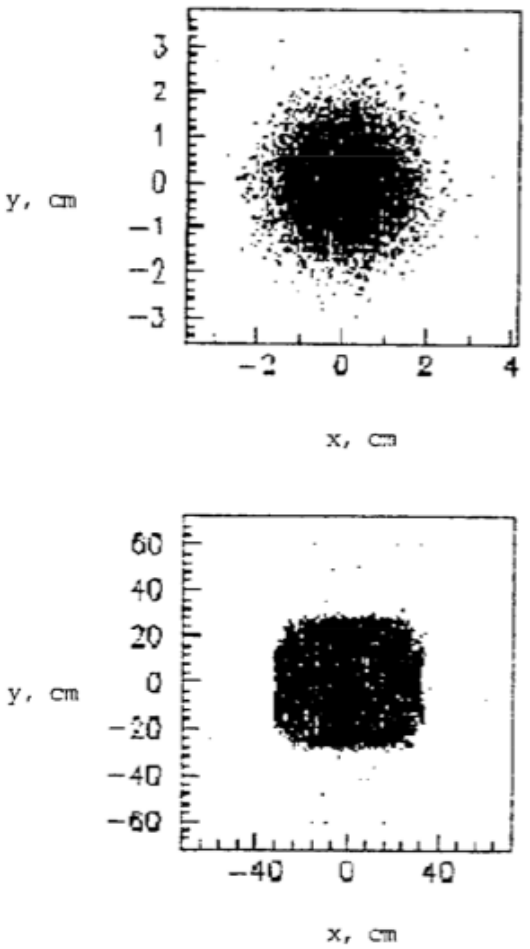

Fig. 1. Projections of computer simulation using code BEAMPATH [7] into real space (x-y) for an initial (upper) and final (lower) beam distribution in a non-linear optics channel.

Consider the one-dimensional problem for a beam of particles with charge q and mass m propagating along the z-axis with a longitudinal velocity $v_z = \beta_z c$. Suppose that a particle at $z = 0$ has the velocity modulation:

$$v_x = v_{x0} + a_2 x_0 + a_3 x_0^2 + a_4 x_0^3 + \cdots + a_n x_0^{n-1}, \qquad (1)$$

where v_{x0} and x_0 are the initial transverse velocity and position of the particle, a_2 is a linear modulation coefficient, and a_3, a_4,... are nonlinear modulation coefficients. After a drift of the beam the x-coordinate of the particle at any z is

$$x = x_0 + \frac{z}{v_z}\left(v_{x0} + a_2 x_0 + a_3 x_0^2 + a_4 x_0^3 + \cdots\right). \qquad (2)$$

The number of particles dN inside the element $(x, x + dx)$ is invariable, hence the particle density $\rho(x) = dN/dx$ at any z is connected with the initial density $\rho(x_0)$ by

$$\rho(x) = \rho(x_0)\frac{dx_0}{dx} \qquad (3)$$

or

$$\rho(x) = \rho(x_0)\left(1 + \alpha_2 + 2\alpha_3 x_0 + 3\alpha_4 x_0^2 + 4\alpha_5 x_0^3 + \cdots (n-1)\alpha_n x_0^{n-2}\right)^{-1}, \qquad (4)$$

where $\alpha_n = a_n z / v_z$. From eq. (4) it follows that redistribution of the particle density can be obtained using the nonlinear velocity modulation coefficients α_3, α_4, α_5 ··· while the linear modulation coefficient α_2 only scales the density.

Experimental Observation of Beam Profile Uniforming

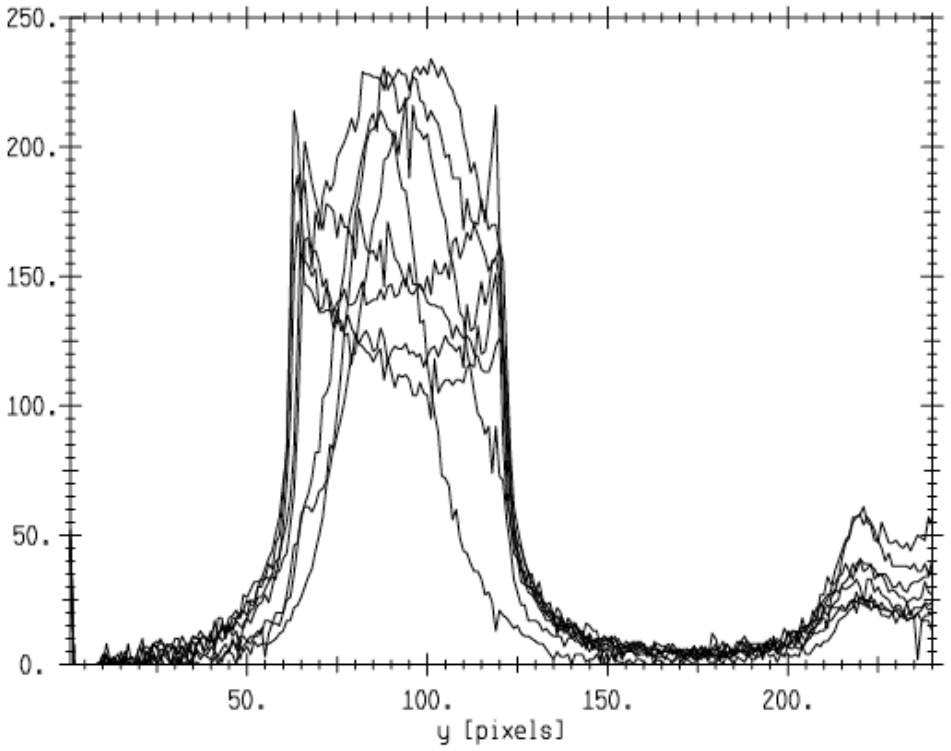

Observed beam profile at LANL beam expander experiment (1997).

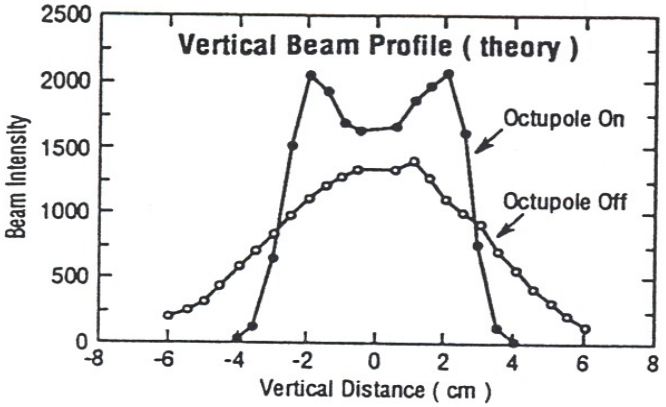

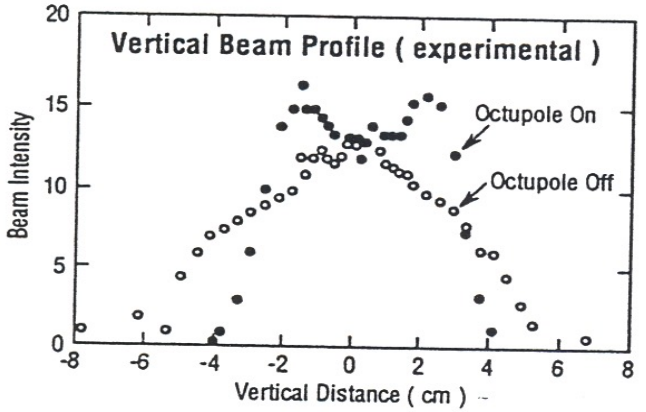

Theoretical calculations (top graph) and the experimental results (bottom graph) of the vertical beam profiles at the target location of the REF facility, with octupoles on and off.

REF (Radiation Effects Facility, 200 MeV H- BNL Linac)

Beam Uniforming in Free Space

$\eta = 0$

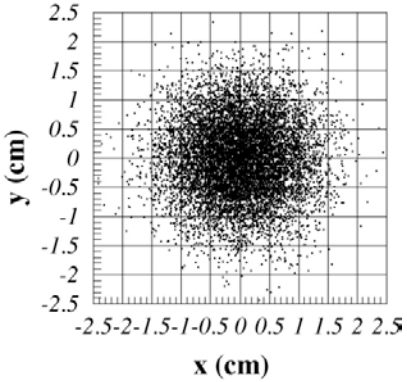

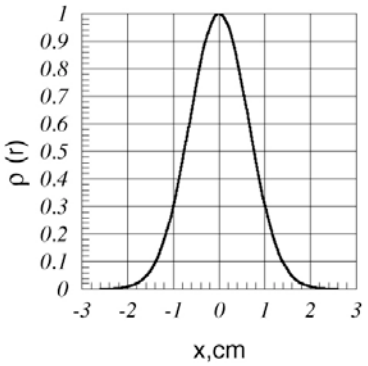

$\eta = 3.8$

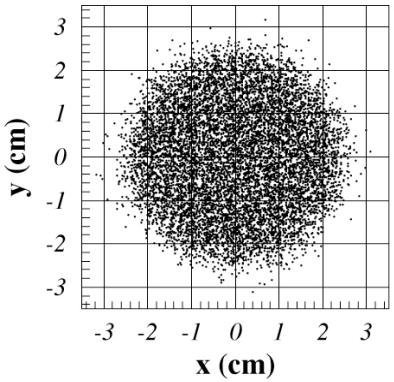

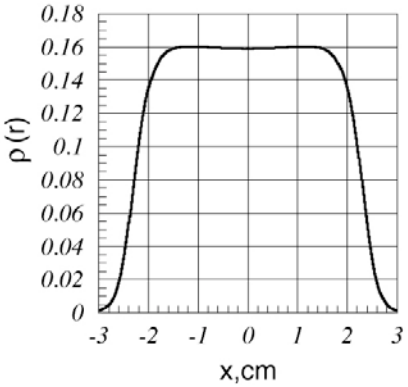

Redistribution of Gaussian beam in drift space.

Beam Uniforming in Free Space

Redistribution of the Gaussian beam under self space charge forces:

$$\rho(r) = \frac{\rho_o \, exp\,(-2\xi_o^2)}{a_o + a_1 F + a_2 F^2 + a_3 F^3 + a_4 F^4 + a_5 F^5 + a_6 F^6}\,, \qquad (3.42)$$

where: $\xi_o = \frac{r_o}{R_o}\,,$ $F = \sqrt{\frac{1 - exp(-2\xi_o^2)}{\xi_o^2}}$ $\eta = \frac{4I}{I_c(\beta\gamma)^3}\left(\frac{z}{R_o}\right)^2$ (3.43)

$$a_o = 1 + \eta \; exp(-2\xi_o^2), \qquad (3.45)$$

$$a_1 = -0.102 \, \eta^{3/2} \; exp(-2\xi_o^2), \qquad (3.46)$$

$$a_2 = \frac{1}{4}\eta^2 \; exp(-2\xi_o^2)\,, \qquad (3.47)$$

$$a_3 = 0.017 \, \eta^{3/2} - 0.0425 \, \eta^{5/2} \; exp(-2\xi_o^2) \qquad (3.48)$$

$$a_4 = 1.734 \cdot 10^{-3} \; \eta^3 exp\,(-2\xi_o^2) - \frac{1}{16}\eta^2\,, \qquad (3.49)$$

$$a_5 = 0.01275 \, \eta^{5/2}\,, \qquad (3.50)$$

$$a_6 = -5.78 \cdot 10^{-4} \; \eta^3\,. \qquad (3.51)$$

The beam with initial Gaussian distribution becomes more uniform when the parameter η is close to 4.

Circular Irradiation of Beam Targets

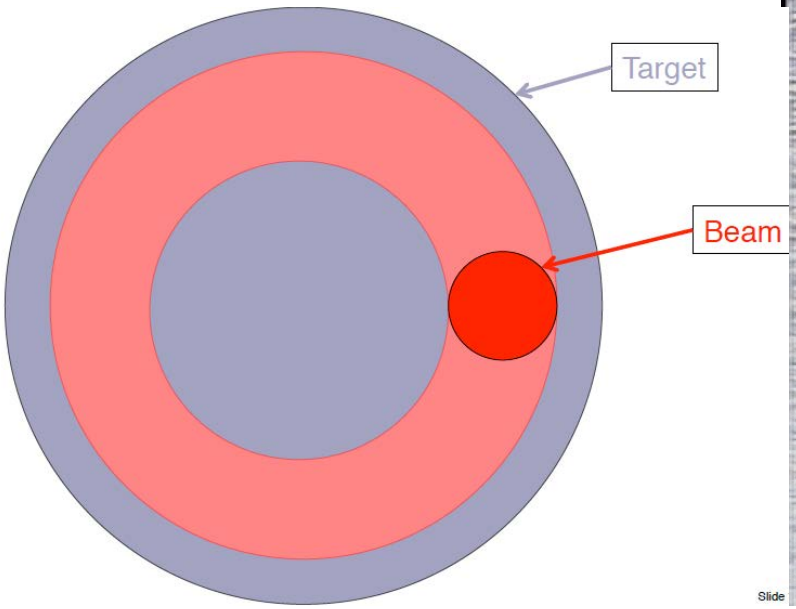

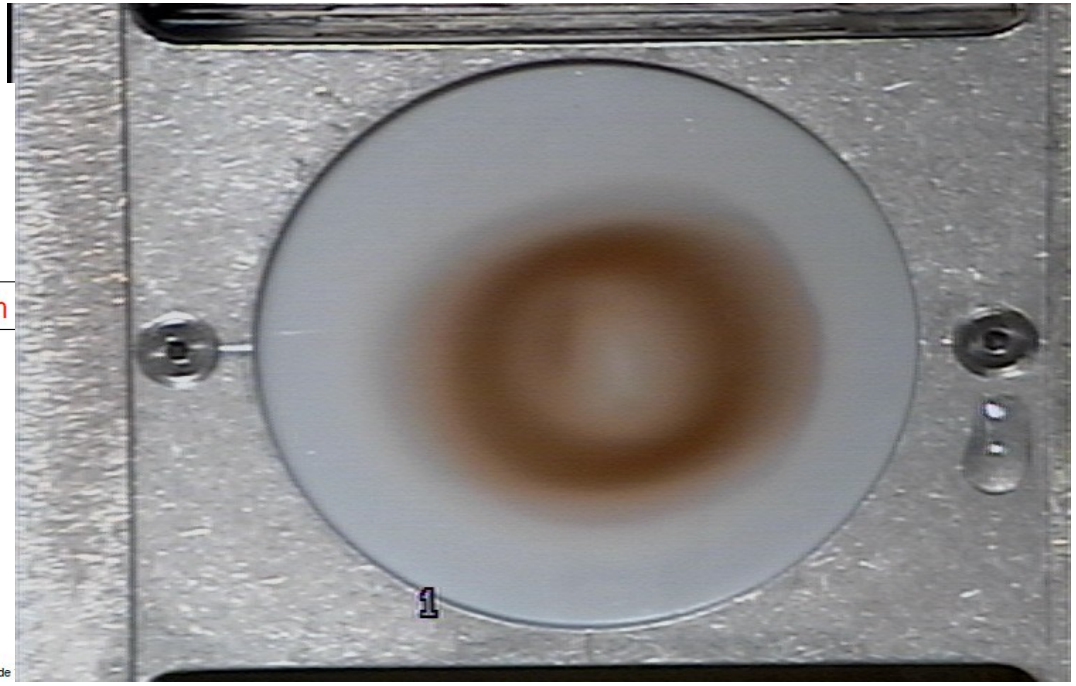

Circular irradiation of LANSCE Isotope Production Target by 100 MeV proton beam with simple one-circle raster

Circular Beam Sweeping

For uniform irradiation of a large target let us change the radius of the beam trajectory slowly in such a way that the increase of the area dS irradiated by the beam per one revolution is a constant:

$$dS = 2\pi r(t)\, dr(t) = \text{const}. \quad (7)$$

Eq. (7) is a condition of uniform irradiation of a target in the radial direction while the equation $\omega = \text{const}$ is a condition of a uniform irradiation in the azimuth direction. Having combined Eq. (7) with the equation of rotation $d\varphi = \omega dt$ the radius of the beam trajectory at the target is given by

$$r = \sqrt{\frac{dS\omega t}{d\varphi \pi}}\,. \quad (8)$$

The value $dS/d\varphi$ can be defined from the condition that after N revolutions (i.e. during the period of irradiation $T = 2\pi N/\omega$) the beam radius reaches its maximum value $r = R$ which is equal to the radius of the target:

$$\frac{dS}{d\varphi} = \frac{R^2}{2N}. \quad (9)$$

Finally the equation for increasing the beam radius with time for a uniform irradiation of a target is

$$r = R\sqrt{\frac{t}{T}} = R\sqrt{\frac{\omega t}{2\pi N}}\,. \quad (10)$$

Eq. (10) describes the untwisted spiral trajectory of the beam which starts at the center of a target (see Fig. 1). The Cartesian coordinates of the particles are changing according to

$$x = R\sqrt{\frac{t}{T}}\sin\,\omega t; \quad y = R\sqrt{\frac{t}{T}}\cos\,\omega t. \quad (11)$$

Spiral

$$r\,(t) = R_{\text{target}}\sqrt{\frac{t}{T}}$$

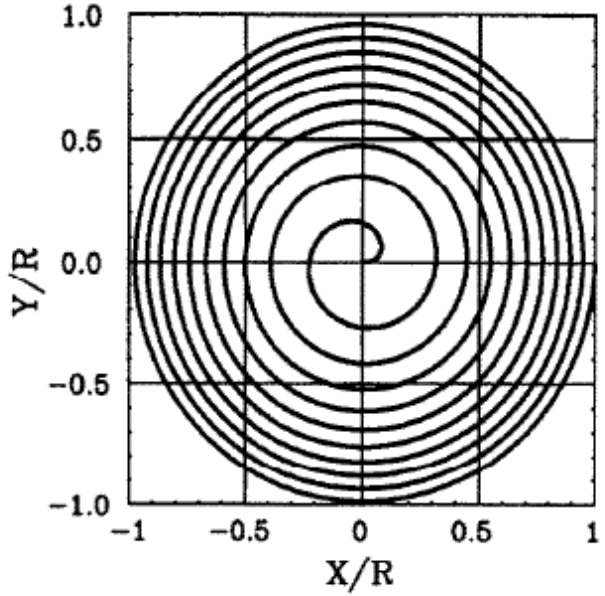

Concentric Rings

$$r_i = R_{\text{target}}\sqrt{\frac{i}{N}}$$

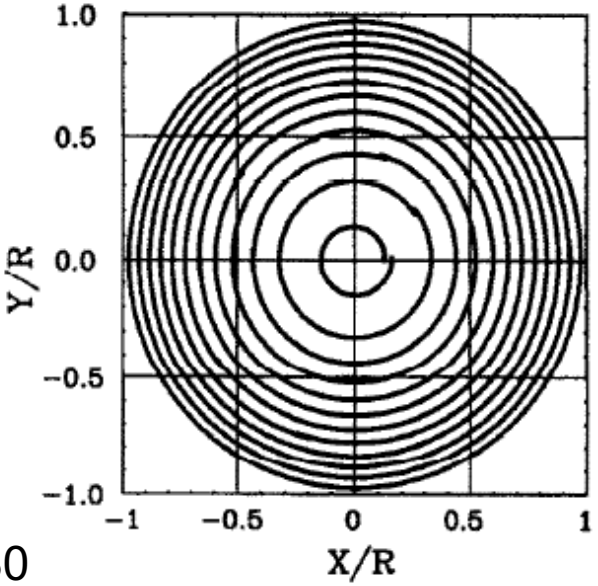

Y.B. et al, NIM-A 363(1995) 128-130

Circular Uniform Irradiation of Beam Targets

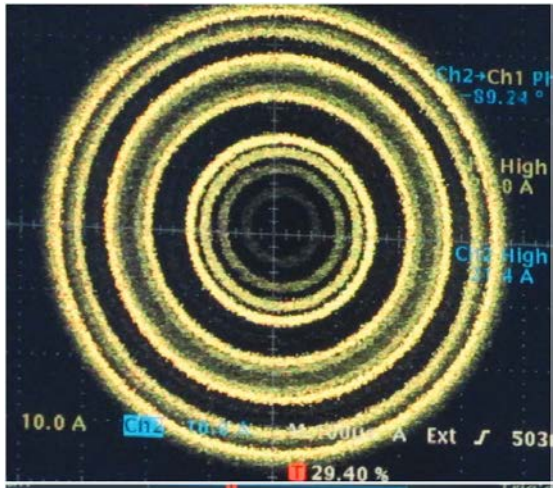

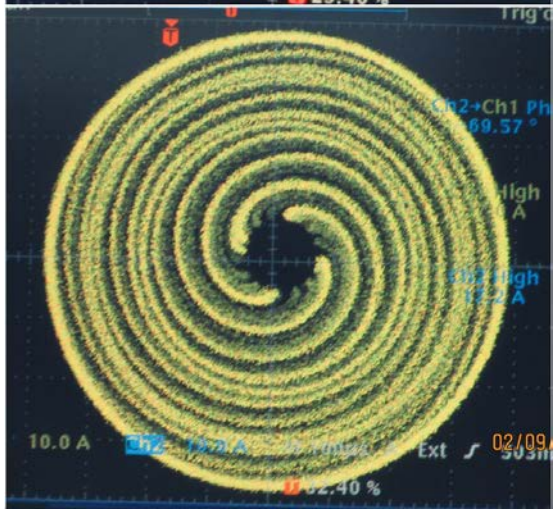

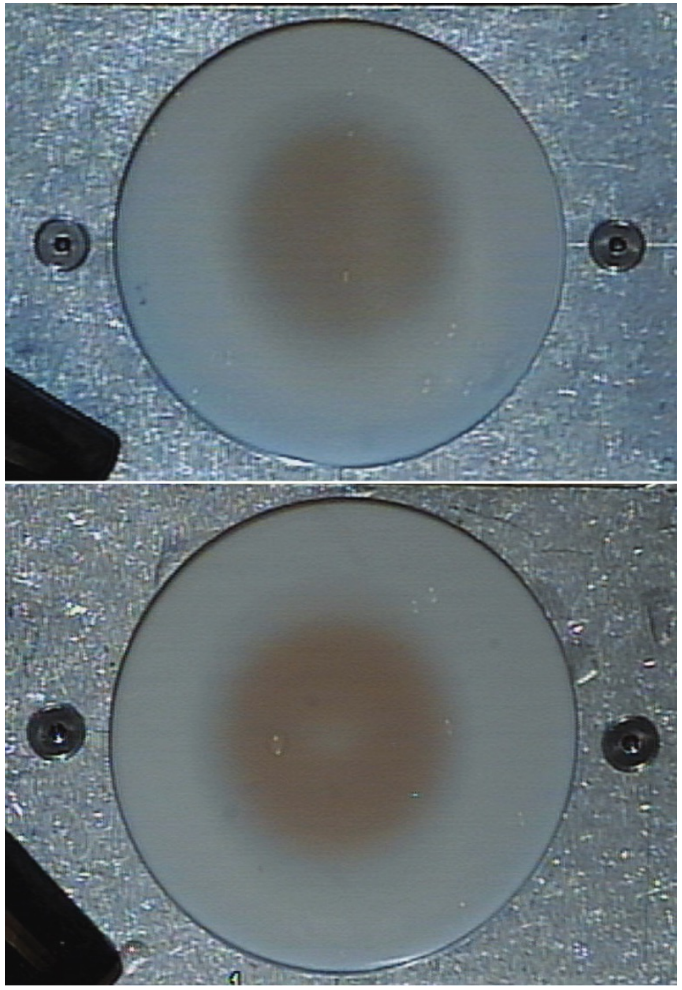

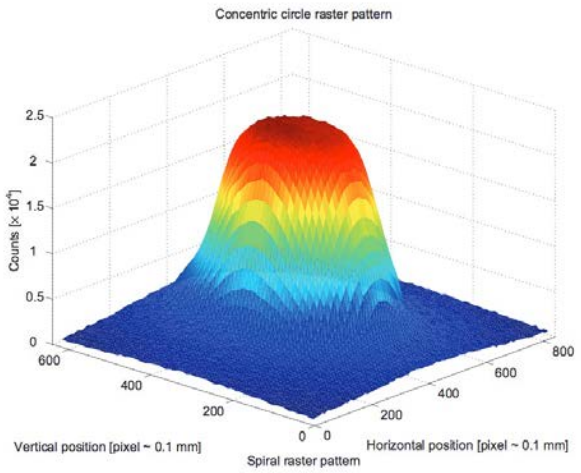

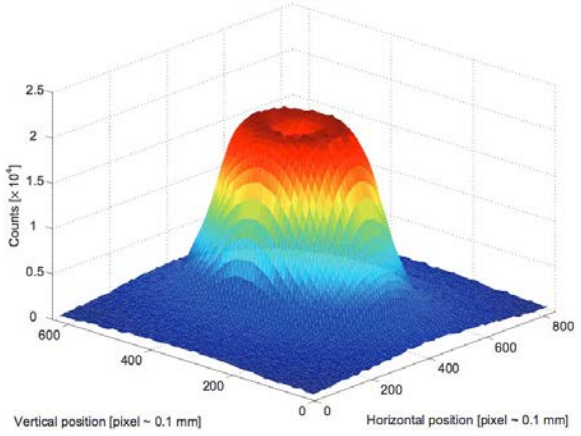

Experimental verification of uniform target irradiation by 100 MeV proton beam at LANSCE Isotope Production Facility (J.Kolski et al, TUPWI028, IPAC15).